



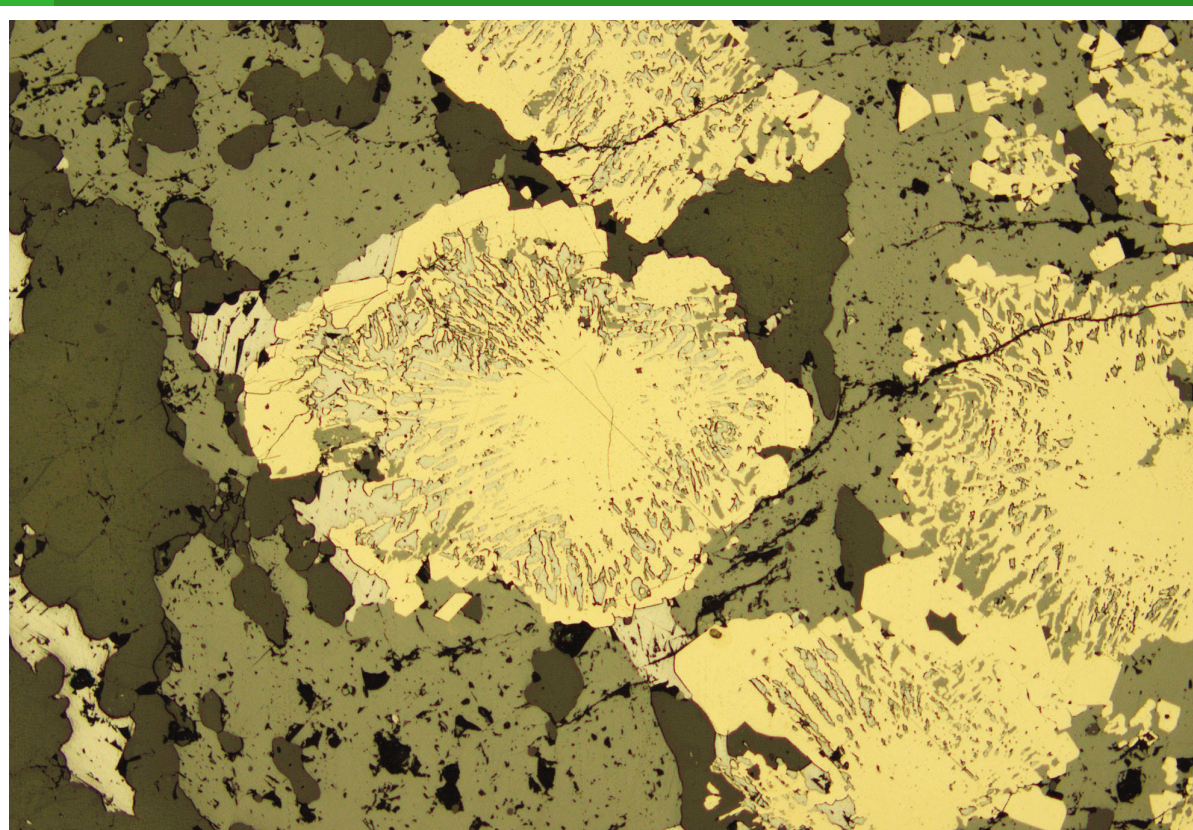
Government of  
Western Australia

Department of  
Mines and Petroleum

REPORT  
141

# ASSESSING THE POTENTIAL FOR VOLCANIC-ASSOCIATED MASSIVE SULFIDE MINERALIZATION AT WELD RANGE, USING GOLDEN GROVE FOR COMPARISON

by  
JN Guilliamse



Geological Survey of Western Australia



Government of **Western Australia**  
Department of **Mines and Petroleum**

**REPORT 141**

# **ASSESSING THE POTENTIAL FOR VOLCANIC-ASSOCIATED MASSIVE SULFIDE MINERALIZATION AT WELD RANGE, USING GOLDEN GROVE FOR COMPARISON**

by  
**JN Guilliamse**

**Perth 2014**



**Geological Survey of  
Western Australia**

**MINISTER FOR MINES AND PETROLEUM**  
**Hon. Bill Marmion MLA**

**DIRECTOR GENERAL, DEPARTMENT OF MINES AND PETROLEUM**  
**Richard Sellers**

**EXECUTIVE DIRECTOR, GEOLOGICAL SURVEY OF WESTERN AUSTRALIA**  
**Rick Rogerson**

#### **REFERENCE**

**The recommended reference for this publication is:**

Guilliamse, JN 2014, Assessing the potential for volcanic-associated massive sulfide mineralization at Weld Range, using Golden Grove for comparison: Geological Survey of Western Australia, Report 141, 61p.

#### **National Library of Australia Cataloguing-in-Publication entry:**

**Author:** Guilliamse, Joshua N., author.  
**Title:** Assessing the potential for volcanic-associated massive sulfide mineralization at Weld Range, using Golden Grove for comparison / J.N. Guilliamse.  
**ISBN:** 9781741685947 (ebook)  
**Series:** Report (Geological Survey of Western Australia) ; 141.  
**Subjects:** Greenstone belts--Western Australia--Yilgarn Craton. Igneous rocks--Western Australia--Weld Range. Igneous rocks--Western Australia--Golden Grove. Minerals--Western Australia--Yilgarn Craton. Hydrothermal alteration--Western Australia--Yilgarn Craton. Spectrum analysis.  
**Other Authors/Contributors:** Geological Survey of Western Australia, issuing body.  
**Dewey Decimal Classification:** 552.1099414  
**ISSN 1834-2280**

Grid references in this publication refer to the Geocentric Datum of Australia 1994 (GDA94). Locations mentioned in the text are referenced using Map Grid Australia (MGA) coordinates, Zone 50. All locations are quoted to at least the nearest 100 m.

Copy editor: RL Hitchings  
Cartography: AK Symonds  
Desktop publisher: RL Hitchings

#### **Disclaimer**

This product was produced using information from various sources. The Department of Mines and Petroleum (DMP) and the State cannot guarantee the accuracy, currency or completeness of the information. DMP and the State accept no responsibility and disclaim all liability for any loss, damage or costs incurred as a result of any use of or reliance whether wholly or in part upon the information provided in this publication or incorporated into it by reference.

#### **Published 2014 by Geological Survey of Western Australia**

This Report is published in digital format (PDF) and is available online at <[www.dmp.wa.gov.au/GSWApublications](http://www.dmp.wa.gov.au/GSWApublications)>.

#### **Further details of geological publications and maps produced by the Geological Survey of Western Australia are available from:**

Information Centre  
Department of Mines and Petroleum | 100 Plain Street | EAST PERTH | WESTERN AUSTRALIA 6004  
Telephone: +61 8 9222 3459 Facsimile: +61 8 9222 3444 [www.dmp.wa.gov.au/GSWApublications](http://www.dmp.wa.gov.au/GSWApublications)

**Cover image:** Pyrite replacing sphalerite and galena, Golden Grove Gossan Hill deposit, plane-polarized reflected-light photograph from ore zone in diamond drillhole GG274

## Contents

Abstract .....	1
Introduction .....	1
Regional geological setting .....	4
Methods .....	9
Sampling .....	9
Mineralogy (including mineral chemistry) .....	9
Whole-rock geochemistry .....	11
Geochronology .....	12
Results .....	12
Stratigraphy .....	12
Golden Grove .....	12
Glenview .....	12
Felsic volcanic geochemistry .....	13
Golden Grove .....	13
Glenview .....	13
Sulfide mineralization .....	17
Golden Grove .....	17
Glenview .....	17
Geochronology .....	18
Alteration mineralogy .....	21
Golden Grove .....	21
White mica .....	21
Chlorite .....	28
Glenview .....	30
White mica .....	30
Chlorite .....	32
Discussion .....	32
Paleodepositional environment .....	32
Tectonic setting .....	38
Host rock ages .....	38
VMS fertility of felsic volcanic rocks .....	39
Alteration vectors to mineralization .....	40
Conclusions .....	41
Acknowledgements .....	42
References .....	42

## Appendices

Appendix 1 – Geochemistry .....	45
Appendix 2 – SEM .....	49
Appendix 3 – TIR results .....	52

## Figures

1. The Yilgarn Craton showing terrane subdivisions within the Eastern Goldfields Superterrane and the domain subdivision of the Youanmi Terrane .....	2
2. The Murchison Domain showing the location of Golden Grove and Glenview .....	3
3. Stratigraphic scheme for the Murchison Domain .....	6
4. Stratigraphic scheme for the Golden Grove area showing the stratigraphic location of the Gossan Hill and Scuddles deposits .....	7
5. The northern Warriedar Fold Belt with stratigraphy of the Golden Grove area .....	8
6. Map of the Weld Range .....	9
7. Cross-section of the Golden Grove deposits showing the approximate location of the six drillholes used for this study .....	10
8. Aerial photo of the Glenview prospect showing the location of the four drillholes used for this study ....	10
9. The electromagnetic spectrum showing the regions of interest in visible/infrared reflectance spectroscopy .....	11

10.	Diagnostic absorption features of white mica and chlorite .....	12
11.	Drillcore photographs of rocks from Golden Grove .....	13
12.	Photographs of rocks from Glenview .....	14
13.	Photographs of rocks from the Weld Range .....	15
14.	Volcanic discrimination diagram for felsic volcanic rocks from Golden Grove and Glenview .....	15
15.	Felsic fertility plot for felsic volcanic rocks from Golden Grove and Glenview .....	15
16.	Chondrite normalized REE spider diagram for footwall and mineralized horizon felsic volcanic rocks from Golden Grove .....	16
17.	Chondrite normalized REE spider diagram for hangingwall dacites from Golden Grove. ....	16
18.	Chondrite normalized REE spider diagram for felsic volcanic rocks from Glenview .....	17
19.	Tectonic setting discrimination diagram for felsic volcanic rocks from Golden Grove and Glenview ....	17
20.	Stylized cross-section of the Gossan Hill deposit showing individual units of the Scuddles and Golden Grove Formations .....	18
21.	Photographs of mineralization intersected in drillcore from Glenview .....	19
22.	U–Pb analytical data for zircons from samples: a) 155569: metarhyolite, Weld Range; b) 155572: felsic volcanoclastic metasandstone, Weld Range .....	20
23.	Graphic log of Golden Grove drillhole CUDD001 .....	22
24.	Graphic log of Golden Grove drillhole GG274 .....	23
25.	Graphic log of Golden Grove drillhole GG276D1 .....	24
26.	Graphic log of Golden Grove drillhole RHDD034 .....	25
27.	Graphic log of Golden Grove drillhole SC098D1 .....	26
28.	Graphic log of Golden Grove drillhole SC107 .....	27
29.	Change in paragonite abundance with increasing proximity to sulfide mineralization .....	28
30.	Downhole variation in the wavelength intersection of the AlOH absorption feature related to white mica .....	29
31.	Change in the intersection of the AlOH absorption feature between drillholes at Golden Grove .....	30
32.	Downhole variation in the wavelength intersection of the FeOH absorption feature related to chlorite .....	31
33.	Change in the intersection of the FeOH absorption feature between drillholes at Golden Grove .....	32
34.	Graphic log of Glenview drillhole 95WGD006 .....	33
35.	Graphic log of Glenview drillhole 95WGD002 .....	34
36.	Graphic log of Glenview drillhole 95WGD004 .....	35
37.	Graphic log of Glenview drillhole 96GVDI001 .....	36
38.	Change in the intersection of the AlOH and FeOH absorption features between drillholes .....	37
39.	Summary of age determinations for felsic volcanic rocks from Golden Grove and the Weld Range .....	39
40.	Conceptual petrogenetic model for the formation of FI-FII-FIII felsic volcanic rocks .....	40

## Tables

1.	Characteristics of each classification type defined by Lesher et al (1986) .....	4
2.	Geochemical classification, petrogenetic models, and tectonic environments proposed for the formation of FI, FII, FIII, and FIV felsic volcanic rocks .....	5

# Assessing the potential for volcanic-associated massive sulfide mineralization at Weld Range, using Golden Grove for comparison

by

JN Guilliamse

## Abstract

The Archean Yilgarn Craton in Western Australia appears to be poorly endowed in volcanogenic massive sulfide (VMS) deposits, but the occurrence of some conspicuous examples, such as Golden Grove, indicates that the geological processes required for their formation were present and that other factors are hindering exploration success. This study evaluated the VMS prospectivity of the Glenview prospect in the Weld Range greenstone belt in the northern Murchison Domain of the Yilgarn Craton, by comparing geological characteristics considered important for VMS mineralization — lithology, age, paleodepositional environment, tectonic setting, VMS fertility and alteration — with those for Golden Grove. Changes in the chemistry of alteration minerals were also examined as potential vectors towards mineralization at Glenview.

From core logging and thin section analysis, Golden Grove and Glenview have similar volcano-sedimentary stratigraphies, dominated by subaqueous felsic volcanic rocks, some of which were probably deposited more than 500 m underwater. SHRIMP U–Pb dating of zircon in a sample near Glenview returned an age of  $2977 \pm 3$  Ma, similar to reported ages of 2960–2945 Ma for Golden Grove. The lithogeochemistry of host rocks in both regions indicate that they formed in active continental margins, which are conducive to VMS formation, and that they are potentially fertile for VMS mineralization. Mineral spectroscopy of drillcore from Golden Grove showed that white mica and chlorite alteration changed systematically in chemistry and intensity with respect to sulfide mineralization, and provides a vector towards VMS mineralization. When applied to Glenview, such changes in white mica and chlorite alteration suggest the core of the system lies east of the present focus of exploration.

**KEYWORDS:** Archean, felsic volcanic rocks, geochemical exploration, hydrothermal alteration, spectroscopic analysis, volcanogenic deposits

## Introduction

Volcanogenic massive sulfides (VMS), also known as volcanic-associated, volcanic-hosted, and volcano-sedimentary hosted massive sulfides, are economically important sources for Cu, Zn, Pb, Ag, Au, Co, Sn, Se, Mn, Cd, In, Bi, Te, Ga, and Ge (Galley et al., 2007). VMS deposits are lensoidal accumulations of massive sulfide that form at or near the sea floor by the focused emission of metal-enriched hydrothermal fluids sourced from large hydrothermal convection cells. Host rocks may be either volcanic or sedimentary, but are always related to tectonic extension because thinning of the crust promotes the formation and shallow level emplacement of intrusions that drive hydrothermal convection (Galley et al., 2007). VMS deposits are found in rocks ranging from Archean to modern, with analogues presently forming on the ocean floor (Herzig and Hannington, 1995).

The formation and preservation of VMS deposits require appropriate tectonic settings, hydrothermal processes, and local environmental conditions. Exploration in ancient settings seeks evidence that these requirements were operating; hence, whether a region had the potential to produce and preserve VMS mineralization. Belford (2001) and Galley et al. (2007) describe characteristic features of ancient assemblages that can be linked to VMS-forming processes. These features include: 1) extensional settings, indicated by bimodal volcanism; 2) sub-volcanic intrusions that act as heat sources to generate hydrothermal convection; 3) an upper stratigraphy dominated by chemical or siliciclastic sedimentary rocks that indicate a hydrothermally active paleo-sea floor; 4) a complex and permeable lower stratigraphy that would have promoted fluid flow; and 5) broad zones of semiconformable alteration that indicate large-scale hydrothermal processes have occurred. Once a geological terrane is recognized





greenstone belt of the Murchison Domain. Pre-mining resources at Gossan Hill were 9.2 Mt at 2.7% Zn, 2.6% Cu, 0.4 g/t Au and 24 g/t Ag, and at Scuddles were 10.5 Mt at 11.7% Zn, 1.2% Cu, 0.8% Pb, 1.1 g/t Au and 89 g/t Ag (MMG Limited, 2012a). Additional resources have recently been defined to the south of the current mines at the Gossan Valley and Felix prospects. As at June 2011, the Gossan Valley and Felix resource was 1.5 Mt of zinc ore at 7.9% Zn, 10 g/t Ag and 0.9 g/t Au; plus 1.3 Mt of copper ore at 2.3% Cu, 14 g/t Ag and 0.3 g/t Au (MMG Limited, 2012b).

Subeconomic VMS mineralization is also known in the Weld Range greenstone belt, in the northern Murchison Domain. Exploration for VMS mineralization first

occurred here in the early 1990s when felsic volcanic rocks on the northern side of the Weld Range were correlated with the felsic volcanic rocks that host the VMS deposits at Golden Grove (Martin et al., 1997). Exploration resulted in the discovery of gossans at the Glenview prospect (Figs 2 and 6), and subsequent drilling intersected VMS-style base metal stringer mineralization in the majority of holes, with significant intersections that included 2 m at 1.47% Pb and 5.73% Zn, and 2.55 m at 11.9% Cu (Martin et al., 1997). Belford (1996) defined an extensive alteration zone that was consistent with circulating hydrothermal fluids, and used the presence of base-metal sulfide stringer mineralization to infer that the circulating fluid was metal laden. Subsequent exploration failed to discover any significant resource

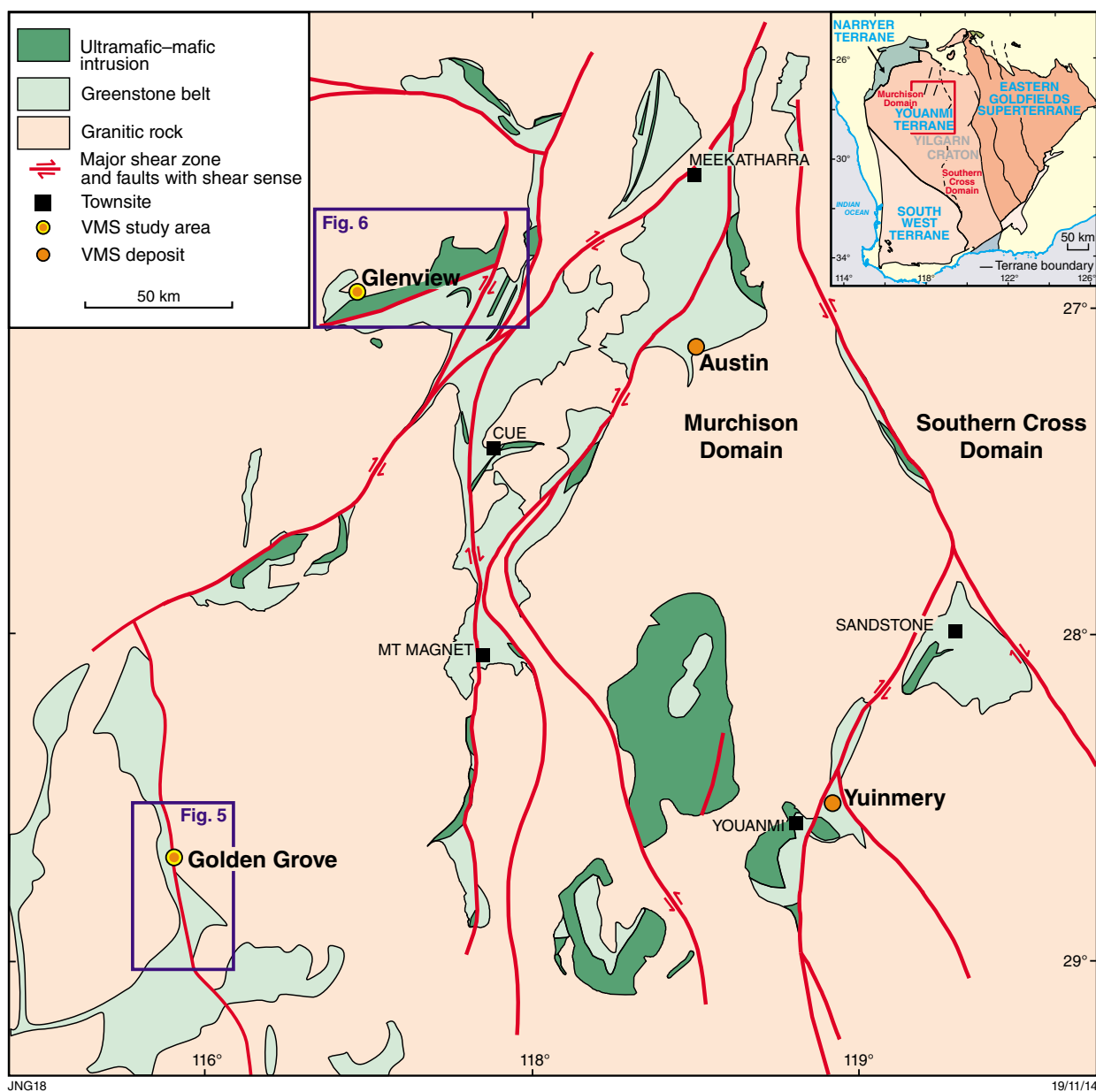


Figure 2. The Murchison Domain showing the location of Golden Grove and Glenview (modified from Van Kranendonk et al., 2010).



at the Glenview prospect, but the presence of sulfides is encouraging. The aim of this study was to examine in more detail the geological setting and VMS prospectivity of Archean strata in the vicinity of the Glenview prospect by comparing this with stratigraphy, ages, tectonic setting, and paleodepositional environment at Golden Grove, and to define possible vectors for exploration.

Data used for evaluation of VMS prospectivity were obtained by visual and hyperspectral logging of representative drillcore, petrography, whole-rock and mineral geochemistry, and geochronology. Interpretations of rock types, tectonic setting, and water depth prevailing at Glenview and Golden Grove are supported by geochemistry and petrography. New and previously published geochronology data were used to re-evaluate depositional ages of both areas. Major and trace-element analysis on felsic volcanic samples from Golden Grove and Glenview were used to determine VMS fertility (FI–FIV) of felsic volcanic rocks using the scheme devised by Leshner et al. (1986; Tables 1 and 2) and to determine tectonic setting using the tectonic discrimination diagrams of Schandl and Gorton (2002). Drillcore from both Glenview and Golden Grove was scanned using the Geological Survey of Western Australia's (GSWA) HyLogger spectrometer to assess changes in mineral abundance and speciation, and to define alteration vectors to mineralization at Golden Grove, then test whether similar vectors can be applied at Glenview.

## Regional geological setting

The Golden Grove and Weld Range districts are part of the Murchison Domain, which comprises the western half of the Youanmi Terrane in the central western part of the Yilgarn Craton (Fig.1, Cassidy et al., 2006). Early interpretations of stratigraphic associations in the Murchison Domain were made by Watkins and Hickman (1990) and Pidgeon and Hallberg (2000). These were superseded by a new lithostratigraphic scheme developed following remapping of parts of the northern Murchison Domain by GSWA (Van Kranendonk and Ivanic, 2009; Fig. 3).

The oldest preserved stratigraphy in the Murchison Domain records mafic to felsic magmatism, manifested by widespread deposition of greenstones and emplacement of associated granites from 2960 to 2935 Ma. This initial phase of magmatism was followed by a 110 million-year hiatus, then the superposition by younger crust created

by voluminous mantle melting at 2825 Ma, possibly in response to a deep mantle plume (Barley et al., 2000; Van Kranendonk et al., 2012). The onset of mantle melting marked the start of 225 million years of almost continuous crustal growth, incorporating two major cycles of ultramafic to felsic magmatism during 2825–2740 Ma and 2735–2710 Ma. The early stages of each cycle involved ultramafic–mafic volcanism and emplacement of large volumes of ultramafic–mafic intrusions into older rocks, followed by voluminous granitic magmatism and felsic volcanism in the later stages. The emplacement of granitic rocks continued until 2600 Ma, marking the end of cratonization of the Murchison Domain.

Golden Grove is located in the southern Murchison Domain on the northeastern flank of the Warriedar Fold Belt, a region defined by Clifford (1992) as the 'Golden Grove Domain', and comprising a steeply west-southwest dipping (and younging), layered succession divided by Clifford (1992) into the Minjar, Thundelarra, and Gossan Hill Groups (Figs 4 and 5). Base-metal mineralization in the Gossan Hill and Scuddles deposits is largely restricted to sedimentary units of the Golden Grove Formation within the Gossan Hill Group (Fig. 4). SHRIMP U–Pb zircon dating of rocks from Golden Grove indicate deposition of the Gossan Hill Group between 2960 and 2945 Ma (Wang, 1998).

The Glenview prospect lies in the northern Murchison Domain on the northern side of the Weld Range greenstone belt, a steeply southward dipping and younging succession of ultramafic to felsic volcanic, volcanoclastic, and clastic and chemical sedimentary rocks that is intruded by dolerite and gabbro sills of the c. 2745 Ma Gnanagooragoo Igneous Complex (Figs 2 and 6; Ivanic, 2009; Ivanic et al., 2010). Mineralization occurs on the northern side of the Weld Range greenstone belt in a sequence of felsic volcanic, volcanoclastic and chemical sedimentary rocks showing marked variability in thickness along strike. The host sequence is capped by a >1 km thick accumulation of banded iron-formation (BIF). This sequence was previously inferred to be part of the c. 2750 Ma Wilgie Mia Formation, based on an interpretation by Van Kranendonk et al. (2012) and Ivanic (2009) that zircons U–Pb SHRIMP dated by Wang (1998) at c. 2960 Ma, are xenocrysts. The zircon age and inferences were both tested with further sampling and U–Pb SHRIMP geochronology. Supracrustal rocks in the Weld Range greenstone belt are metamorphosed to lower-greenschist facies ( $300 \pm 50$  °C) at pressures of about 2–3 kbars (Gole, 1980).

**Table 1. Characteristics of each classification type of felsic volcanic rocks defined by Leshner et al (1986)**

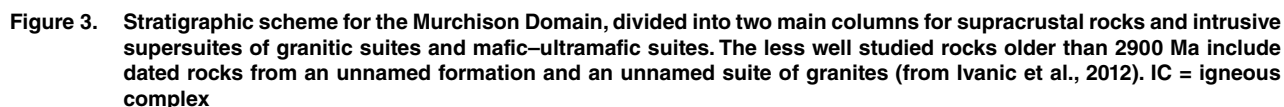
<i>Fertility</i>	<i>REE patterns</i>	<i>Eu anomaly</i>	<i>Zr/Y</i>	<i>HFSE abundances</i>
FI	Steep	Weakly negative to moderately positive	High	Low
FII	Gently sloping	Variable	Moderate	Intermediate
FIIIa	Flat	Variable negative	Low	Intermediate
FIIIb	Flat	Pronounced negative	Low	High

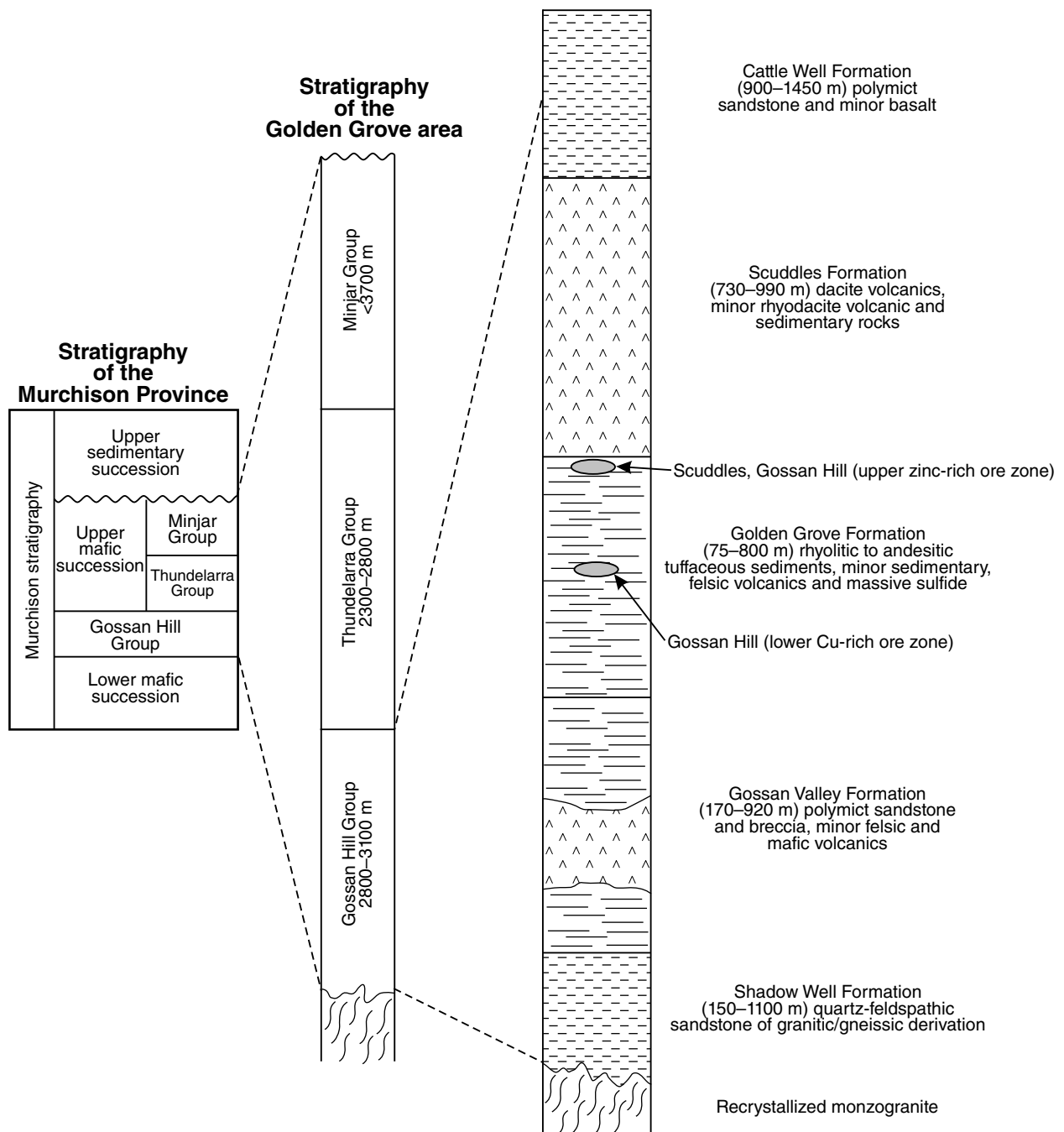
Table 2. Geochemical classification, petrogenetic models, and tectonic environments proposed for the formation of FI, FII, FIII, and FIV felsic volcanic rocks (from Hart et al., 2004)

	FI	FII	FIIIa	FIIIb	FIV
<b>Lithology</b>	Dacite–rhyolite	Dacite–rhyolite	Rhyodacite – high-silica rhyolite	Rhyodacite – high-silica rhyolite	Rhyolite – high-silica rhyolite
SiO <sub>2</sub> (wt %)	64–72	64–81	67–78	67–84	69–81
TiO <sub>2</sub>	0.16 – 0.65	0.16 – 0.89	0.21 – 0.99	0.09 – 0.73	0.09 – 0.57
Y (ppm)	6–31	11–73	25–96	72–238	18–63
Zr/Y	8.8 – 31	3.2 – 12.12	3.9 – 7.7	1.7 – 6.2	0.67 – 4.8
Yb (ppm)	0.43 – 3.8	1.3 – 7.9	3.4 – 9.3	5–32	1.5 – 8.4
[La/Yb] <sub>Cr<sup>(a)</sup></sub>	5.8 – 34	1.7 – 8.8	1.5 – 3.5	1.1 – 4.9	0.22 – 2.1
Eu/Eu*	0.87 – 1.5	0.35 – 0.91	0.37 – 0.94	0.20 – 0.61	–
<b>Affinity</b>	Alkaline–calc–alkaline	Calc–alkaline	Tholeiitic	Tholeiitic	Tholeiitic
<b>Petrogenetic models</b>	Low-degree partial melting of mafic source at high pressure with minimal fractionation; do not appear to be associated with high-level magma chambers (Leshner et al., 1986)	Fractional crystallization of intermediate magma (Campbell et al., 1981, 1982; Leshner et al., 1986); high-degree partial melting of felsic granulite at intermediate crustal depths (Leshner et al., 1986); partial melting related to metasomatism of mantle wedge over subducted slab fractional crystallization of resulting mafic magma (Barrett and MacLean, 1999); high-temperature partial melting of crustal material with magma compositions controlled by differences in composition of crust (Lentz, 1998)	Low-pressure partial melting of tholeiitic basalt with no residual amphibole (Hart, 1984) or garnet (Campbell et al., 1981, 1982; Leshner et al., 1986; Barrie et al., 1993) in a subvolcanic magma chamber; low-pressure plagioclase-dominated fractional crystallization of intermediate magma (Leshner et al., 1986); partial melting of different crustal material producing a variety of felsic magma compositions (Lentz, 1998); partial melting of continental crust with minor assimilation fractional crystallization forming alkaline to subalkaline rhyolites (Barrett and MacLean, 1999)	Partial melting of granulite lower crust with fractionation producing higher silica contents; extreme fractional crystallization of tholeiitic mafic liquid resulting in liquid immiscibility with possible wallrock contamination (Thurston and Fryer, 1983); high-temperature partial melting of crustal material magma compositions controlled by differences in composition of crust (Lentz, 1998)	Low-pressure moderate degree partial melting of depleted tholeiitic basalt (Hart et al., 2004)
<b>Tectonic environment</b>	Arc-related suites derived from metasomatized wedge with variable crustal contamination (Barrie et al., 1993)	Continental arc (Barrie et al., 1993); rifted mature arc/continental back-arc floored by oceanic crust (Barrett and MacLean, 1999); extensional environments (e.g. intra-oceanic intra-arc, and back-arc rift; Lentz, 1998)	Rifted island-arc (Barrie et al., 1993); rifted continental margin (Barrett and MacLean, 1999); extensional environments (e.g. intra-arc, and back-arc intra-oceanic intra-arc, and back-arc rift; Lentz, 1998)	Oceanic rift (Hart, 1984; Barrie et al., 1993)	Intra-oceanic island-arc on oceanic crust (Barrett and MacLean, 1999)
<b>Examples</b>		Sturgeon Lake, Kuroko, Rio Tinto, Bathurst, Myra Falls, Mt Windsor, Tulsequah Chief, Mt Chalmers, Thalanga, Mt Read, Boliden, Selbale, Salt Creek, Murgul, Benambra	Noranda, Jerome, United Verde, Teutonic Bore, Parys, Mountain, Ambler, Avoca, Woodlawn, Buchans, Pieska, Fox Lake, Manito Uwadge, Hood River, Sulphur Springs, Scuddles, Berslagen, Winston Lake	Kidd Creek, Kamiskotia, Eskay Creek, Neves Corvo, Shasta, Crandon Lake, Mons Cupri, South Bay	Stekerjokk, Snow Lake, Flin Flon, West Shasta, Kutchok Creek, Canatuan
<b>Source depth</b>	Deep (>30 km)	Intermediate (>10 but <5 km) for mineralized FI	Shallow (<10 km)	Shallow (<10 km)	Shallow (<10 km)

**NOTES:** (a) on Chondrite-normalizing values from Nakamura (1974)

\* Eu calculated by linear interpolation between chondrite-normalized Sm and Tb

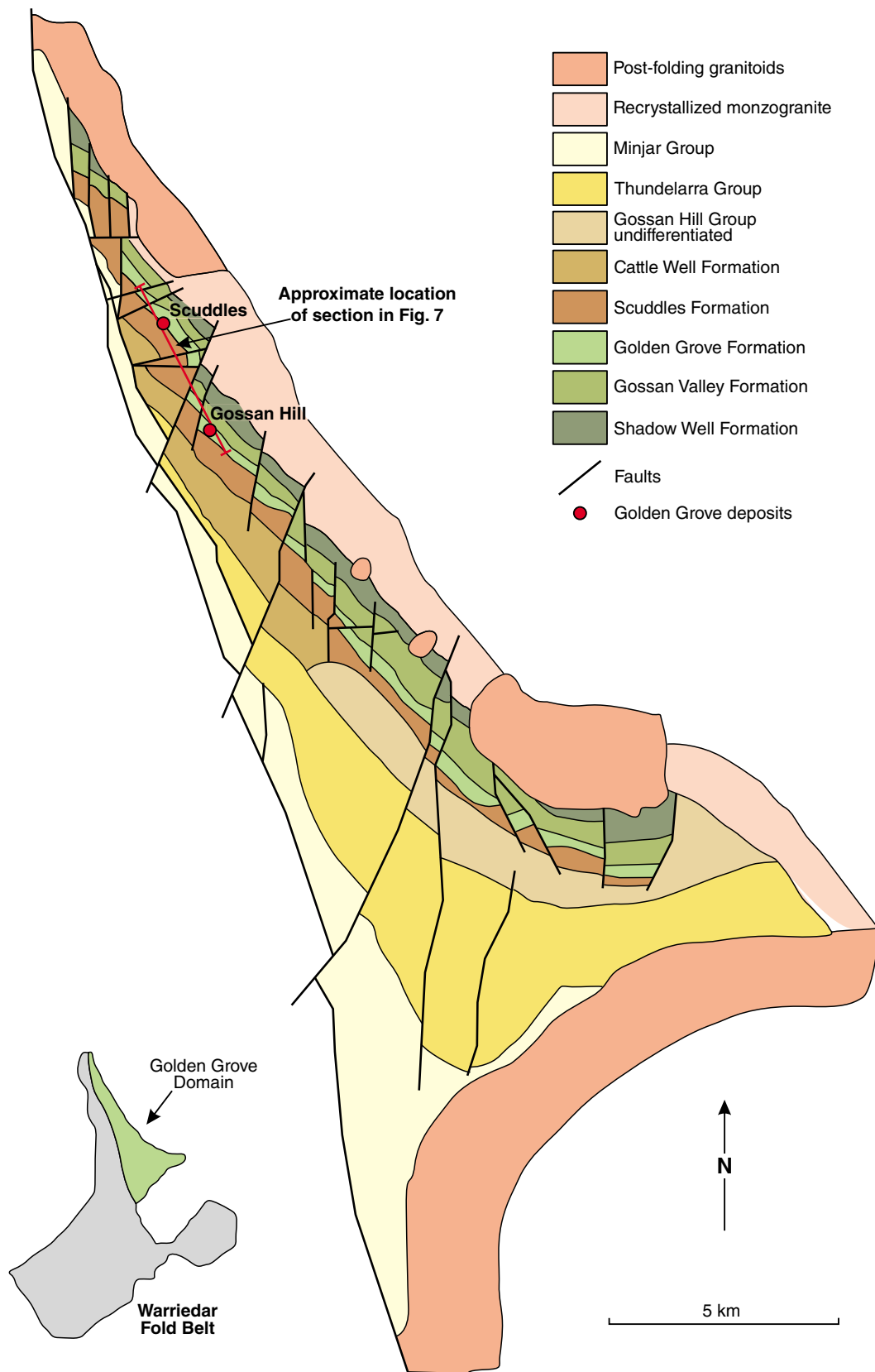




JNG20

18/11/14

**Figure 4. Stratigraphic scheme for the Golden Grove area showing the stratigraphic location of the Gossan Hill and Scuddles deposits (modified from Clifford, 1992)**



JNG19

01/12/14

**Figure 5.** The northern Warriedar Fold Belt with stratigraphy of the Golden Grove area as defined by Clifford (1992). Modified from Clifford (1992).

## Methods

### Sampling

MMG Limited and Hampton Hill Mining NL donated diamond drillcore for six drillholes from Golden Grove and four drillholes from the Weld Range for this study. These are held in the GSWA Perth core library. The drillholes from Golden Grove each span an equivalent section of the footwall, mineralized horizon, and hangingwall stratigraphy that hosts the Gossan Hill and Scuddles deposits, and collectively sample host rocks distal and proximal to mineralization (Fig. 7). The four drillholes from the Glenview prospect sample part of the felsic volcanic sequence, and all intersect VMS-style base metal stringer mineralization (Fig. 8).

All core was scanned using the GSWA HyLogger spectrometer (Hancock and Huntington, 2010a), then graphically logged and selectively sampled for thin section

petrography and whole-rock geochemistry (Appendix 1) to identify host rocks and to validate mineral assemblages interpreted from HyLogger data. Forty samples of felsic volcanic rock were collected from drillcore for geochemical analysis, 11 samples from Glenview and 29 samples from Golden Grove (Appendix 1). Felsic volcanic rocks were chosen, as they are a requirement of fertility plots used in this study. Rocks appropriate for geochronology were identified during field observations (Fig. 6).

### Mineralogy (including mineral chemistry)

All drillcore was scanned in the near-infrared (NIR; 600–300 nm), shortwave infrared (SWIR; 1300–2500 nm), and thermal infrared (TIR; 2500 nm – 1 mm; Fig. 9) spectral ranges using the HyLogger and operational parameters and scanning procedures as described by Hancock and Huntington (2010b).

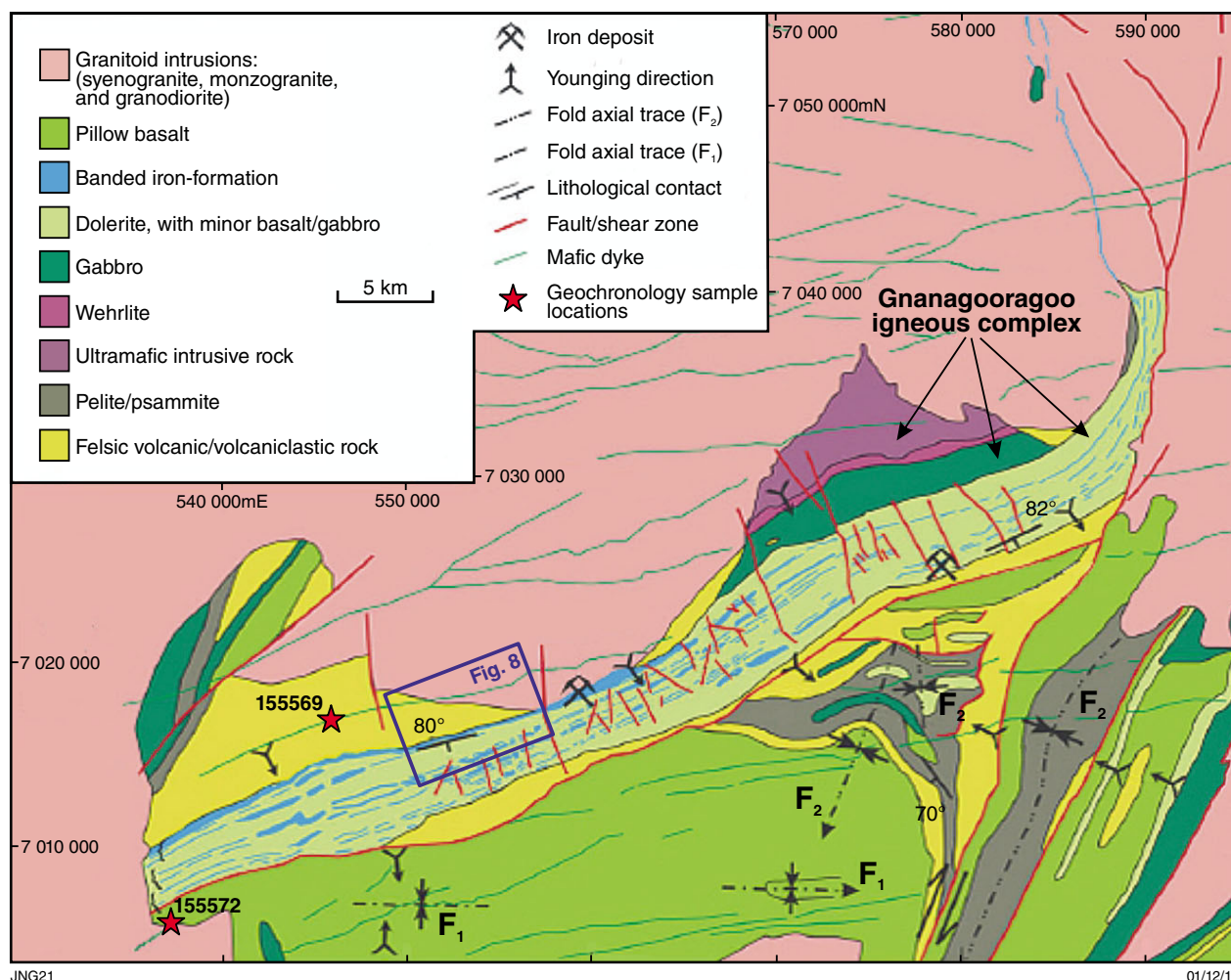


**Figure 6. Map of the Weld Range. The blue square indicates the approximate location of the Glenview prospect. Modified from Duuring and Hagemann (2013), after Ivanić (2009).**



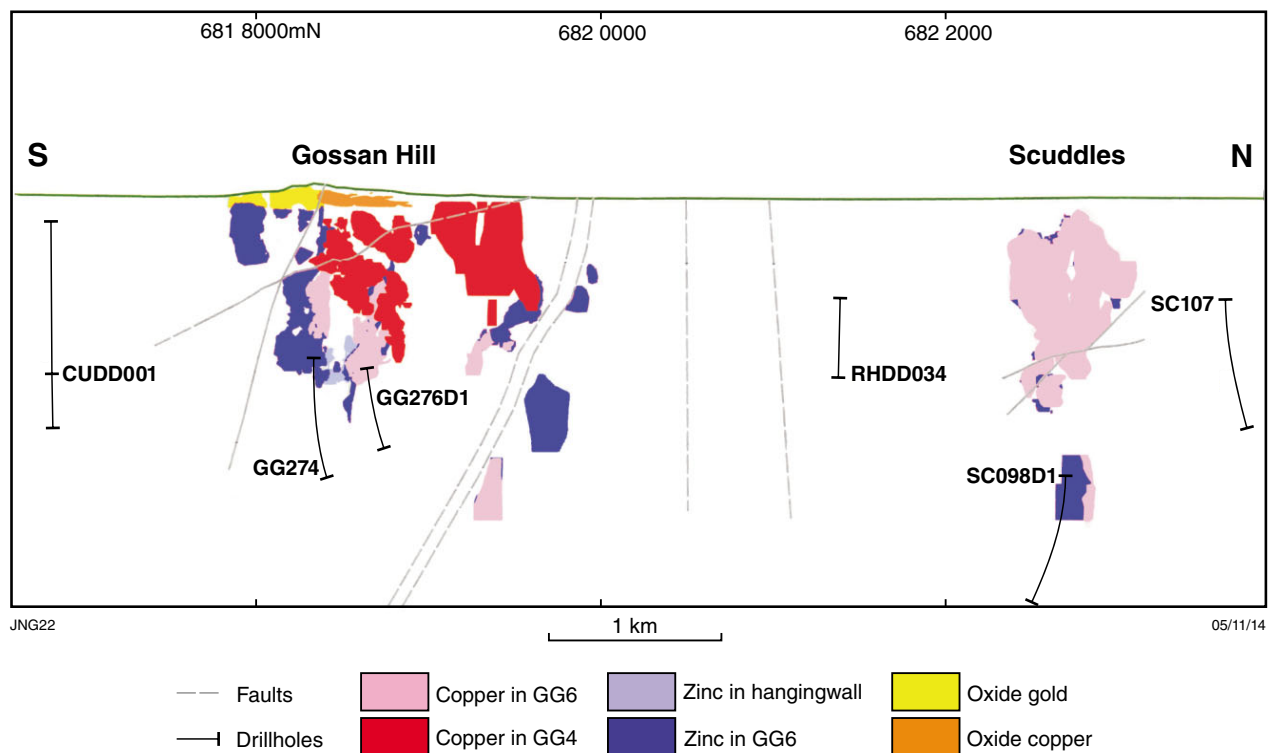


**Figure 7.** Cross-section of the Golden Grove deposits showing the approximate location of the six drillholes used for this study relative to main mineralization styles (modified from Gawlinski, 2004)

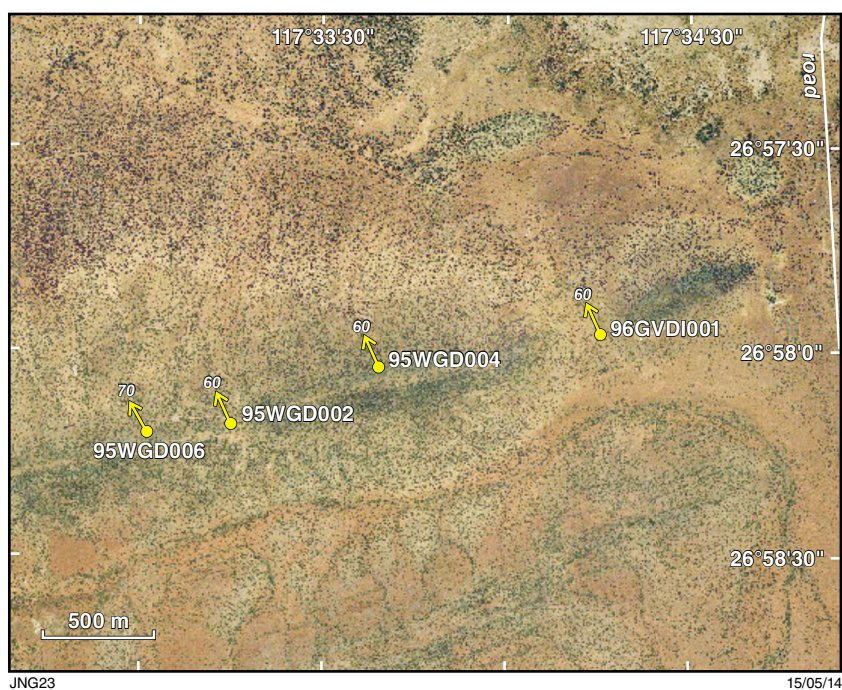
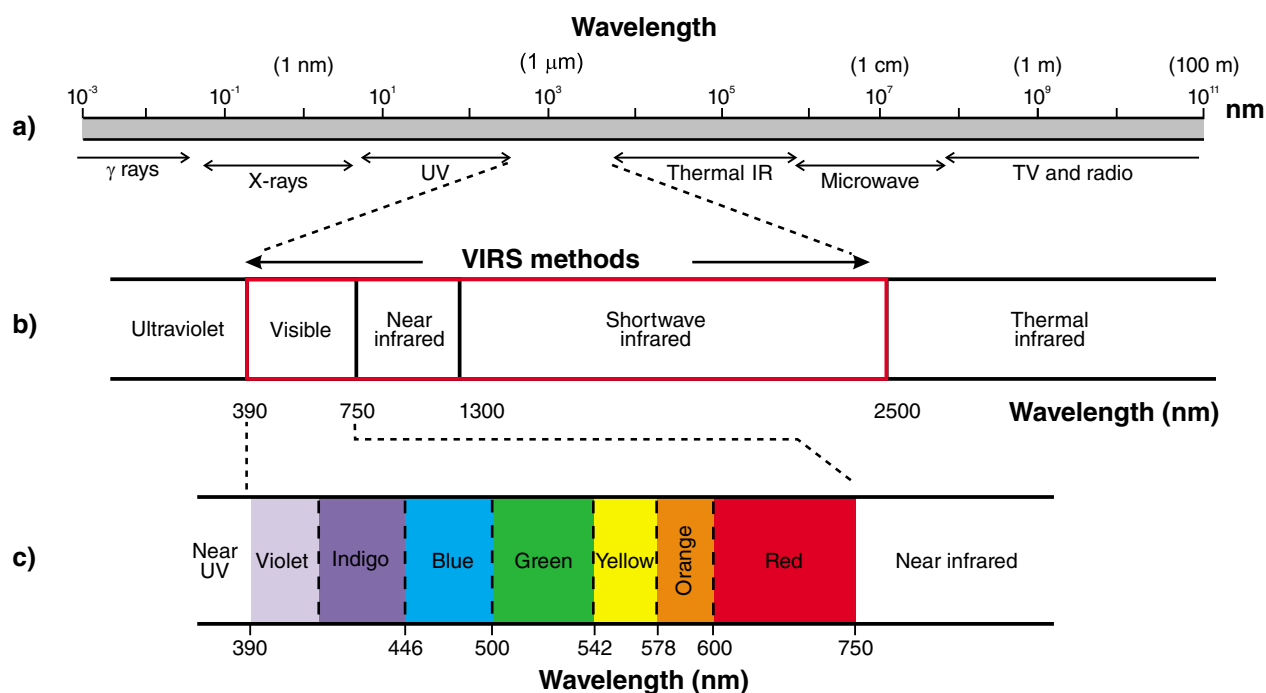


**Figure 8.** Aerial photo of the Glenview prospect showing the location of the four drillholes used for this study





JNG34

05.11.14

**Figure 9. The electromagnetic spectrum showing the regions of interest in visible/infrared reflectance spectroscopy (from Kerr et al., 2011)**

Raw spectral data was analysed using The Spectral Geologist (TSG) 7.1, a commercial software that assists with mineral identification, provides estimates of mineral abundance, and measures positions of specific absorption features by matching collected spectra against a library of known mineral responses (Merry et al., 1999). This study largely used The Spectral Assistant (TSA) approach — a routine within TSG that uses a training library of spectra either to match the unknown project spectrum against a single mineral spectrum, or to create a simulated mixture of two mineral spectra that match the observed spectrum. Major minerals are predicted on the basis of the match that returns the lowest error result (Pontual, 2008). Changes in identified mineral species were analysed in relation to proximity to VMS mineralization, focusing on white mica and chlorite species because they are common VMS alteration minerals that are known to vary in chemistry.

Two user-defined calculations known as ‘scalars’ were produced using a method developed by Jon Huntington from CSIRO to focus on absorption features within the SWIR spectrum related to white mica and chlorite. The AlOH absorption feature between 2190 and 2210 nm (Fig. 10a) and the FeOH absorption feature between 2240 and 2260 nm (Fig. 10b). If an absorption feature occurs in the specified wavelength range, the scalar returns the wavelength of the minimum point. These values were plotted to test for any spatial relationship between recorded wavelength values and proximity to sulfide mineralization. A description of data processing using the TSG software is provided by Hancock and Huntington (2010a, 2010b).

Polished thin sections were made and examined using transmitted and reflected light petrography, and a small subset of these were analysed using an XL40 scanning electron microscopy (SEM) at the Earth Science and Resource Engineering division of CSIRO, to validate chlorite and white mica identification and chemistry. Samples were tested at 30 kV using a standardless EDAX ZAF quantification. Samples were not carbon-coated prior to testing, on the advice of the instrument technician.

## Whole-rock geochemistry

All samples were crushed and pulverized at the GSWA laboratories using a tungsten carbide mill to minimize potential contaminations with Co, W, rare earth elements (REE) and high field strength elements (HFSE; Morris, 2007). Pulps were then sent to Intertek Genalysis for major and trace-element analysis. Major elements were determined using X-ray fluorescence spectrometry (XRF) on discs prepared using lithium-metacarbonate fusion. Trace elements were analysed using inductively coupled plasma-mass spectrometry (ICP-MS) after a lithium-metaborate fusion was used prior to dissolution of discs in  $\text{HNO}_3$  to address potential problems stemming from incomplete dissolution of refractory minerals (Kerrick and Said, 2011). Duplicate samples and blind GSWA reference materials BB1, KG1, and MW1 were submitted to check precision and accuracy of the results, which were found to be acceptable (Appendix 1). Both ioGAS and Microsoft Excel were used to analyse, interpret and present the data.

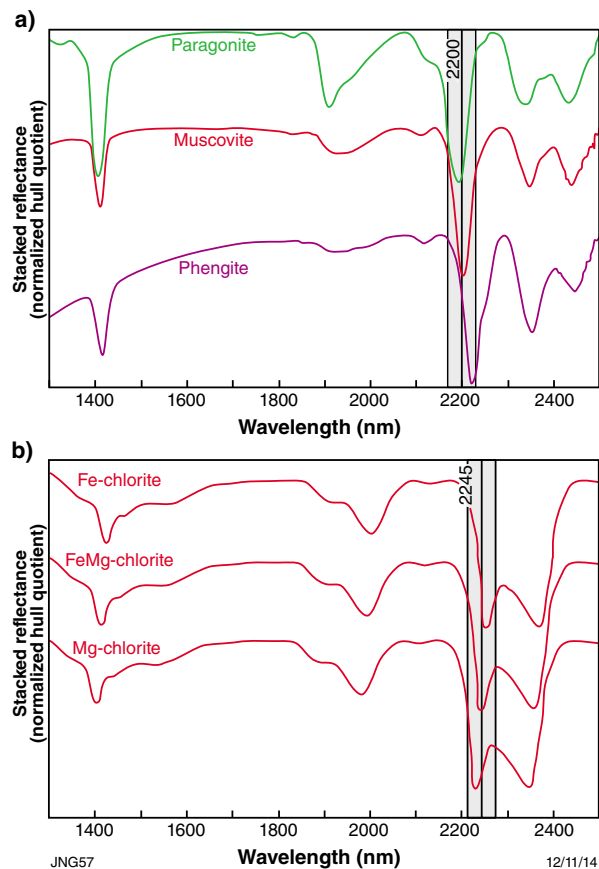


**Figure 10.** a) Diagnostic absorption features of white mica, split between paragonite, muscovite, and phengite. The highlighted area indicates the AIOH absorption feature of white mica at ~2200 nm. Note that the vertical scale is arbitrary and that the stacked spectra are offset for clarity. Modified from Hinchey (2011); b) diagnostic absorption features of chlorite, split between iron-rich, mixed sample, and magnesium-rich chlorite. The highlighted area indicates the FeOH absorption feature of chlorite at ~2250 nm. Note that the vertical scale is arbitrary and that the stacked spectra are offset for clarity. Modified from Hinchey (2011).

## Geochronology

Previous studies of Weld Range geology disagree with the age of the rock succession. Two samples were therefore collected from key locations in the Weld Range by GSWA and submitted for SHRIMP U–Pb analysis at the John de Laeter Centre of Mass Spectrometry at Curtin University, Perth, Western Australia. Wingate and Kirkland (2013) give a comprehensive overview of sample preparation, analysis, and data interpretation.

## Results

### Stratigraphy

#### Golden Grove

Stratigraphic logging reported here (Figs 23–28) show, as previously described in Clifford (1992), that the geology of the Golden Grove district comprises a layered succession of mafic to felsic volcanic, volcanoclastic, and clastic and chemical sedimentary rocks. The footwall is largely sedimentary, ranging from fine laminated siltstones to coarse-grained conglomerates and breccias. Sedimentary breccias are polymictic, poorly sorted, and clast supported, with angular to rounded lithic clasts and pumice fragments generally less than 20 mm in diameter. The footwall also contains minor felsic to mafic volcanic rocks, some of which have hyaloclastite textures. Chlorite and sericite alteration are significant through most of the footwall.

Fine-grained volcanoclastic rocks host and underlie mineralization at both the Gossan Hill and Scuddles mines. These volcanic packages are tens of metres thick and interbedded with epiclastic units. The upper part of each section contains up to 5 cm-thick chert beds that in the upper mineralized package are interlayered with sulfide mineralization (Fig. 11a). Sericite, chlorite, and carbonate alteration are prevalent in the mineralized section, with chlorite most prevalent in direct contact with sulfide mineralization.

Dacite and rhyodacite make up the bulk of the hangingwall sequence, although subordinate fine grained laminated sediments occur in the lower hangingwall (Fig. 11b), overlying the mineralized unit. Sericite and chlorite alteration is pervasive in the lower hangingwall sediments, becoming less apparent up stratigraphy away from mineralization.

#### Glenview

Petrographic examination of 22 samples of felsic lava obtained from drillcore at the Glenview prospect show mineralogical variation from rhyodacite to dacite. These typically display hyaloclastite and perlitic textures indicating subaqueous emplacement (Fig. 12f). Most are extensively altered by sericite and chlorite, making interpretation of the original rock difficult. Komatiitic basalts and coeval volcanic breccias outcrop northeast of the Glenview prospect in the basal part of the stratigraphy and are interpreted to have been deposited subaerially, and to have been derived by high-temperature mantle melting (Fig. 13a,b; Van Kranendonk et al., 2010).

Sedimentary units make up a significant portion of the Glenview stratigraphy. Petrographic examination of

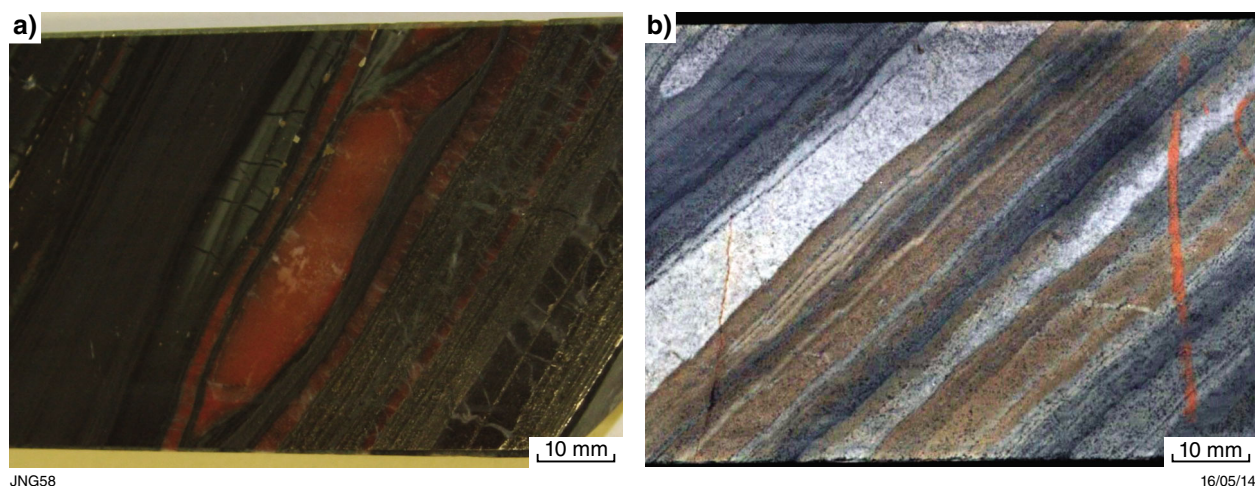


**Figure 11.** Drillcore photographs of rocks from Golden Grove: a) Marker horizon that occurs in the upper section of the GG6 mineralized zone at Golden Grove. Jasper and magnetite bands in laminated siltstone, RHDD011; b) laminated volcaniclastic unit which forms the GG6 mineralized horizon at Golden Grove, RHDD034.

40 drillcore samples indicates that these sedimentary units include immature and reworked volcaniclastic, chemical sedimentary, and fine- to coarse-grained epiclastic rocks. Immature volcaniclastic material is pyroclast rich, coarse to fine grained, and forms massive to finely laminated units from a metre to tens of metres thick (Fig. 12c). Pyroclastic components include curvilinear lithic and crystal fragments and chlorite-altered relict pumice and bubble wall shards originally derived from explosive volcanic eruptions (Fisher and Schmincke, 1984; Cas and Wright, 1987; McPhie et al., 1993; Fig. 12d). Laminated pyroclastic units have interspersed millimetre- to centimetre-thick chert and jaspilite layers, indicating that hydrothermal processes were taking place during times of quiescence when minimal detritus was being deposited (Fig. 21e). BIF up to 150 m thick caps the entire Glenview stratigraphy and forms much of the overlying stratigraphy assigned to the Wilgie Mia Formation, which is also host to the Weld Range iron ore deposits (Duuring and Hagemann, 2013). Coarse-grained epiclastic rocks include polymictic breccias, conglomerates, and redeposited hyaloclastites (Fig. 12b). Polymictic breccias are lithic rich and include broken and rounded crystal fragments, relict pumice, rounded felsic lava, and angular chert and jaspilite fragments. Conglomerates have well-rounded clasts commonly greater than 10 cm in diameter (e.g. Fig. 12a,b), indicative of high-energy deposition.

## Felsic volcanic geochemistry

### Golden Grove

The 29 assayed samples of volcanic rocks from Golden Grove mostly plot within the rhyodacite/dacite field on the volcanic discrimination diagram of Winchester and Floyd

(1977), supporting rock type classification made during core logging (Fig. 14).

Dacites and rhyodacites from the footwall, mineralized horizon, and lower hangingwall have Eu anomalies and heavy rare earth element (HREE) enrichment, and plot within the FIIIa and FII fields on a Y versus Zr/Y felsic fertility diagram. Dacites in the upper hangingwall have no Eu anomaly, are relatively depleted in HREE and plot within the low fertility FI field (Table 2; Figs 15–17).

All felsic volcanic rocks plot in the active continental margin (ACM) field on a Ta versus Th tectonic setting discrimination diagram (Fig. 19).

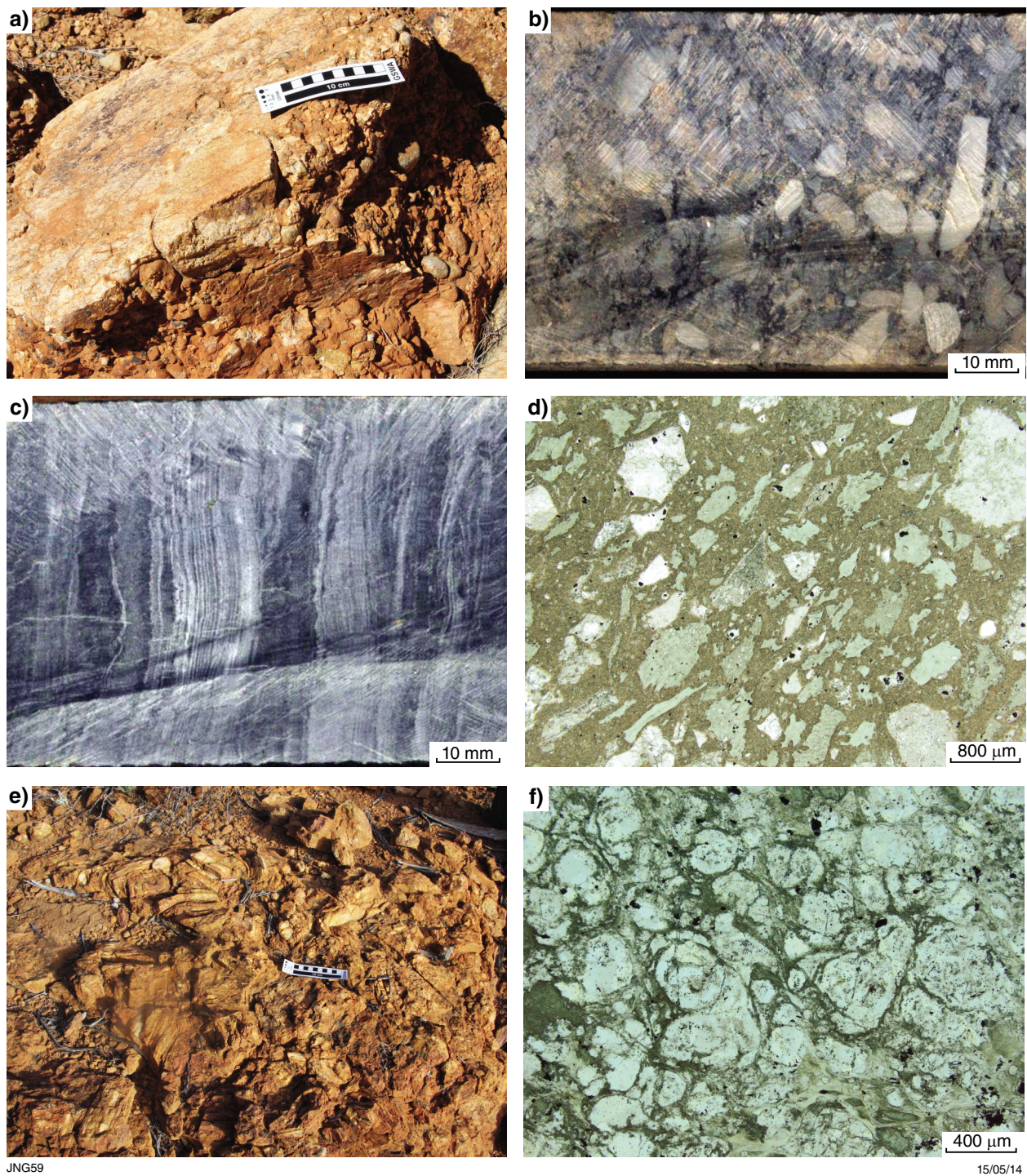
### Glenview

The 11 assayed samples of volcanic rocks from Glenview mostly plot within the upper section of the rhyodacite/dacite field on the volcanic discrimination diagram of Winchester and Floyd (1977), and match observations made during core logging (Fig. 14).

On a Y versus Zr/Y plot for felsic fertility, these rhyodacites and rhyodacitic hyaloclastites mostly fall within the FIIIa and FII zones associated with prospective Archean successions (Leshner et al., 1986; Lentz, 1998); three samples plot just to the left of the FII field (Fig. 15). Samples lying within the FII and FIIIa fields have Eu anomalies and HREE enrichment, whereas the other three samples, though also having Eu anomalies, are relatively depleted in REE (Fig. 18).

All felsic volcanic rocks plot in the ACM field on a Ta versus Th tectonic setting discrimination diagram (Fig. 19).





JNG59

15/05/14

**Figure 12.** Photographs of rocks from Glenview: a) Conglomerate with cobbles >10 cm in diameter. The cobbles are rounded, inferred to indicate erosion from wave or fluvial processes; b) conglomerate intersected in drillcore. Occurs at ~270 m in drillhole 95WGD002; c) drillcore image of finely laminated volcaniclastic unit intersected in several drillholes; d) plane-polarized light thin section photo of coarser section of the volcaniclastic unit showing inferred pyroclastic material; e) chaotic chert breccia in outcrop at Glenview; f) plane-polarized light thin section photo of apparent perlitic texture in felsic hyaloclastite intersected at Glenview, 95WGD004



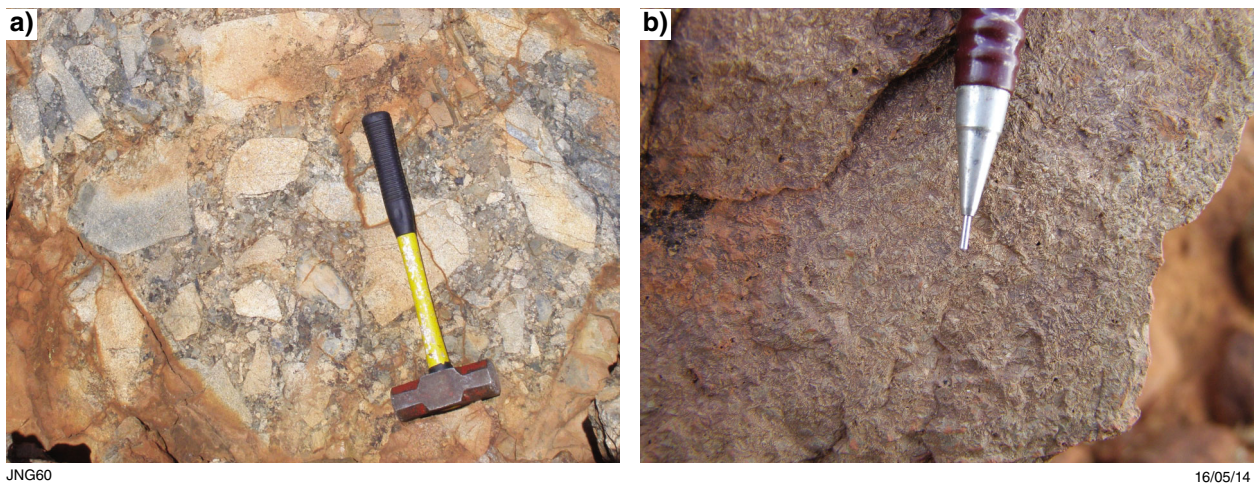


Figure 13. Photographs of rocks from the Weld Range: a) Outcrop of subaerial breccia to the northeast of the Glenview prospect. Hammer is ~1 m in length; b) outcrop of komatiitic basalt to the northeast of the Glenview prospect.

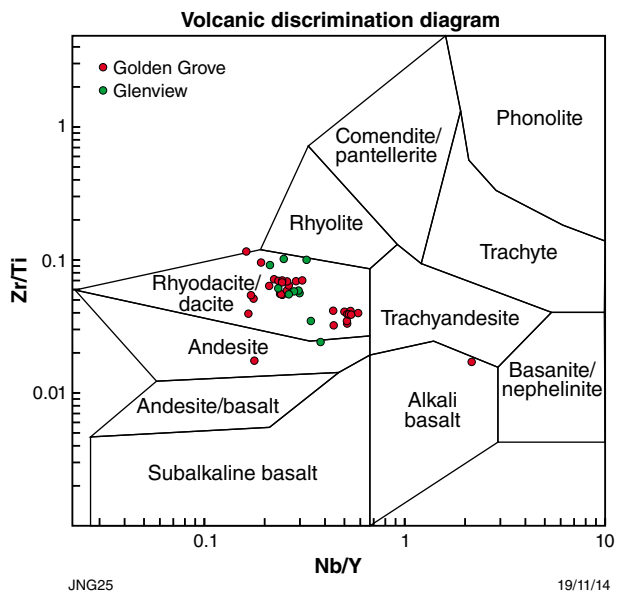


Figure 14. Volcanic discrimination diagram for felsic volcanic rocks from Golden Grove and Glenview (modified from Winchester and Floyd, 1977)

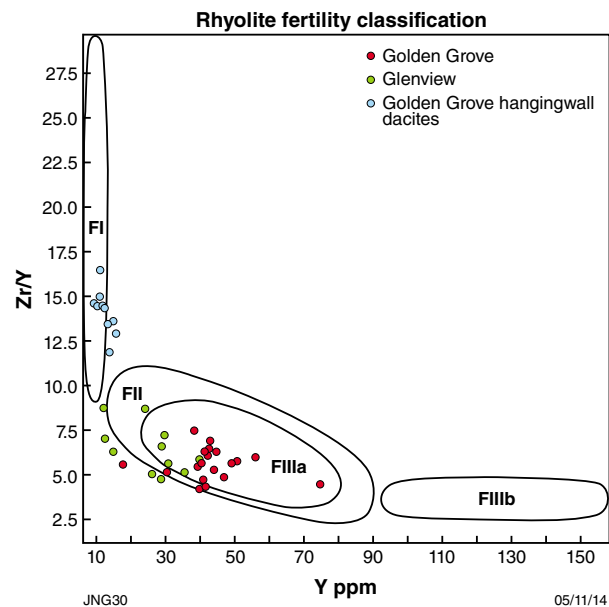


Figure 15. Felsic fertility plot diagram showing felsic volcanics from both the Weld Range and Golden Grove considered prospective for VMS mineralization. Fields from Lesher et al. (1986); see Table 2.

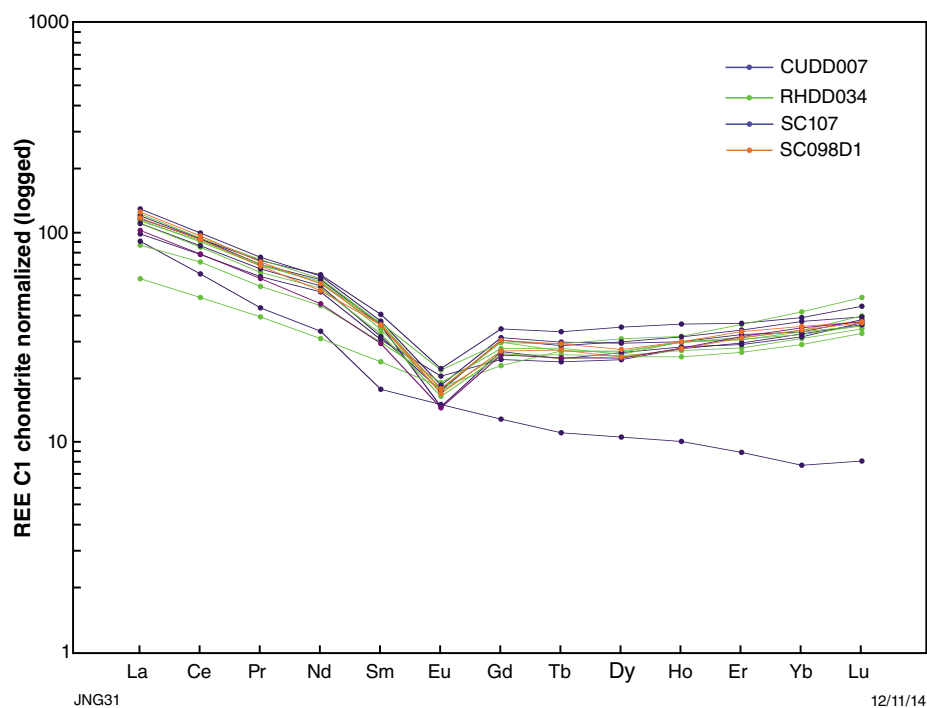


Figure 16. Chondrite-normalized REE spider diagram for footwall and mineralized horizon felsic volcanic rocks from Golden Grove (McDonough and Sun, 1995)

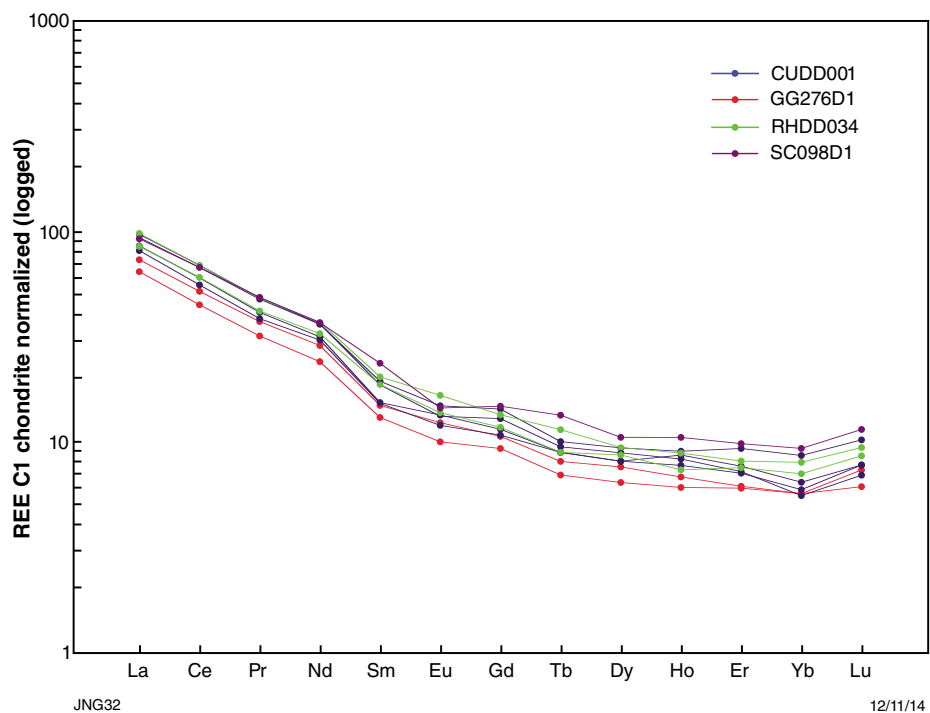


Figure 17. Chondrite-normalized REE spider diagram for hangingwall dacites from Golden Grove (McDonough and Sun, 1995)

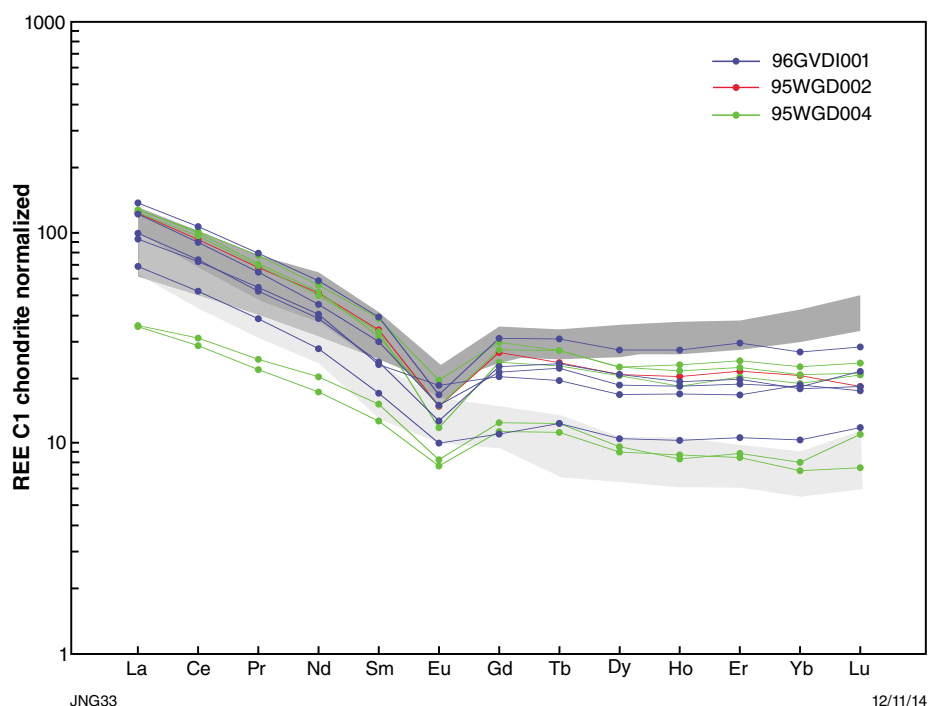


Figure 18. Chondrite-normalized REE spider diagram for felsic volcanic rocks from Glenview (McDonough and Sun, 1995). Note that the three lowest samples correspond to the three samples left of the FII zone in Figure 15.

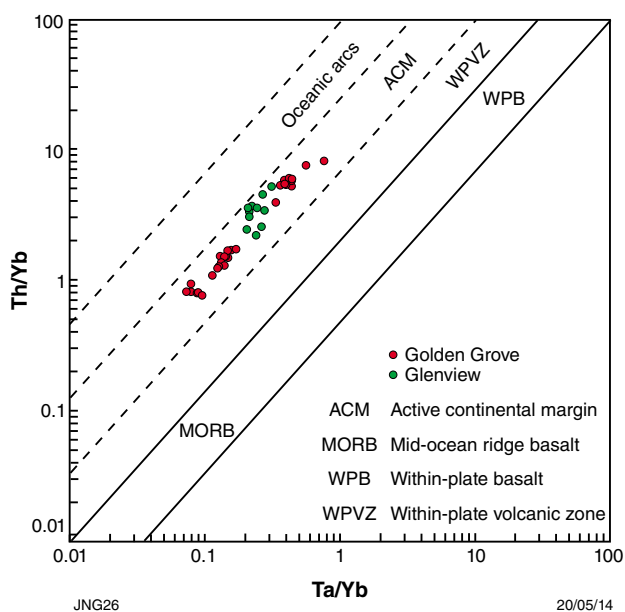


Figure 19. Tectonic setting discrimination diagram suggests that felsic volcanic rocks from both the Weld Range and Golden Grove formed in an active continental margin setting (modified from Schandl and Gorton, 2002).

## Sulfide mineralization

### Golden Grove

Sulfide mineralization at Golden Grove is well defined (Sharpe, 1999; Sharpe and Gemmell, 2001, 2002; Ashley et al., 1988), and is summarized here. Broadly stratabound, sheet-like bodies of massive sulfide mineralization are present in two distinct stratigraphic intervals, separated by a 150 m-thick volcanoclastic unit (Sharpe, 1999; Fig. 20). The lower mineralized zone is massive pyrite  $\pm$  chalcopyrite overlain by massive magnetite, contained within finely bedded, quartz-rich, tuffaceous sandstone and pebble breccia of the GG4 unit. The upper mineralized zone occurs in volcanoclastic sedimentary rocks and pebble breccias of the GG6 unit, and is characterized by massive pyrite  $\pm$  chalcopyrite overlain by, and interfingering with laterally continuous massive sphalerite (Fig. 20). Zinc mineralization is more abundant than Cu at Scuddles, in contrast to Gossan Hill where Cu is more abundant (Ashley et al., 1988).

### Glenview

Known mineralization at Glenview occurs primarily as sulfide veins; there is only minor massive sulfide. The bulk of sulfide mineralization intersected in drillcore occurs as pyrite-rich veins, with minor chalcopyrite, sphalerite and galena interstitial to subhedral-euhedral pyrite (Fig. 21a).



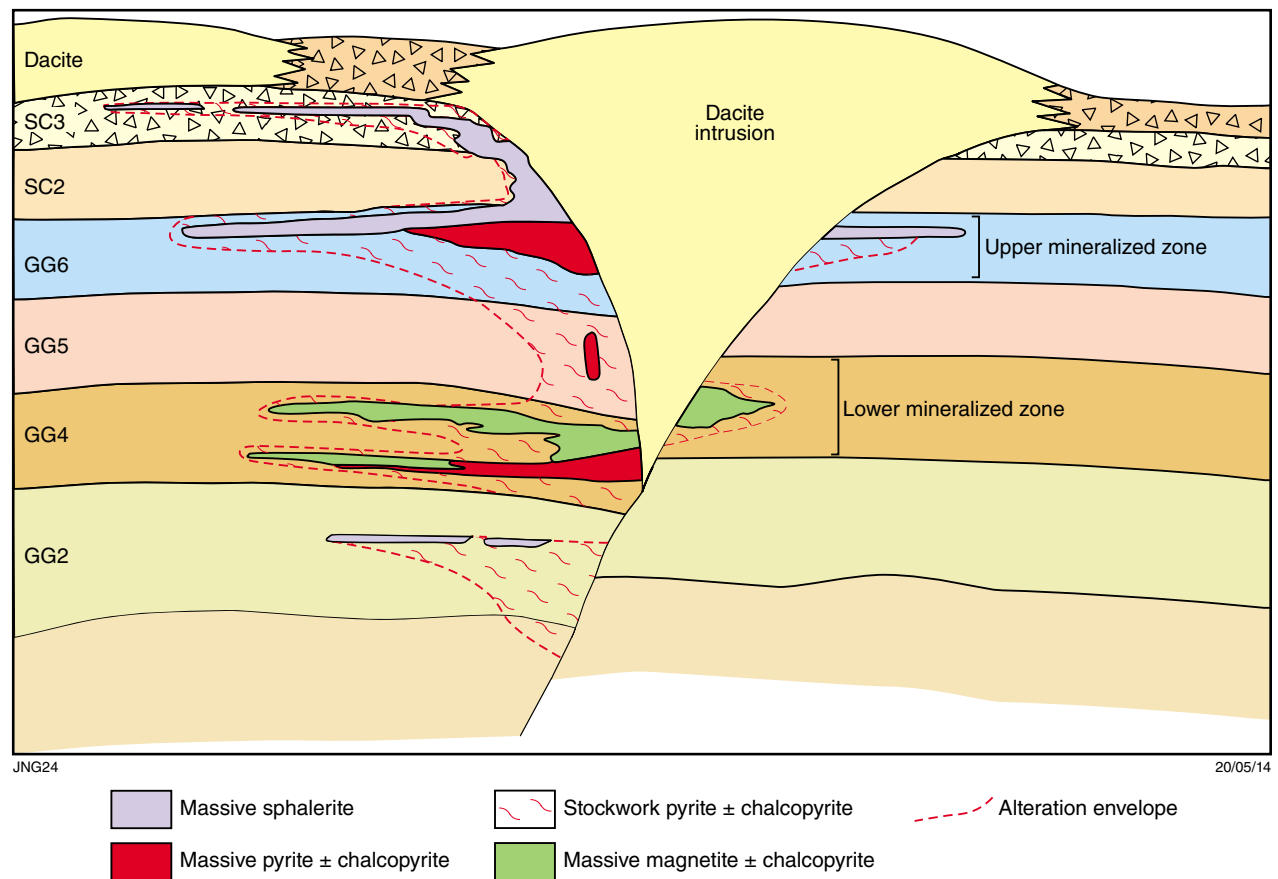


**Figure 20. Stylized cross-section of the Gossan Hill deposit showing individual units of the Scuddles and Golden Grove Formations, as defined by Clifford (1992). Modified from Sharpe, (1999). GG = Golden Grove; SC = Scuddles**

Zinc-dominant mineralization was intersected in three of the studied holes (95WGD002; 95WGD006; 96GVDI001) as sphalerite veins. Mineralization intersected in 95WGD004 is copper rich, occurring as chalcopyrite and pyrite in veins and as massive sulfides (Fig. 21d). Sphalerite-rich stringer veins are typically flanked by fibrous sericite and minor platy chlorite. The sphalerite is overprinted by anhedral chalcopyrite grains, and galena overprints both sphalerite and chalcopyrite, giving timing relationships of sphalerite → chalcopyrite → galena. Vein-hosted and massive chalcopyrite is typically overprinted by accessory anhedral to euhedral grains of pyrite, and is also associated with intense, massive and platy chlorite (Fig 21b,c).

Sericite and chlorite alteration form haloes to mineralization in all studied drillcore. The predominance of chlorite or sericite around sulfide mineralization depends on the sulfides present. Chlorite is associated with all significant sulfide accumulations and tends to be closer to sulfide mineralization than sericite. Chlorite occurs as both massive accumulations in the groundmass proximal to sulfide mineralization and as platy-textured rims to sulfide veins. Sericite occurs more commonly as fibrous accumulations along the margin of sphalerite-rich veins. Sericite is also more pervasive throughout the rock package than chlorite.

## Geochronology

Twenty-one zircons from a metarhyolite sample collected from a large, well-exposed outcrop on the northern side of the Weld Range, yielded a pooled magmatic crystallization age of  $2977 \pm 3$  Ma (Fig. 22a; Wingate et al., 2013b). One analysis that was more than 5% discordant was considered unreliable and not geologically significant. The remaining 20 analyses are divided on the basis of  $^{207}\text{Pb}^*/^{206}\text{Pb}^*$  ratios into Group I of 19 analyses that yielded the magmatic crystallization age, and one analysis that yielded a  $^{207}\text{Pb}^*/^{206}\text{Pb}^*$  date of  $2960 \pm 6$  Ma, interpreted by Wingate et al. (2013b) to reflect minor ancient loss of radiogenic Pb.

Another 21 zircons were analysed from a sample of a felsic volcanoclastic metasandstone collected from a low outcrop on the southern side of the Weld Range (Fig. 22b). Four zircon analyses were more than 5% discordant and considered unreliable by Wingate et al. (2013a). The remaining 17 analyses were divided on the basis of  $^{207}\text{Pb}^*/^{206}\text{Pb}^*$  ratios into Group Y comprising a single analysis yielding a  $^{207}\text{Pb}^*/^{206}\text{Pb}^*$  age of  $2729 \pm 9$  Ma, and Group S comprising 16 analyses yielding  $^{207}\text{Pb}^*/^{206}\text{Pb}^*$  ages between 2968 and 2735 Ma. It was considered that a weighted mean  $^{207}\text{Pb}^*/^{206}\text{Pb}^*$  age of  $2747 \pm 4$  Ma for the 17 analyses from the combined Y and S groups to be the most conservative estimate of maximum depositional age (Wingate et al., 2013a).



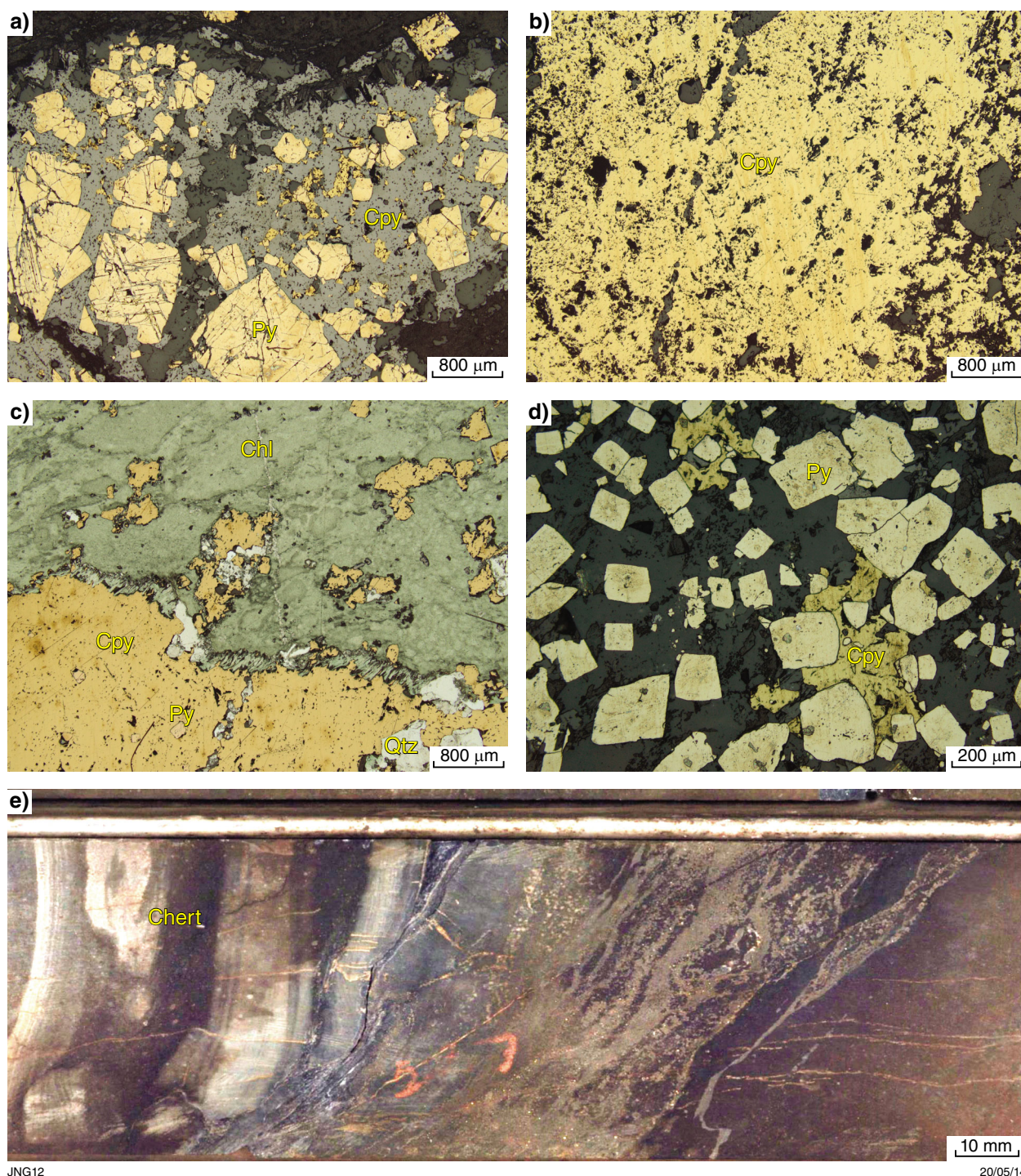


**Figure 21.** Plane-polarized reflected light photomicrographs of mineralization intersected in drillcore from Glenview: a) Euhedral to subhedral pyrite with interstitial sphalerite and minor chalcopyrite, 95WGD002; b) massive chalcopyrite with small occurrences of sphalerite, 95WGD002; c) intense chlorite alteration rimming massive chalcopyrite with minor pyrite, 95WGD002; d) euhedral to anhedral pyrite grains with interstitial chalcopyrite, 95WGD004; e) photograph of chert layers interspersed with sulfide stringers, 95WGD002.

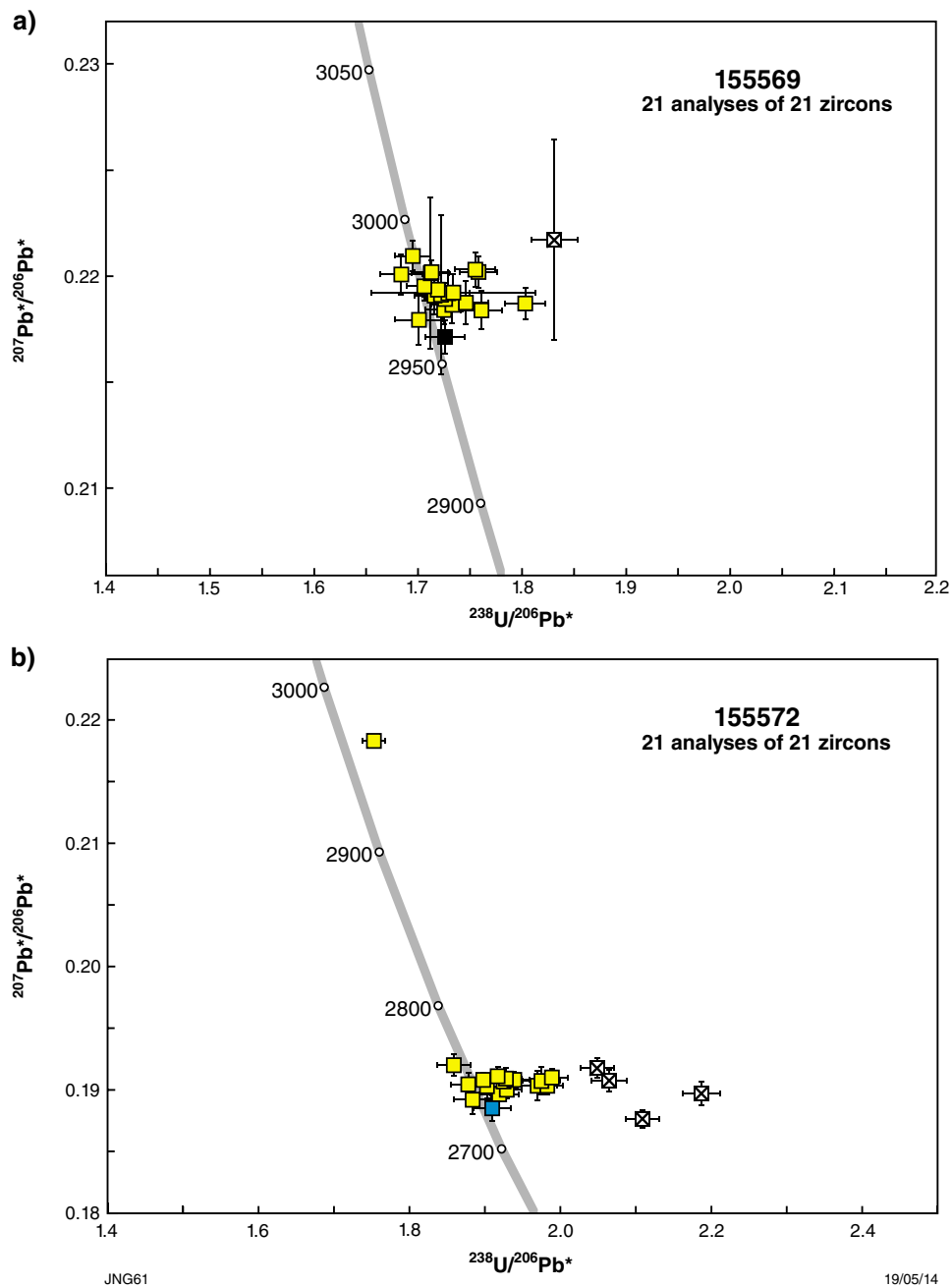


**Figure 22.** a) U–Pb analytical data for zircons from sample 155569: metarhyolite, Weld Range. Yellow squares indicate Group I (magmatic zircons); black square indicates Group P (radiogenic-Pb loss); crossed square indicates Group D (discordance >5%), from Wingate et al. (2013b); b) U–Pb analytical data for zircons from sample 155572: felsic volcanoclastic metasandstone, Weld Range. Blue square indicates Group Y (youngest detrital zircon); yellow squares indicate Group S (older detrital zircons); crossed square indicates Group D (discordance >5%), from Wingate et al. (2013a).



## Alteration mineralogy

### Golden Grove

Hyperspectral data for the six drillholes from Golden Grove indicate the predominance of white mica, chlorite, quartz, and feldspar with minor amounts of ankerite, calcite, dolomite, gypsum, siderite, montmorillonite, biotite, phlogopite, epidote, hornblende, actinolite, tourmaline, and other mineral species (Figs 23–28, Appendix 3a–f). Of those minerals that were detected in SWIR, only white mica and chlorite show a systematic association with sulfide mineralization and were therefore chosen as a focus for this study. Sharpe (1999) documented carbonate and talc gangue phases in the lower mineralized zone at Gossan Hill, occurring with massive magnetite and sulfide mineralization in conjunction with intense chlorite alteration, but both were only detected in TIR and have no discernible chemical variation, and are not considered further. TIR is useful for showing feldspar alteration in drillholes at Golden Grove. In GG274 (Appendix 3b), feldspars are present in the upper hangingwall and in dacite and rhyolite intrusions, but are absent proximal to mineralization apart from in the late intrusions, indicating the breakdown of feldspar in the footwall and mineralized zone. However, TIR data needs to be used with caution. In 96GVDI001, amphiboles are shown to occur in a fine-grained volcanoclastic unit, but none were found using SWIR or thin-section analysis (Appendix 3j, 210–270 m).

### White mica

The TSA routine within TSG automatically interprets white mica, in part, by recognizing the diagnostic AIOH absorption feature ~2200 nm (Fig. 10a). White micas are interpreted to be paragonite or muscovite based on the wavelength that the AIOH absorption feature occurs, with shorter wavelengths (<2195 nm) indicating paragonite and longer wavelengths (>2195 nm) muscovite. SEM analyses of selected white mica samples show that all white micas tested from Golden Grove are muscovite, and that paragonite has higher Al and lower Fe and Mg relative to muscovite (Appendix 2). There are systematic variations in mineral identity and spectral feature wavelengths in relation to mineralization at Golden Grove, which differ between the Scuddles and Gossan Hill deposits.

At Gossan Hill, white mica is abundant in all drillholes within and flanking mineralization (CUDD001, GG274, GG276D1, RHDD034; Fig. 7), and shows a clear change in composition with distance from sulfide mineralization (Figs 23–26).

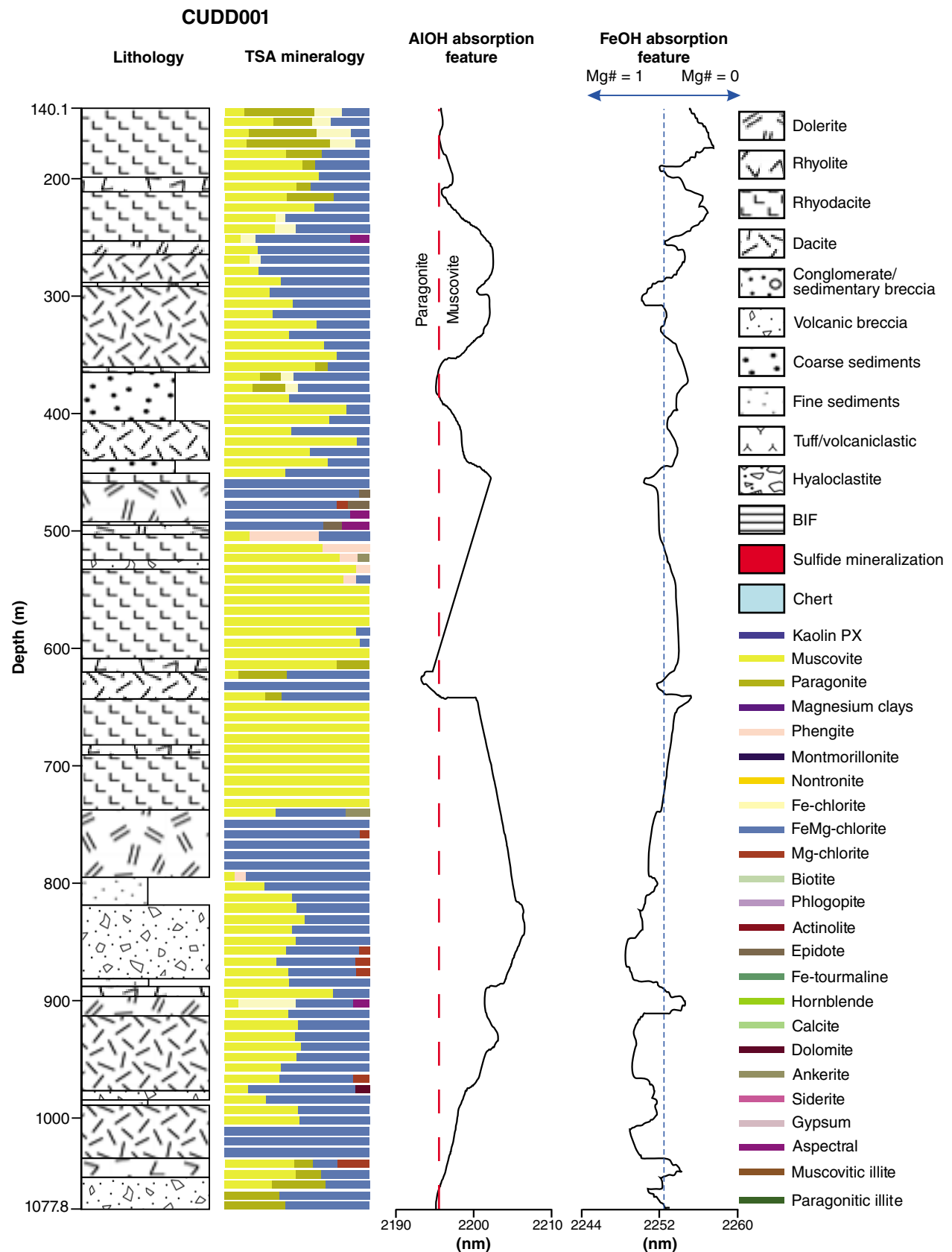
In the two non-mineralized holes flanking Gossan Hill, white mica composition is variable and shows some association with rock type. In CUDD001 (Fig. 23), white mica is present through most of the sequence, is dominantly muscovite, and is particularly prominent in rhyodacites. Small amounts of paragonite and phengite

are present in CUDD001 and display no distinct pattern or association (Fig. 23, 29). The variation in white mica composition is reflected in the AIOH absorption feature, which shows significant wavelength variation, ranging between 2193 and 2205.8 nm (Fig. 30a). The predominance of muscovite is also reflected with wavelength averages above 2200 nm for the hangingwall and mineralized zone, and ~2198 nm in the footwall (Fig. 31).

White mica in RHDD034 is predominantly paragonite in the footwall, the lower part of the mineralized unit and in parts of the hangingwall. Muscovite is the dominant white mica species in the upper section of the mineralized unit and throughout the bulk of the hangingwall, where it is associated with volcanic rocks. The AIOH absorption feature averages 2196 nm in the hangingwall and mineralized zone where muscovite is most dominant, and 2194 nm in the paragonite-rich footwall (Fig. 31). The AIOH absorption feature is much less variable in RHDD034 than in CUDD001, ranging between 2191.4 and 2197.3 nm (Fig. 30d).

In the mineralized hole GG274, white mica in the hangingwall is a varied mix of paragonite and muscovite well away from sulfides, but is predominantly paragonite (>50%) within 120 m of the mineralized zone (Fig. 29). Small amounts of muscovite are present immediately below the mineralized horizon for ~50 m into the footwall. White mica is absent between 50 and 100 m below mineralization, and paragonite makes up about 50% of the rock to the end of the hole (Fig. 24). In GG276D1 white mica is present in the bulk of the hangingwall. This mica is muscovite in the distal hangingwall. Paragonite appears within 80 m above mineralization, and within 30 m of the mineralized zone is the dominant white mica mineral (Fig. 29). White mica is also prominent in the upper 100 m of the footwall, decreasing in abundance downhole. This mica is a variable mix of paragonite and muscovite in the upper 50 m of the footwall, and predominantly muscovite in the lower 50 m (Fig. 25). The predominance of paragonite in these mineralized holes is reflected by the AIOH absorption feature occurring at shorter wavelengths (~5 nm in the footwall and hangingwall; ~10 nm in the mineralized zone; Fig. 31) and being significantly less variable (2191.8 – 2196.9 nm for GG274; 2192.7 – 2199.2 nm for GG276D1; Fig. 30b, c) compared to the non-mineralized CUDD001 hole (Fig. 30a, 31).

At Scuddles, white mica in drillcore from SCO98D1 and SC107 is predominantly muscovite and shows no systematic variation in composition with respect to sulfide mineralization, and is much less abundant than at Gossan Hill (Figs 27 and 28). The wavelengths of the AIOH feature for white mica in SCO98D1 and SC107 ranged between 2194.4 and 2202.8 nm, and 2194.4 and 2200.1 nm, respectively. On average, these are slightly higher (by 1–5 nm) than for those in holes GG274, GG276D1, and RHDD034, but show a similar low degree of variability and are significantly lower and less variable than in CUDD001 (Figs 30a,e,f and 31).



JNG44

18/11/14

**Figure 23.** Graphic log of Golden Grove drillhole CUDD001 showing lithology, TSG predicted mineral species, change in the wavelength intersection of the AIOH absorption feature, and change in the wavelength intersection of the FeOH absorption feature. Dashed red line indicates predicted wavelength where change from muscovite to paragonite occurs. Dashed blue line corresponds with middle value between Mg# = 1 (Mg-chlorite) and Mg# = 0 (Fe-chlorite). Note that aspectral is usually associated with sulfide occurrence.



19/11/14

**Figure 24.** Graphic log of Golden Grove drillhole GG274 showing lithology, TSG predicted mineral species, change in the wavelength intersection of the AIOH absorption feature, and change in the wavelength intersection of the FeOH absorption feature. Dashed red line indicates predicted wavelength where change from muscovite to paragonite occurs. Dashed blue line corresponds with middle value between  $Mg\# = 1$  (100% Mg-chlorite) and  $Mg\# = 0$  (100% Fe-chlorite). Note that spectral is usually associated with sulfide occurrence.

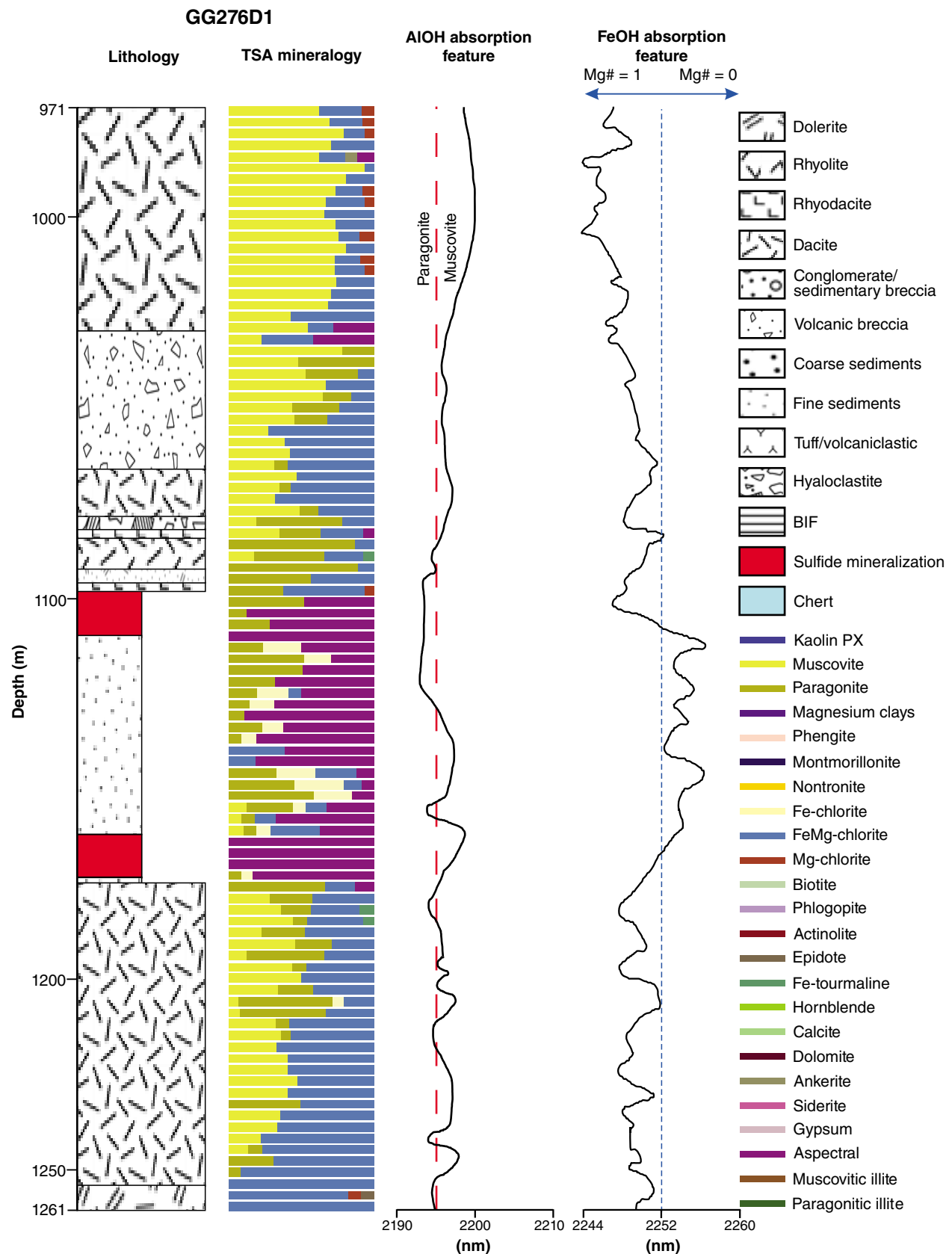
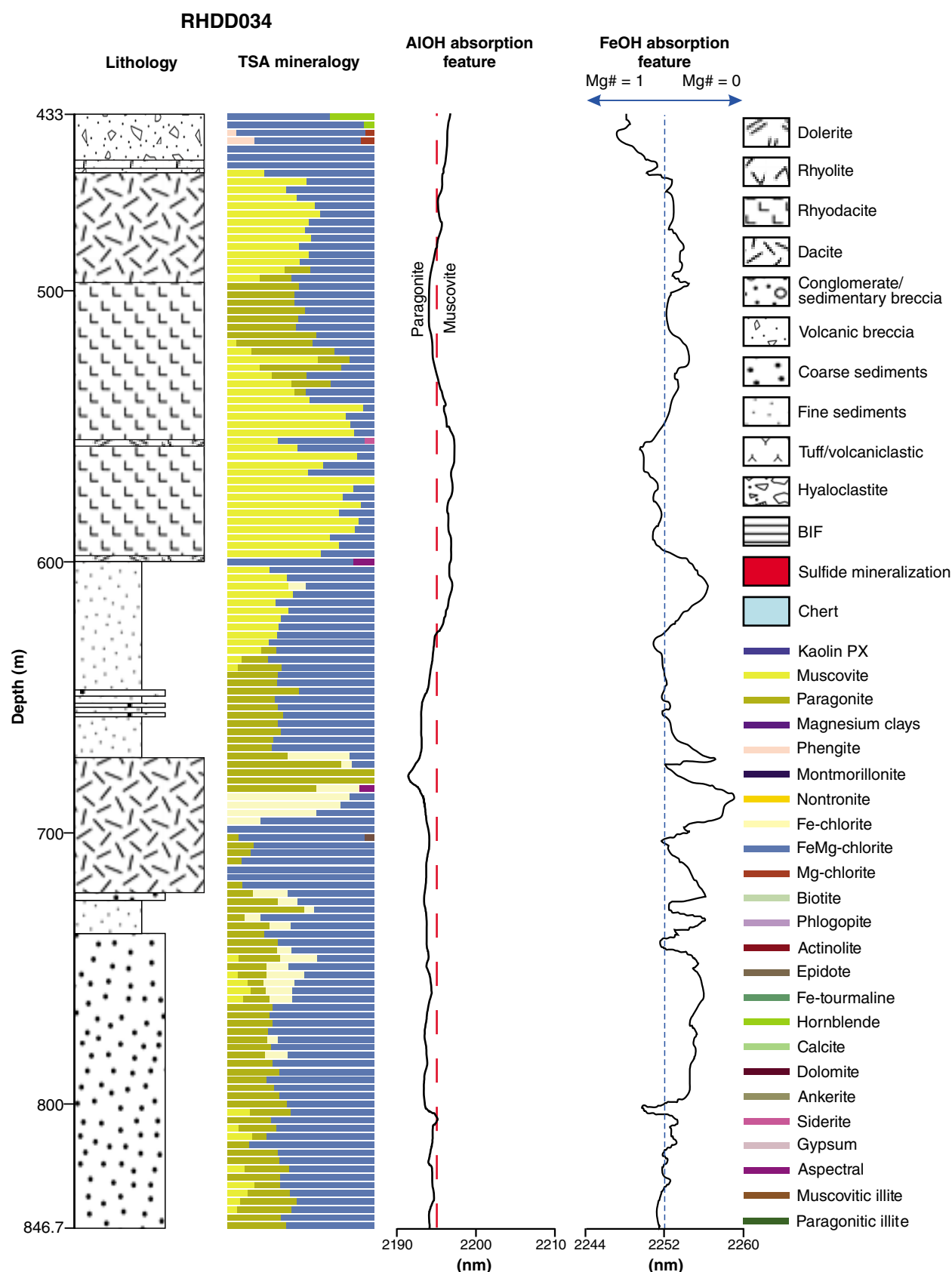


**Figure 25.** Graphic log of Golden Grove drillhole GG276D1 showing lithology, TSG predicted mineral species, change in the wavelength intersection of the AIOH absorption feature, and change in the wavelength intersection of the FeOH absorption feature. Dashed red line indicates predicted wavelength where change from muscovite to paragonite occurs. Dashed blue line corresponds with middle value between Mg# = 1 (Mg-chlorite) and Mg# = 0 (Fe-chlorite). Note that aspectral is usually associated with sulfide occurrence.

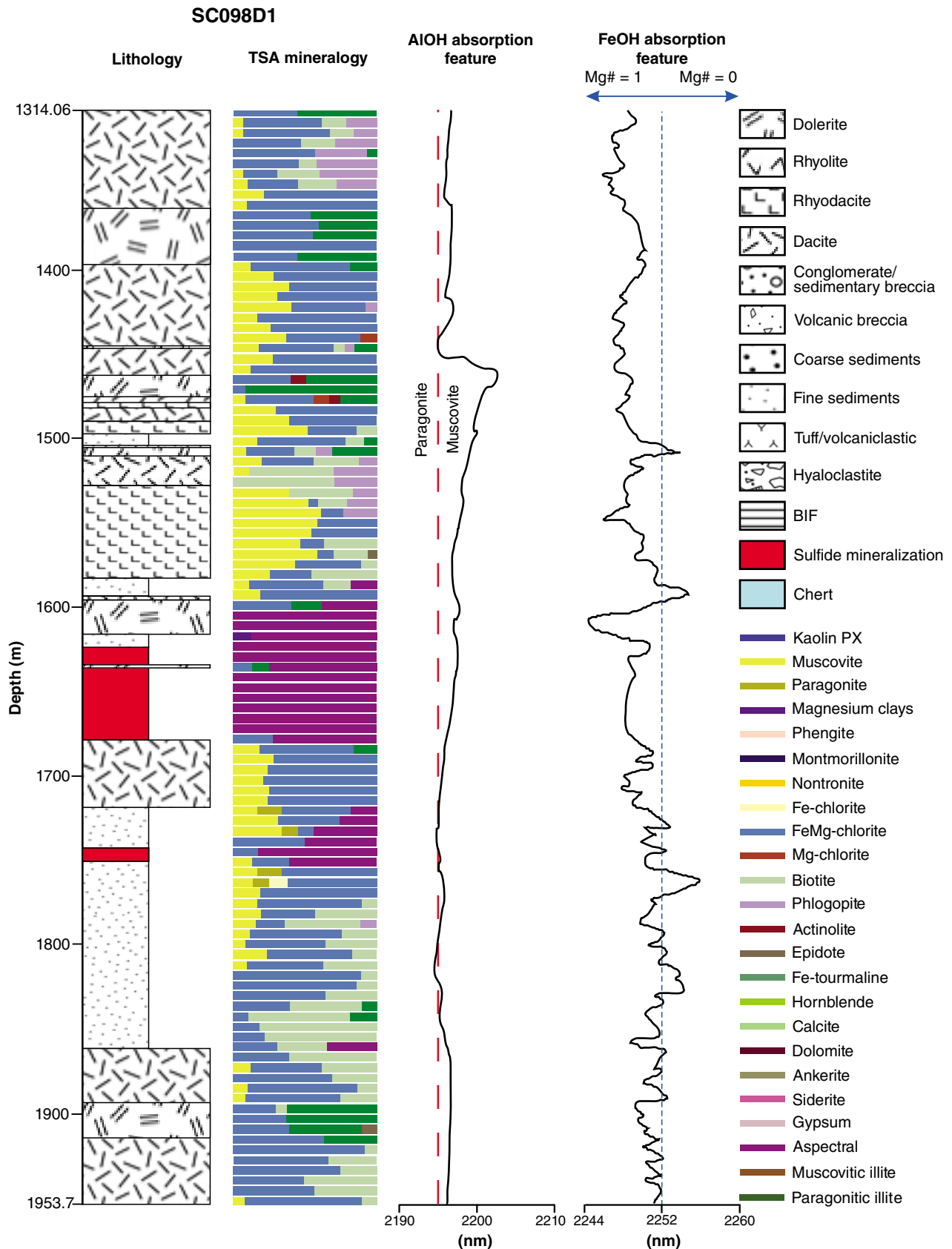




JNG42

12/11/14

**Figure 26.** Graphic log of Golden Grove drillhole RHDD034 showing lithology, TSG predicted mineral species, change in the wavelength intersection of the AIOH absorption feature, and change in the wavelength intersection of the FeOH absorption feature. Dashed red line indicates predicted wavelength where change from muscovite to paragonite occurs. Dashed blue line corresponds with middle value between Mg# = 1 (Mg-chlorite) and Mg# = 0 (Fe-chlorite). Note that aspectral is usually associated with sulfide occurrence.



JNG47

12/11/14

**Figure 27.** Graphic log of Golden Grove drillhole SC098D1 showing lithology, TSG predicted mineral species, change in the wavelength intersection of the AIOH absorption feature, and change in the wavelength intersection of the FeOH absorption feature. Dashed red line indicates predicted wavelength where change from muscovite to paragonite occurs. Dashed blue line corresponds with middle value between Mg# = 1 (Mg-chlorite) and Mg# = 0 (Fe-chlorite). Note that aspectral is usually associated with sulfide occurrence.

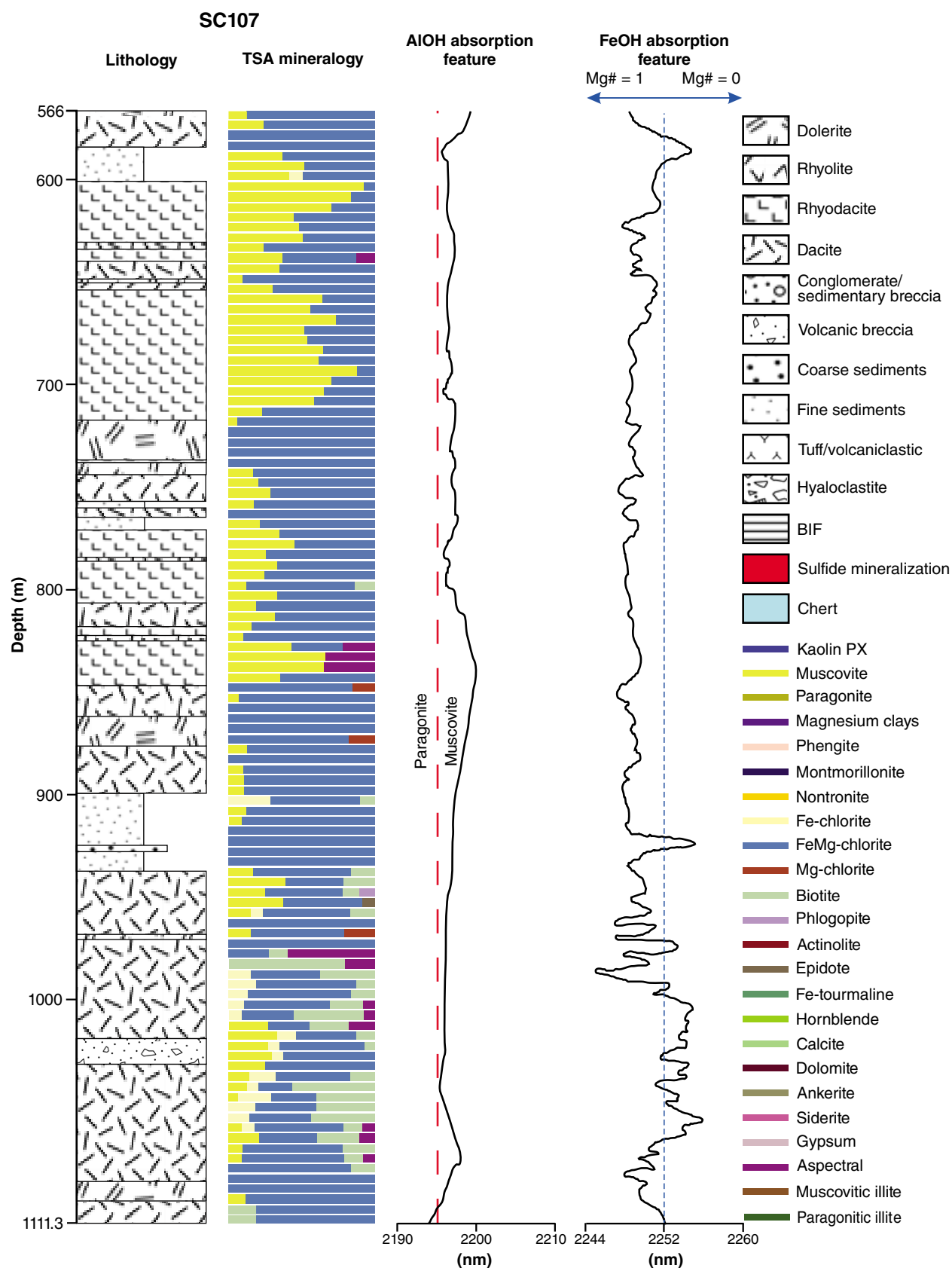


**Figure 28.** Graphic log of Golden Grove drillhole SC107 showing lithology, TSG predicted mineral species, change in the wavelength intersection of the AIOH absorption feature, and change in the wavelength intersection of the FeOH absorption feature. Dashed red line indicates predicted wavelength where change from muscovite to paragonite occurs. Dashed blue line corresponds with middle value between Mg# = 1 (Mg-chlorite) and Mg# = 0 (Fe-chlorite). Note that aspectral is usually associated with sulfide occurrence.

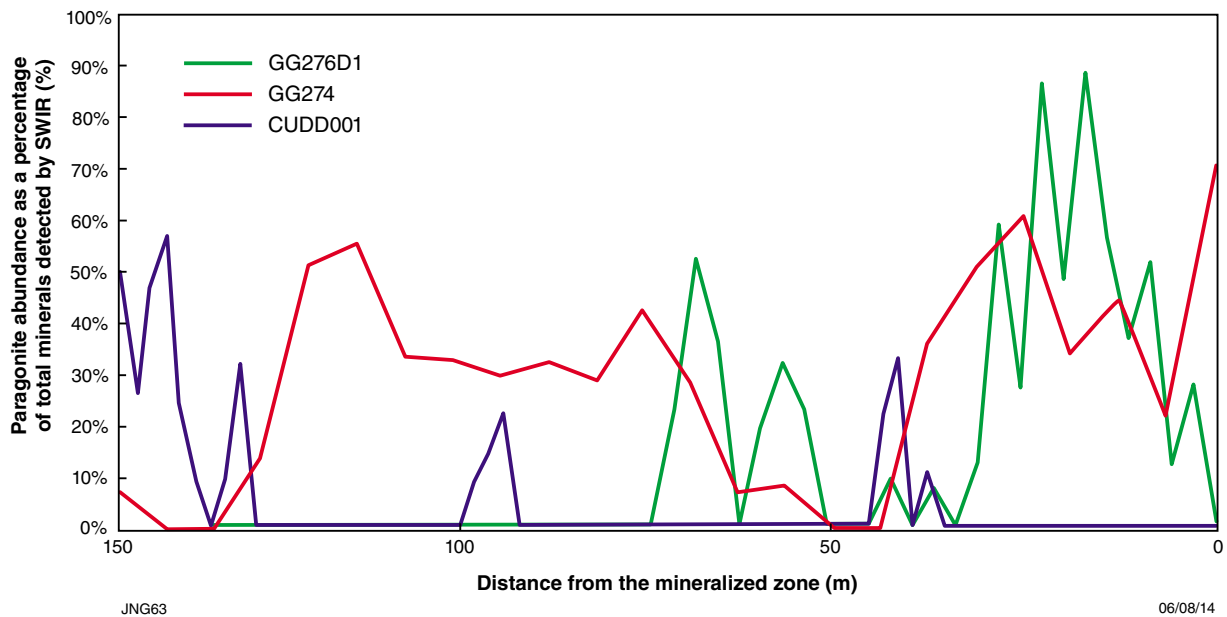


Figure 29. Change in paragonite abundance with increasing proximity to sulfide mineralization

### Chlorite

TSA interprets chlorites to be Fe rich or Mg rich based on the wavelength of the FeOH absorption feature at ~2250 nm, with shorter wavelengths being more Mg rich and longer wavelengths more Fe rich (Fig. 10b). SEM analyses of selected chlorite samples show that TSA is accurate at depicting these changes in Fe and Mg abundance, with Fe content in samples where Fe-chlorite was interpreted being around 8% higher than in samples identified as FeMg-chlorite (Appendix 2). No Mg-rich samples were tested by SEM as appropriate thin sections were not available. Chlorite is abundant in the six drillholes at Golden Grove, but shows a systematic variation with proximity to sulfide mineralization.

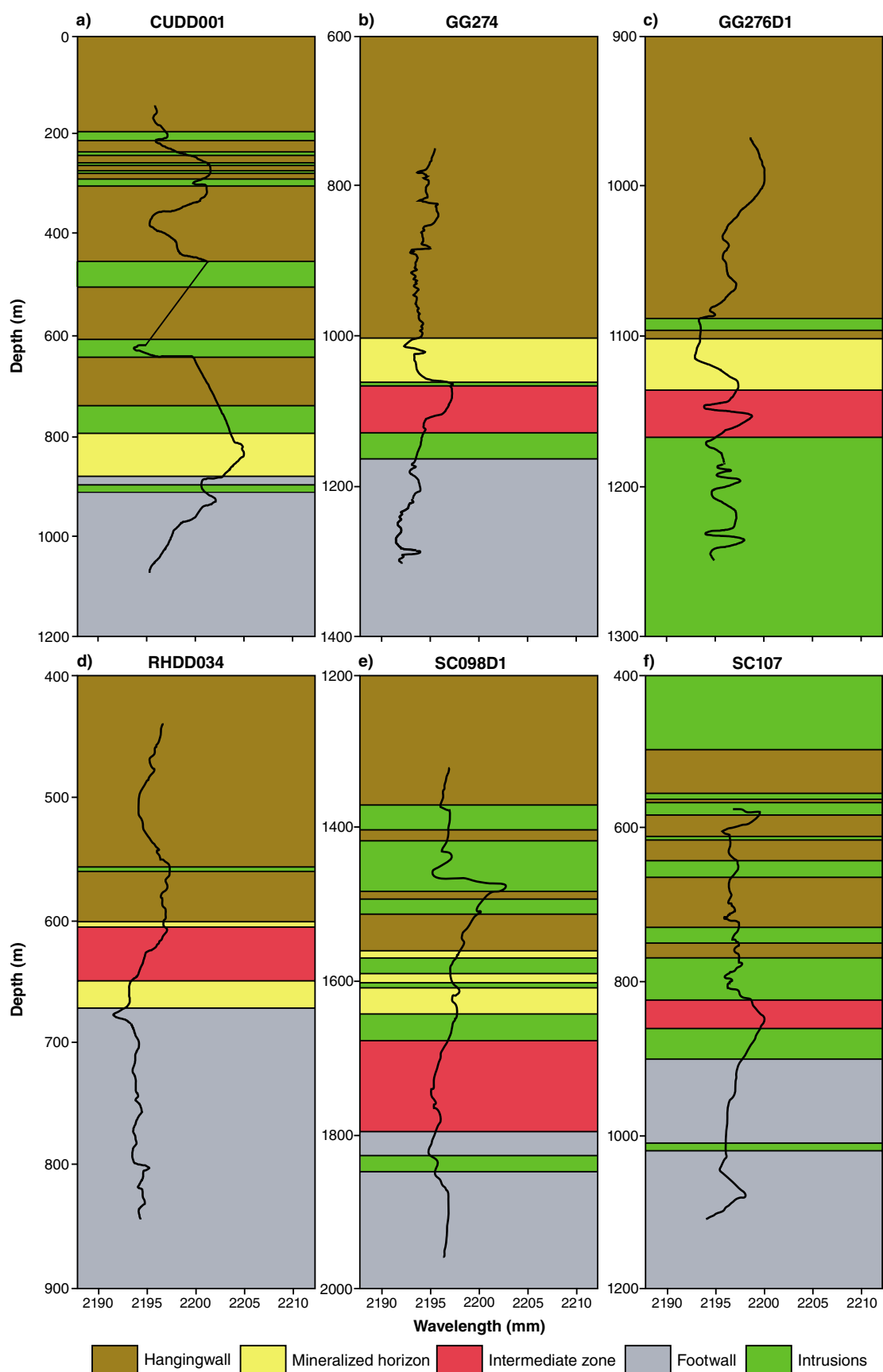
CUDD001 has large areas of FeMg-chlorite, and only minor Fe-chlorite associated with paragonite in the hangingwall (Fig. 23). The FeOH absorption feature, though variable, generally shifts to shorter wavelengths towards the mineralized zone (Fig. 32a). There is no marked change at the contact between the hangingwall and the mineralized zone, but there is a significant ~7 nm shift in the immediate footwall to the mineralized zone (Fig. 32a). Average wavelengths are highest in the hangingwall and decrease by about 3 nm in the mineralized zone and footwall (Fig. 33).

Chlorites in the two mineralized holes at Gossan Hill (GG274 and GG276D1) are predominantly FeMg-chlorite, but Fe-chlorite is directly associated with the mineralized

zone. Both varieties show a dramatic increase in wavelength of the FeOH absorption feature passing from the hangingwall into the mineralized zone, thence a gradual decrease in wavelength into the footwall, punctuated by dramatic decreases in wavelength within intrusions in the footwall (Fig. 32b,c). Overall, the average wavelengths of the FeOH absorption feature are about 4 nm higher in the mineralized zone and footwall, and 2–3 nm lower in the hangingwall, compared to CUDD001 (Fig. 33).

In RHDD034, FeMg-chlorite is present through the entire hole, but there are also moderate amounts of Fe-chlorite in the footwall (Fig. 26). The FeOH response in RHDD034 is similar to the mineralized holes at Gossan Hill, although was not as well defined (Fig. 32d), and the average wavelength in the footwall is about 2 nm shorter (Fig. 33c).

Chlorite in the two drillholes at Scuddles (SC098D1 and SC107) is largely FeMg-chlorite, but SC107 locally has moderate amounts of Fe-chlorite in the footwall (Fig. 28), and SC098D1 has very minor Fe-chlorite associated with the lower mineralized zone (Fig. 27). Both chlorite varieties have similar average wavelengths for the FeOH absorption feature, that are generally shorter than for chlorites in mineralized holes at Gossan Hill (Fig. 33), but there is no significant change in wavelength between the mineralized zone and the footwall and hangingwall in SC098D1 (Fig. 32e).



JNG62

05/11/14

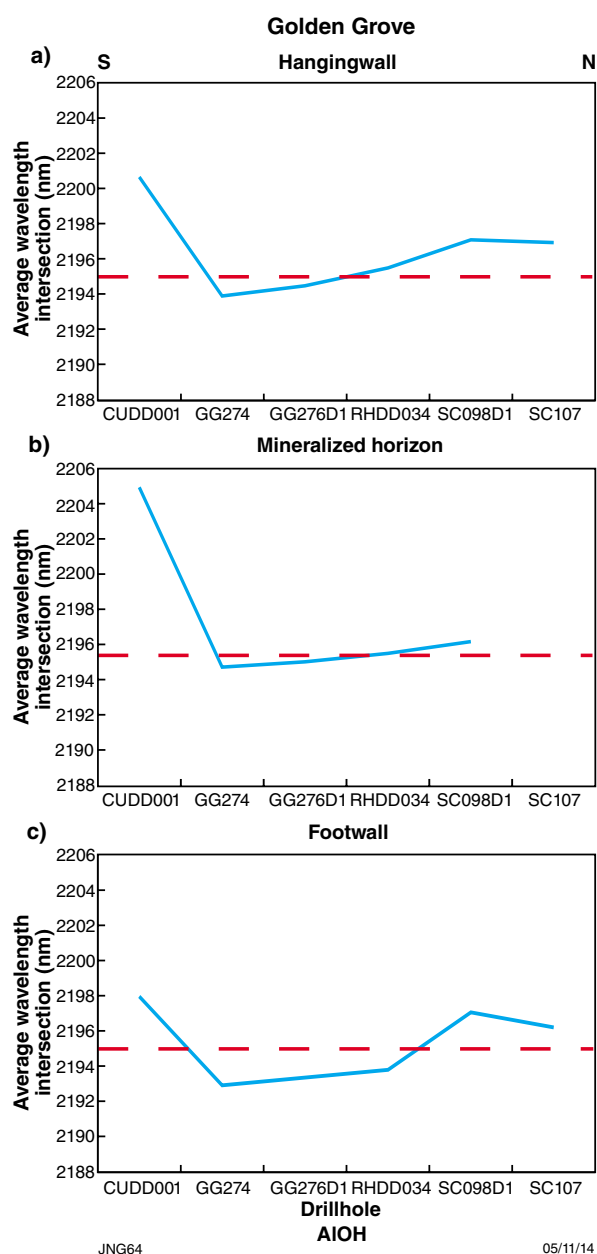


**Figure 31. Change in the intersection of the AIOH absorption feature between drillholes at Golden Grove. Results were averaged for the entire hole to give a representation of the change. The dashed red line indicates the change from muscovite to paragonite.**

## Glenview

Hyperspectral data for the four drillholes at Glenview indicate the predominance of white mica, chlorite, quartz and feldspar, with minor kaolinite, montmorillonite, nontronite, illite, hornblende, calcite, dolomite, ankerite, siderite, gypsum, phlogopite, biotite and other mineral species (Figs 34–37; Appendix 3g–j). As at Golden Grove, only white mica and chlorite showed a systematic relationship with sulfide mineralization and are therefore only considered here. SEM analyses done on selected samples showed that white micas are all muscovite; paragonite has relatively higher Al and lower Fe and Mg relative to muscovite, and little to no Na. Glenview muscovites have higher abundances of Al than those from Golden Grove (Appendix 2). Fe-chlorite has a higher Fe content compared to FeMg-chlorite. No Mg-rich samples were tested by SEM because no appropriate samples were available.

### White mica

There is a general trend in white mica composition from muscovite/phengite in the west to paragonite in the east (Figs 34–37). White mica in the far western hole (95WGD006) is abundant, and changes sharply at about 130 m from paragonite in the upper part of the hole to muscovite and muscovitic illite with minor phengite in the lower 40 m (Fig. 34). Paragonite is absent from the next drillhole to the east (95WGD002). White micas below the BIF unit are predominantly muscovite and muscovitic illite, with minor phengite (Fig. 35). Further east still, in hole 95WGD004, paragonite is present throughout, and is mixed with muscovite in the middle part of the hole, where the rock sequence is dominated by finely laminated volcanoclastic material (Fig. 36). White mica in the easternmost hole (96GVDI001) is almost entirely paragonite, with muscovite only evident in the uppermost part of the hole (Fig. 37).

The AIOH feature varies considerably in the westernmost holes, ranging 2192–2207 nm for 95WGD006, and 2197–2207 nm for 95WGD002 (Figs 34 and 35). Much of the variability appears to relate to changes in rock type. For both these holes, the average wavelength of the AIOH absorption feature is 2201 nm, with a slight decrease eastwards (Fig. 38a). By contrast, the wavelength of the AIOH absorption feature in the eastern holes (95WGD004 and 96GVDI001) varies by less than 5 nm over the entire length of the drillhole, shows no distinct variation with changes in rock type (Figs 36 and 37), and is significantly shorter, averaging 2194 nm for 95WGD004, and 2193 nm for 96GVDI001 (Fig. 38a).

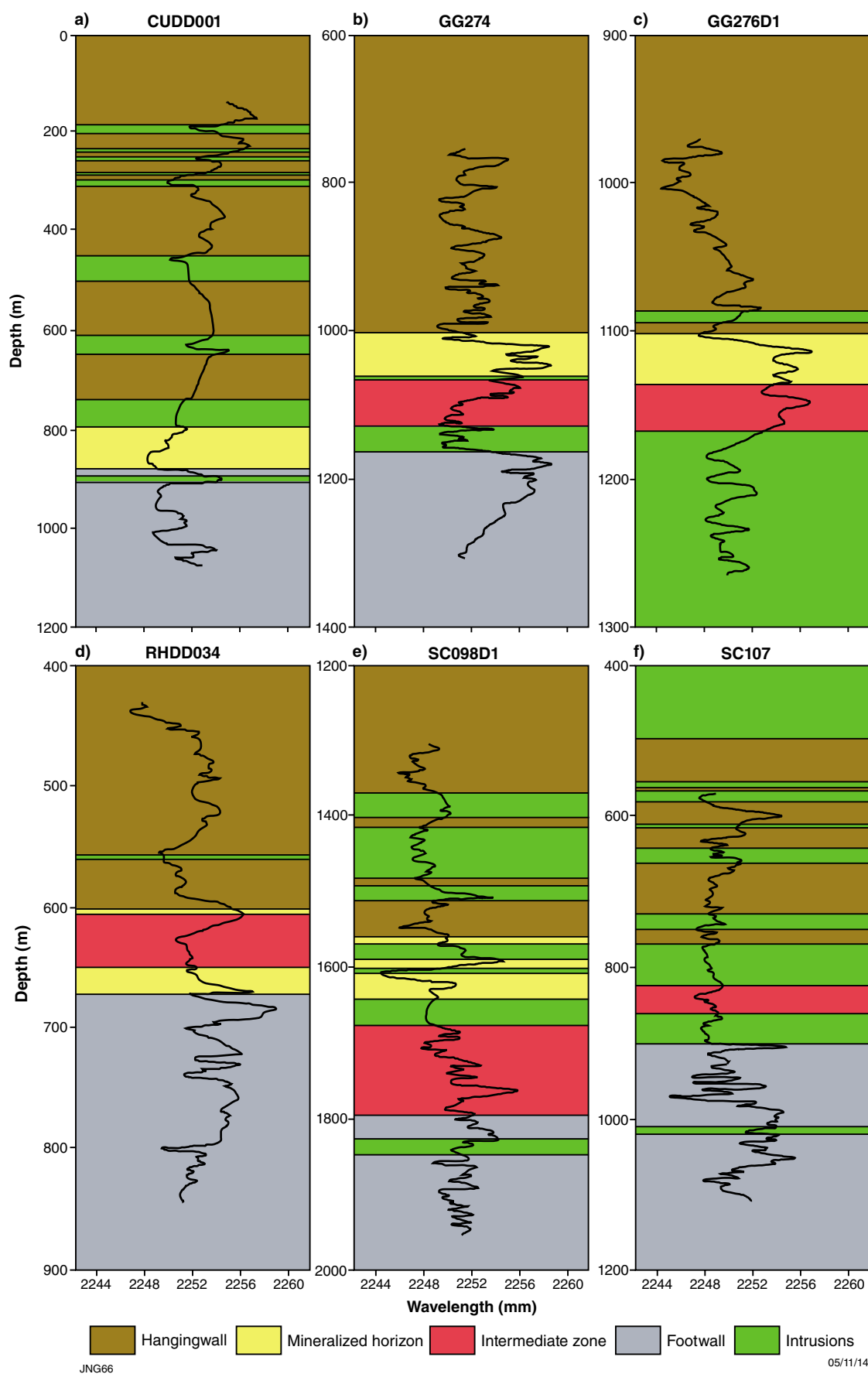


**Figure 32. Downhole variation in the wavelength intersection of the FeOH absorption feature related to chlorite. Drillholes are from Golden Grove and are divided into hangingwall, mineralized horizon, intermediate zone, footwall, and intrusions.**



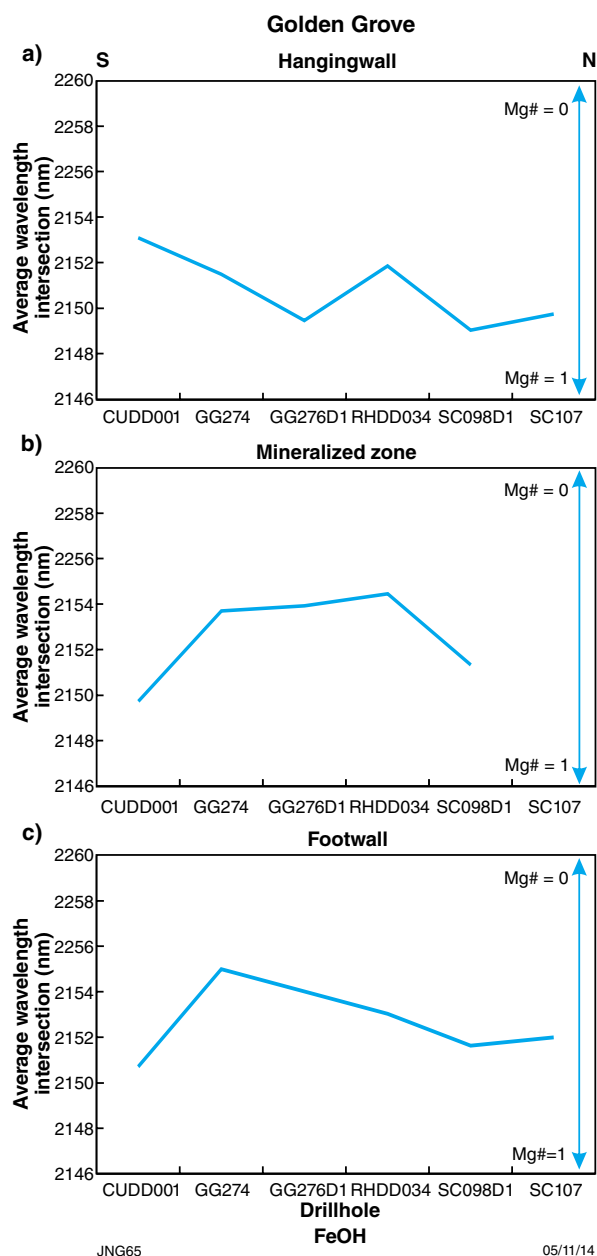


**Figure 33. Change in the intersection of the FeOH absorption feature between drillholes at Golden Grove. Results were averaged for the entire hole to give a representation of the change. The range in the plots indicates the change from 100% Fe-chlorite to 100% Mg-chlorite.**

## Chlorite

The abundance of chlorite increases from west to east at Glenview (Figs 34–37) showing FeMg-chlorite is the dominant composition identified by TSG. Mg-chlorite and Fe-chlorite are generally subordinate, but increase in abundance eastwards (Figs 34–37), and appear to be controlled by rock type. For instance, Fe-chlorite in 96GVDI001 is primarily associated with coarse volcanic breccia and with chert layers within laminated volcanoclastic units (Fig. 37).

There is an overall shift of the FeOH absorption feature to longer (~2 nm) average wavelengths in an easterly direction (Fig. 38b), although data for the two western holes is limited to where chlorite occurs: in the upper 160 m for 95WGD006 (Fig. 34), and in core from greater than 125 m downhole (beneath the BIF) for 95WGD002 (Fig. 35).

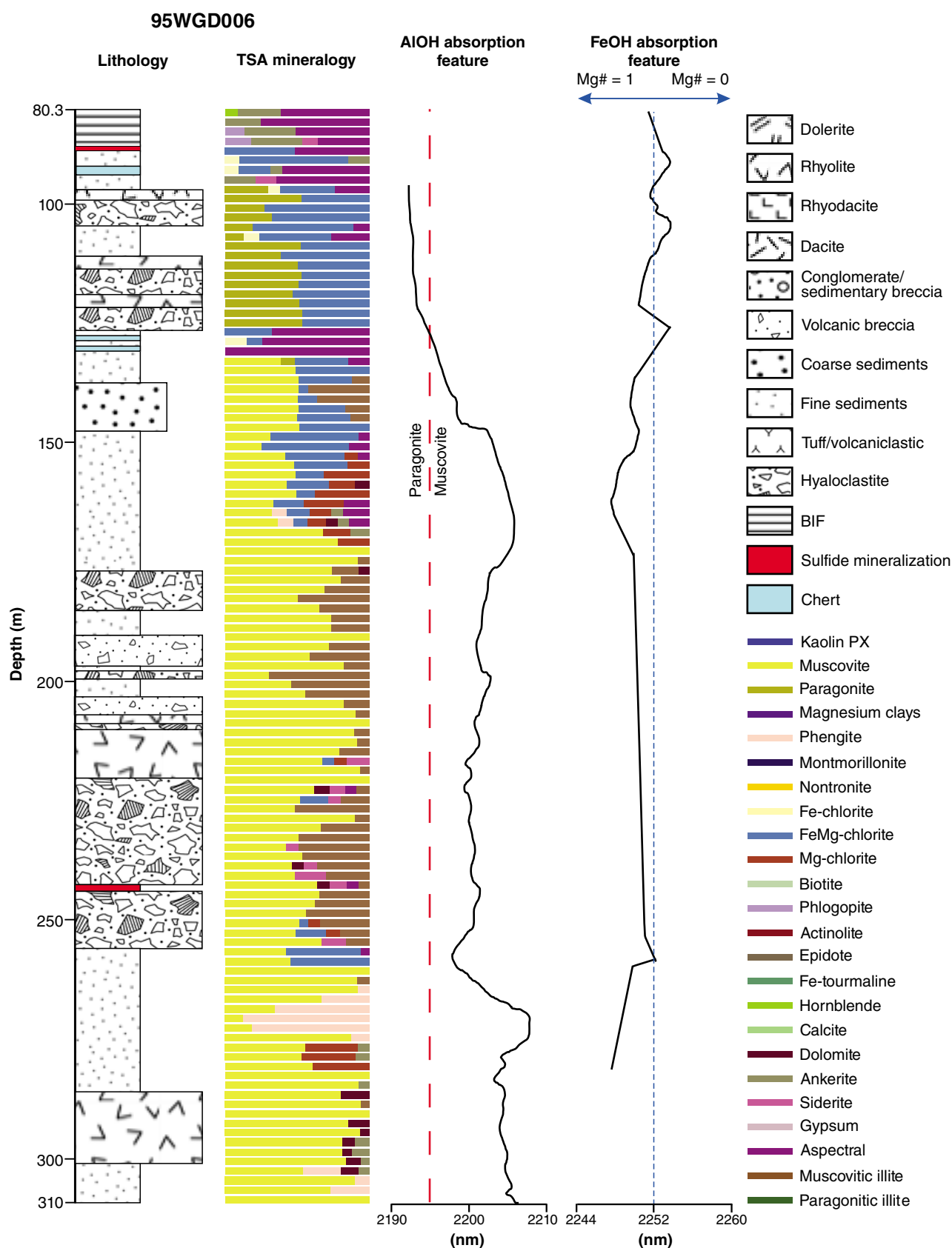
The average wavelength of the FeOH feature is ~2252.5 nm in the two easternmost holes (95WGD004 and 96GVDI001; Fig. 38b), but there is considerable variability, and an overall shift to slightly longer wavelengths downhole, associated with the presence of interbedded chert layers within a fine-grained laminated volcanoclastic unit (Figs 36, 37 and 12c).

## Discussion

### Paleodepositional environment

The paleodepositional environment of a region is a first-order constraint on its prospectivity for VMS deposits. The formation of massive sulfides requires that hot, metal-laden hydrothermal fluids mix with cold seawater at the sediment-water interface under pressures sufficient to prevent boiling and dispersal of metals in the substrate (Cas, 1992). Modern VMS systems are not known to form at water depths shallower than 1500 m, but Cas (1992) suggested that a water depth of as little as 500 m may provide sufficient confining pressure.

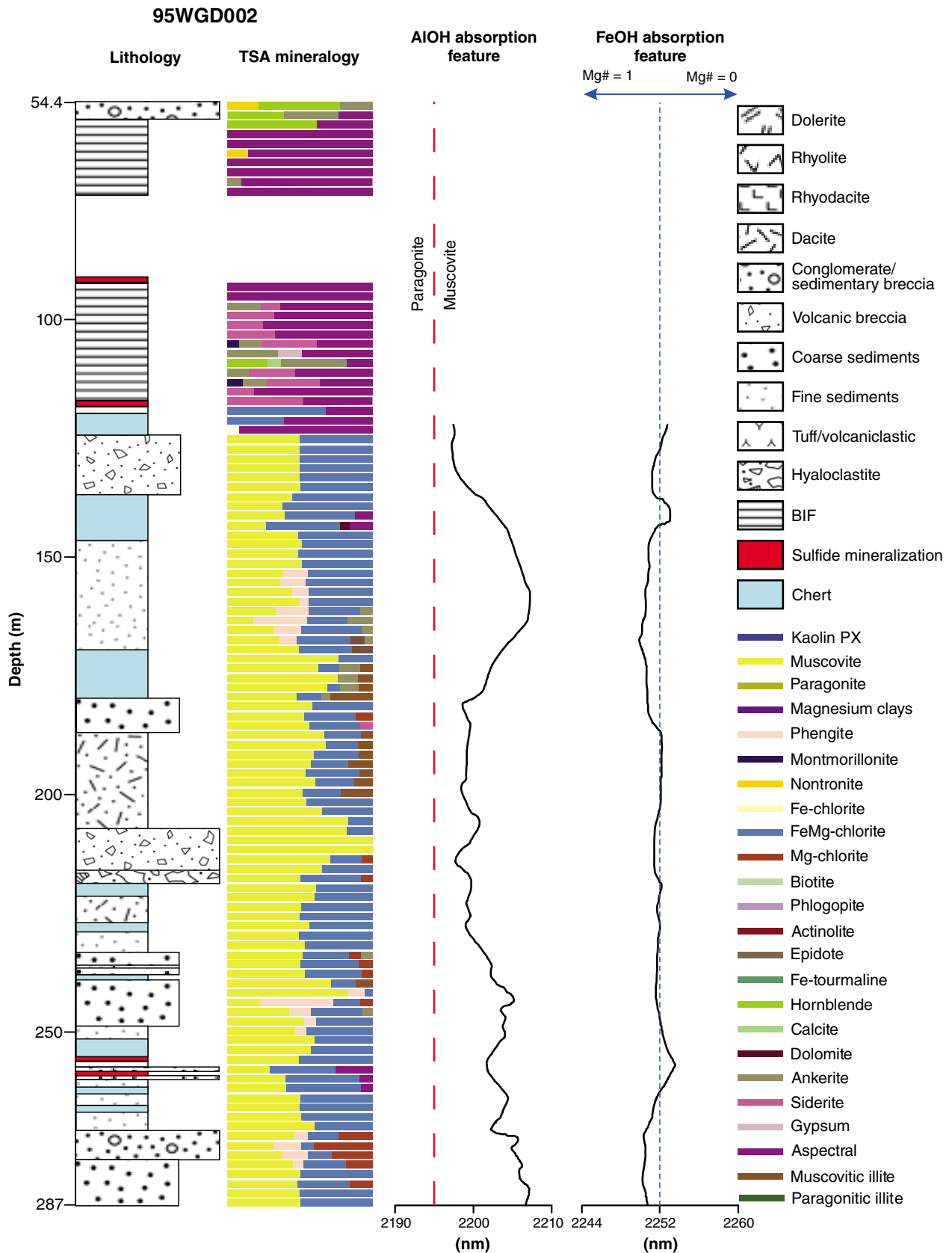
The Glenview and Golden Grove regions are both dominated by felsic volcanic sequences composed of coherent lavas and intrusives interbedded with pyroclastic volcanic, epiclastic and chemical sedimentary units. Evidence that the succession at Golden Grove formed in a deep subaqueous environment includes the presence of pillow basalts (Kerrick and Said, 2011); a subaqueous mass flow style of sedimentation (Clifford, 1992); basalt flows with interflow sediments and hyaloclastite textures (Sharpe, 1999); and the presence of massive sulfides (Cas, 1992). The stratigraphy at Glenview is indicative of an active volcanic environment that alternated between brief periods of short-lived explosive volcanic activity and long periods of quiescence dominated by sedimentary processes. Evidence for subaqueous deposition of the succession includes hyaloclastite-textured volcanic rocks, resedimented hyaloclastites, laminated cherts, and graded and laminated sedimentary rocks.



JNG49

12/11/14

**Figure 34. Graphic log of Glenview drillhole 95WGD006 showing lithology, TSG predicted mineral species, change in the wavelength intersection of the AIOH absorption feature, and change in the wavelength intersection of the FeOH absorption feature. Dashed red line indicates predicted wavelength where change from muscovite to paragonite occurs. Dashed blue line corresponds with middle value between Mg# = 1 (100% Mg-chlorite) and Mg# = 0 (100% Fe-chlorite). Note that aspectral is usually associated with sulfide occurrence.**



JNG50

25/11/14

**Figure 35.** Graphic log of Glenview drillhole 95WGD002 showing lithology, TSG predicted mineral species, change in the wavelength intersection of the AIOH absorption feature, and change in the wavelength intersection of the FeOH absorption feature. Dashed red line indicates predicted wavelength where change from muscovite to paragonite occurs. Dashed blue line corresponds with middle value between Mg# = 1 (100% Mg-chlorite) and Mg# = 0 (100% Fe-chlorite). Note that aspectral is usually associated with sulfide occurrence.

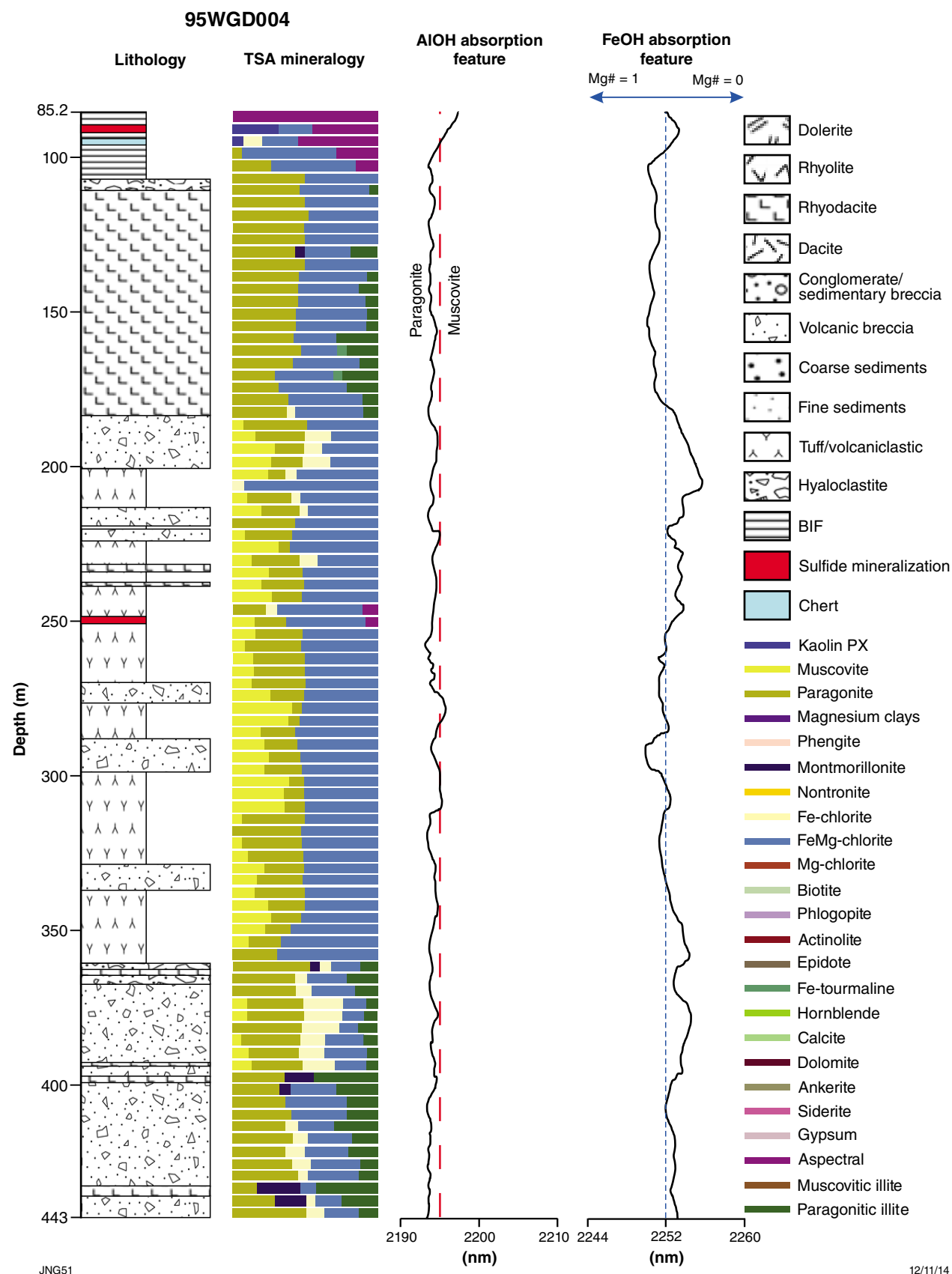


**Figure 36.** Graphic log of Glenview drillhole 95WGD004 showing lithology, TSG predicted mineral species, change in the wavelength intersection of the AIOH absorption feature, and change in the wavelength intersection of the FeOH absorption feature. Dashed red line indicates predicted wavelength where change from muscovite to paragonite occurs. Dashed blue line corresponds with middle value between Mg# = 1 (100% Mg-chlorite) and Mg# = 0 (100% Fe-chlorite). Note that aspectral is usually associated with sulfide occurrence.

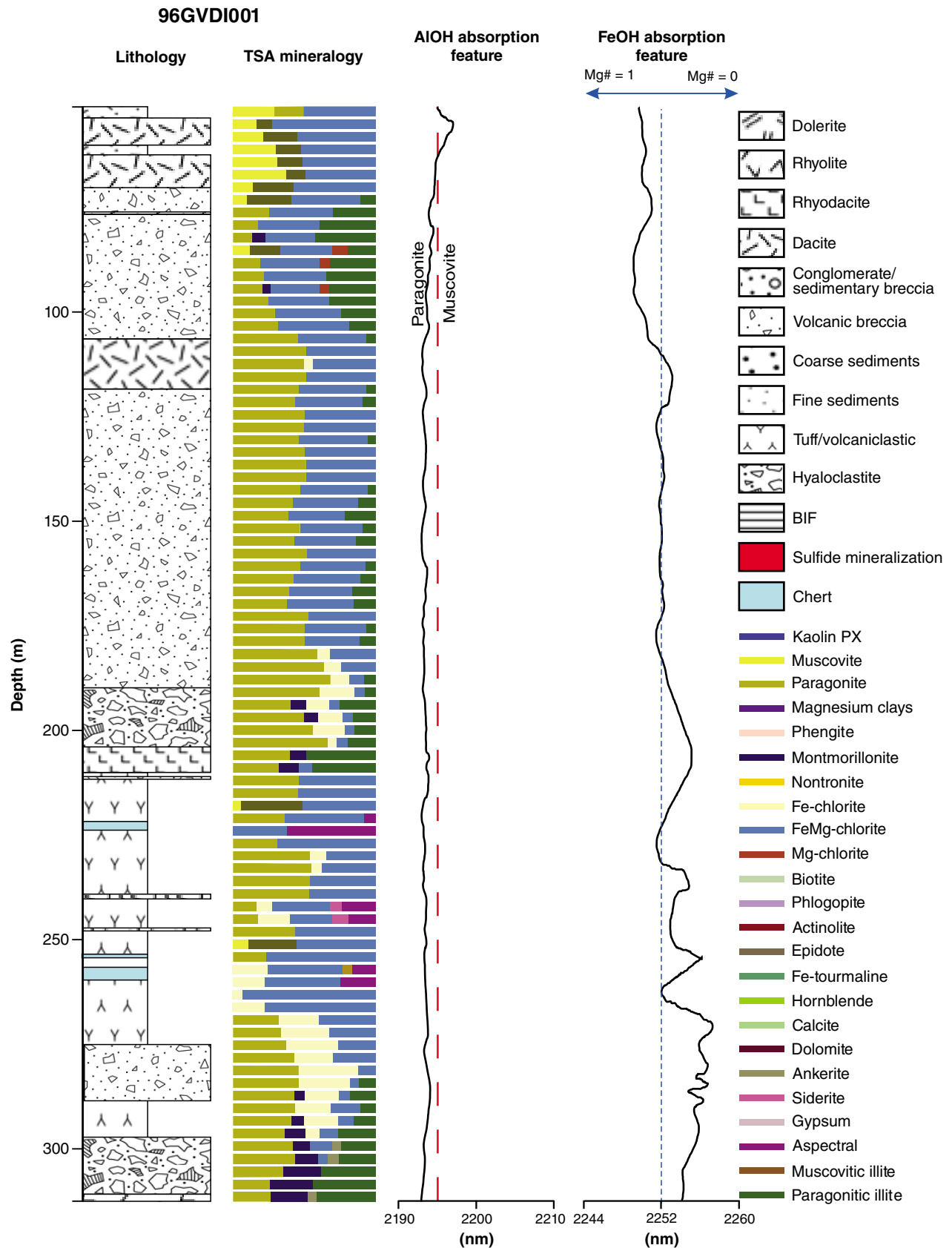


**Figure 37.** Graphic log of Glenview drillhole 96GVDI001 showing lithology, TSG predicted mineral species, change in the wavelength intersection of the AIOH absorption feature, and change in the wavelength intersection of the FeOH absorption feature. Dashed red line indicates predicted wavelength where change from muscovite to paragonite occurs. Dashed blue line corresponds with middle value between Mg# = 1 (100% Mg-chlorite) and Mg# = 0 (100% Fe-chlorite). Note that aspectral is usually associated with sulfide occurrence.

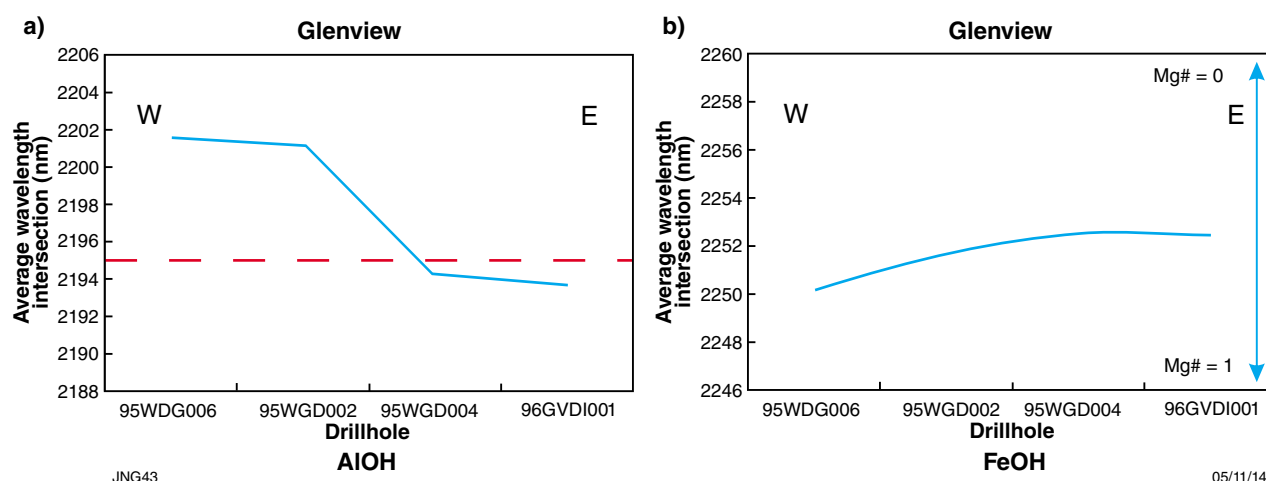


**Figure 38. Change in the intersection of the AIOH and FeOH absorption features between drillholes. Results were averaged for the entire hole to give a representation of the change. The dashed red line in the AIOH graph (a) indicates the change from muscovite into paragonite. The range in the FeOH plots (b) indicates the change from 100% Fe-chlorite to 100% Mg-chlorite.**

Evidence that volcanism and sedimentation were in deep water is more circumstantial. The lack of storm-induced sedimentary structures suggests that deposition of the succession occurred below storm-wave base, typically about 200 m below sea level (Mueller et al., 2009), although storm-induced sedimentary structures might also not form in a restricted setting such as a lake or lagoon. The presence of pyroclastic material that shows no indications of welding suggests emplacement into cold water having a possible minimum depth of 500 m (Cas, 1992; McPhie et al., 1993).

The high amount of immature pyroclastic material is interpreted to represent syneruptive submarine volcanoclastic turbidity currents, sourced from an explosive felsic eruption at a subaerial or shallow marine extrabasinal or basin-margin vent. Redeposited hyaloclastites are interpreted to be locally sourced mass flows, possibly resulting from sector collapse of a felsic dome. These units form a large part of the eastern drillhole (96GVDI001) and lie over a coherent rhyodacite, possibly a source for the hyaloclastites. Finely laminated, tuffaceous volcanoclastic layers possibly represent water-settled, ash-fall deposits of fine-grained ash derived from distal explosive eruptions, or suspension settling of fine-grained debris during the waning phases of pyroclastic-rich turbidity currents (Fig. 12c).

Rounded boulder conglomerates in the lower footwall at Glenview indicate high energy, possibly locally emergent sedimentary processes usually associated with fluvial or shallow marine (above wave base) erosion (Fig. 12a). The presence of vesicles in komatiitic basalts in the lower footwall is also interpreted by Van Kranendonk et al. (2010) as evidence for subaerial volcanism. However, these units are stratigraphically lower than the felsic succession that hosts VMS mineralization at Glenview, and permit the possibility of an environment that evolved from terrestrial to deep marine.

Van Kranendonk et al. (2010) interpreted the rock succession in the Weld Range as belonging to the c. 2750 Ma Polelle Group, and to represent a section through a southward tilted supervolcano fed by mantle and crustal melts, possibly induced by a deep mantle plume. Expulsion of magma led to caldera subsidence, creating a basin into which BIF was deposited from circulating hydrothermal fluids that were driven by heat from subvolcanic intrusions. Evidence cited by Van Kranendonk et al. (2010) in support of this interpretation includes: i) transition of volcanism from the Meekatharra to the Greensleeves Formation; ii) contemporaneous deposition of BIF of the Wilgie Mia Formation with volcanic rocks of the Greensleeves Formation; iii) evidence of abiogenic hydrothermal precipitation of the precursor to the jaspilitic cherts of the Wilgie Mia Formation; and iv) enrichment of jaspilitic cherts by highly reduced hydrothermal fluids prior to emplacement of the c. 2750 Ma Gnanagooragoo Igneous Complex and c. 2740 Ma granitic rocks, and burial unconformably beneath the c. 2735 Ma Glen Group.

A caldera subsidence model for the Weld Range can account for the transition from a subaerial to shallow marine setting evident in the lower stratigraphy, and for VMS formation. Breccias to the northeast of Glenview would then represent remnants of volcanic centres that formed local highpoints (Van Kranendonk et al., 2010). Felsic volcanic rocks were deposited during subsidence of the caldera floor, and the progressively deepening basin would have provided a favourable environment for VMS formation, particularly along synvolcanic faults associated with outer caldera walls, sites known to provide first-order control on the location of large VMS deposits in the Abitibi greenstone belt (Mueller et al., 2009). Synvolcanic faults may be recognized by the presence of chaotic chert breccias (Mueller et al., 2009), examples of which are present in the stratigraphy at Glenview (Fig. 12e; Belford, 1996; John Martyn and Associates Pty Ltd, 2000).



## Tectonic setting

VMS deposits form in extensional environments in both divergent and convergent geodynamic settings, such as oceanic sea-floor spreading ridges, or back-arc environments associated with subduction at convergent margins (Galley et al., 2007). In addition, the Archean Kidd Creek deposit in the Abitibi greenstone belt, Canada, has been interpreted by some to be associated with mantle plume activity (Wyman, 1999). Extensional settings promote necessary lithospheric thinning, mantle depressurization, and creation of basaltic magmas that ascend into and partially melt the crust to form the felsic magmas that are emplaced as subvolcanic intrusions that drive hydrothermal convection (Galley et al., 2007).

The geodynamic settings of modern VMS deposits are readily apparent, but those for ancient deposits are generally less obvious. Some potentially prospective settings (e.g. oceanic crust) are poorly preserved in the geological record, and VMS explorers have historically considered the better preserved ancient arc environments to be more prospective (Allen and Weihed, 2002).

It is more challenging to recognize ancient arc environments in the rock record. A common technique uses geochemical signatures to differentiate volcanic rocks formed in different settings. There are now many geochemical discriminant diagrams for determining tectonic environments of ancient and modern mafic igneous rocks (Wood et al., 1979; Pearce, 1982, 1996, 2008), but most are inappropriate for use with felsic volcanic rocks such as are common at Glenview. However, Gorton and Schandl (2000) have developed a technique to discern between felsic volcanic rocks from oceanic arcs, continental margin arcs, and within-plate settings, using the ratio of Th to Ta as an indicator of volcanic provenance. Thorium is known to increase relative to Ta with increasing fractionation in arc magmas (Hawkesworth et al., 1997). Schandl and Gorton (2002) attribute this trend to Th behaving as a nonconservative element that is preferentially incorporated into the subduction-generated magma either via melting or within an aqueous fluid, whereas Ta is conservative, preferentially remaining in the subducting slab during magma genesis. The mechanisms underpinning these behaviours are poorly understood, but may relate to differing partition coefficients for Th and Ta, or retention of Ta-rich accessory phases such as rutile within the subducting slab (Schandl and Gorton, 2002).

Felsic volcanic rocks from Golden Grove and Glenview all plot on the tectonic setting discrimination diagram of Schandl and Gorton (2002) within the field for active continental margins (Fig. 19). Kerrich and Said (2011) interpreted a similar continental margin arc or continental back-arc basin setting for Golden Grove using basalt geochemistry and the discrimination diagrams of Pearce (2008). Clifford (1992) preferred a rifted island- or back-arc setting with a significant continental component, similar to modern examples such as the Tertiary Hokuroko Basin in Japan (Cathles, 1983), or the Manus Basin in Papua New Guinea (Binns and Scott, 1993), citing the abundance of continentally derived, deep submarine sedimentary facies and the presence of mafic rocks.

A continental arc setting for Glenview is at odds with the interpretation by Van Kranendonk et al. (2010) that the Weld Range succession formed in response to plume-induced mantle melting in an intracontinental setting, based on the presence of komatiitic basalts, a lack of significant thrusting, and a low overall metamorphic grade.

The tectonic settings inferred herein for Glenview and Golden Grove also differ from the within-plate volcanic settings deduced for Canadian Archean VMS deposits by Schandl and Gorton (2002). They proposed that Archean VMS deposits preferentially formed in intraplate oceanic and continental rift environments rather than in subduction-related settings, due to faster spreading rates (owing to higher mantle temperatures), faster consumption of much thinner oceanic plates during subduction, and greater buoyancy of fractionated rhyolites with respect to the subducting mafic slab.

The apparent discrepancy between geochemistry that suggests an active continental margin setting for both Golden Grove and Glenview, and the lack of evidence for convergent tectonics indicates that more work is required to clarify the evolution of both regions.

## Host rock ages

The crystallization age for the felsic volcanics along the northern side of the Weld Range is disputed. Wingate et al. (2008) obtained a maximum depositional age of  $2969 \pm 3$  Ma for a metasandstone in this region. Van Kranendonk (2008) interpreted this as the crystallization age of the felsic volcanics from which the metasandstone was sourced indicating that felsic volcanism on the northern side of the Weld Range was slightly older than in the Golden Grove area (dated at 2960–2945 Ma by Wang, 1998). Wang (1998) obtained an identical age for a felsic porphyry along strike from the metasandstone, but interpreted an age of  $2752 \pm 9$  Ma for crystal tuff interbedded with BIF. When Van Kranendonk and Ivanic (2009) re-evaluated the lithostratigraphic scheme for the northern Murchison Domain, they interpreted the younger age to be that of felsic volcanism on the northern side of the Weld Range, and interpreted the  $2969 \pm 3$  Ma age determined for the metasandstone and felsic porphyry by Wingate et al. (2008) and Wang (1998), respectively, to come from detrital or xenocrystic zircons. Ivanic (2009) subsequently placed the supracrustal sequence at the Weld Range into the c. 2750 Ma Wilgie Mia Formation (the youngest formation of the Polelle Group; Fig. 3), making it ~200 Ma younger than the Gossan Hill Group in the Golden Grove region. Attempts by CSIRO to directly date mineralization at Glenview returned Pb isotope ages of 3162 and 3200 Ma for disseminated galena, and 2860 Ma for galena in a late stage vein (Martin et al., 1997). However, these Pb isotopic ages yielded a large error and do not help resolve the controversy; hence, are not considered further.

In order to resolve the controversy, sampling and age determination was undertaken for a metarhyolite sample from the northern side of the Weld Range, and a felsic volcanoclastic metasandstone from its south side (Fig. 6).

The rhyolite returned an interpreted magmatic crystallization age of  $2977 \pm 3$  Ma and the metasandstone returned a weighted mean age of  $2747 \pm 4$  Ma (Fig. 22; Wingate et al., 2013b). The samples therefore contain zircons from two distinct magmatic crystallization events in volcanic environments separated by a ~200 Ma time gap. The felsic lavas at Glenview that host mineralization are interpreted to have crystallized at c. 2977 Ma, rather than as part of the Polelle Group succession. This older age is similar but outside of error to ages obtained at Golden Grove and Mount Gibson (2935 Ma; Yeats et al., 1996). The younger  $2747 \pm 4$  Ma age corresponds to formation of the Polelle Group, as defined by Ivanic et al. (2012; Figs 3 and 39).

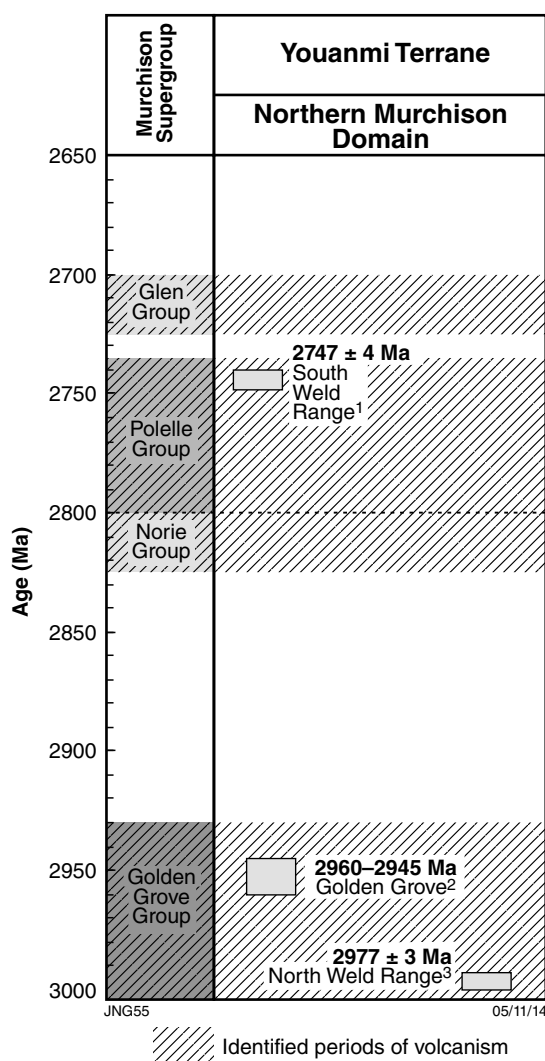


**Figure 39. Summary of age determinations for felsic volcanic rocks from Golden Grove and the Weld Range.** The division of the Murchison Domain as per Van Kranendonk and Ivanic (2009) is shown on the left. Ages: 1 GSWA 155572 (Wingate et al. 2013a); 2 Wang (1998); 3 GSWA 155569 (Wingate et al. 2013b).

This new interpretation of two successions in the vicinity of the Weld Range requires a stratigraphic discordance, possibly an unconformity, somewhere between the northern and southern margins of the Weld Range. The stratigraphic affiliation of the BIF overlying the felsic volcanics at Glenview is not yet known, although a metasilstone sample from within this unit is dated at  $2792 \pm 9$  Ma (Wingate et al., 2014), giving a possible age for deposition of the BIF. Nevertheless, it is clear that the lithostratigraphic scheme for the northern Murchison Domain must be reassessed, as must be the mantle plume-related tectonic model proposed for the geological evolution of this region by Van Kranendonk et al. (2010). A continental arc setting is possible, and would be consistent with that inferred for Golden Grove by Kerrich and Said (2011), and for rocks of similar age in the eastern Yilgarn Craton (e.g. Penneshaw Formation,  $2930 \pm 4$  Ma; Nelson, 1995).

## VMS fertility of felsic volcanic rocks

An association between geochemically distinct felsic volcanic rocks and VMS mineralization has long been recognized and used as an area selection tool for VMS exploration in Archean and Proterozoic successions (Thurston, 1981; Campbell et al., 1982; Barrie et al., 1993; Hart et al., 2004). Several schemes have been devised to distinguish between prospective and barren felsic volcanic successions (Campbell et al., 1982; Barrie et al., 1993; Fig. 40), but the one most commonly used is that of Leshner et al. (1986), who classified felsic volcanic rocks as FI, FII, FIIIa, and FIIIb types on the basis of REE patterns, Eu anomalies, Zr/Y ratios, and HFSE abundances (Tables 1 and 2). Hart et al. (2004) subsequently recognized an FIV suite of felsic volcanic rocks (Table 2). FII and FIII felsic volcanic rocks have the greatest potential for VMS mineralization. Most petrogenetic models for these rocks invoke fractionation in high-level magma chambers (Campbell et al., 1981; Franklin et al., 1981). However, Hart et al. (2004) challenged the fractionation hypothesis, citing the improbability of producing the compositionally uniform felsic volcanics that occur at many VMS deposits, and the paucity of intermediate volcanic rocks that would be expected to form by fractionation of an intermediate-mafic magma. They instead proposed a model invoking partial melting of the crust at progressively shallower depths within a rift environment, with trace-element differences arising because melts coexist with different residual mineral phases at different crustal levels. Hence, FI magmas form in the deep crust in the presence of garnet residua, FII magmas are mid-crustal melts associated with amphibole-plagioclase bearing residua, and FIII magmas form at shallowest crustal levels where plagioclase is present, and amphibole and garnet absent (Fig. 40).

Felsic volcanic rocks from both Golden Grove and Glenview have chemistries considered fertile for VMS mineralization. Dacites and rhyodacites from the footwall, mineralized zone, and lower hangingwall at Golden Grove have FIIIa and FII chemical affiliates with clear Eu anomalies and enrichment in HREE (Figs 15 and 16);

hence, would be considered prospective for VMS-style mineralization (Leshner et al., 1986; Lentz, 1998). The dacites in the upper hangingwall are FI types with REE patterns typical for non-fertile felsic volcanics (Fig. 17), and comprise intrusive and extrusive components of a late proximal dome that is not associated with significant mineralization (Sharpe, 1999).

Rhyodacites and rhyodacitic hyaloclastites at Glenview are largely FII and FIIIa types with distinctive REE patterns similar to those for prospective rocks at Golden Grove; hence, are regarded as chemically prospective for VMS (Figs 15, 16, and 18). Although Y values are lower than in rocks from Golden Grove, several felsic volcanic samples have chemistries to the left of the FII field (Fig. 15). These show REE patterns that fall below 10 times chondritic and are considered to be more comparable to FI non-prospective types (Fig. 18).

## Alteration vectors to mineralization

Once mineral explorers recognize the terrane-scale geological characteristics of an Archean greenstone belt as prospective for VMS mineralization, they shift focus towards finding evidence for VMS mineralization at the district scale, including the large hydrothermal

alteration haloes that form sulfides (Morton and Franklin, 1987; Galley, 1993; Sharpe and Gemmell, 2001), and variations in the mineralogy and alteration intensity within these haloes with respect to proximity to VMS mineralization (Large et al., 2001). Visual identification of such mineralogical changes can be subjective, and more objective techniques have been developed, such as the Ishikawa alteration index (Ishikawa et al., 1976), the chlorite–carbonate–pyrite index (Large et al., 2001), and reflectance spectroscopy (Herrmann et al., 2001; Jones et al., 2005; Hinchey, 2011; van Ruitenbeek et al., 2012).

Reflectance spectroscopy can be used to map and vector within hydrothermal alteration associated with VMS deposits; for instance, discerning compositional changes in chlorite and white mica using variations in wavelengths of their diagnostic FeOH and AlOH absorption features (Thurston and Fryer, 1983; Hart, 1984; Barrett and MacLean, 1999; Hinchey, 2011). Proximity to sulfide mineralization may be indicated by a trend towards a particular mineral composition, or by increased alteration intensity, or reduction in mineral compositional variability. Bulk-rock composition is considered an important first-order control on mineral composition in weakly or non-altered domains, but its influence is overwhelmed in strongly altered zones through which passed the higher temperature fluids required to transport metals, e.g. Cu – 250–270°C; Zn – 175–235°C (Large, 1992).

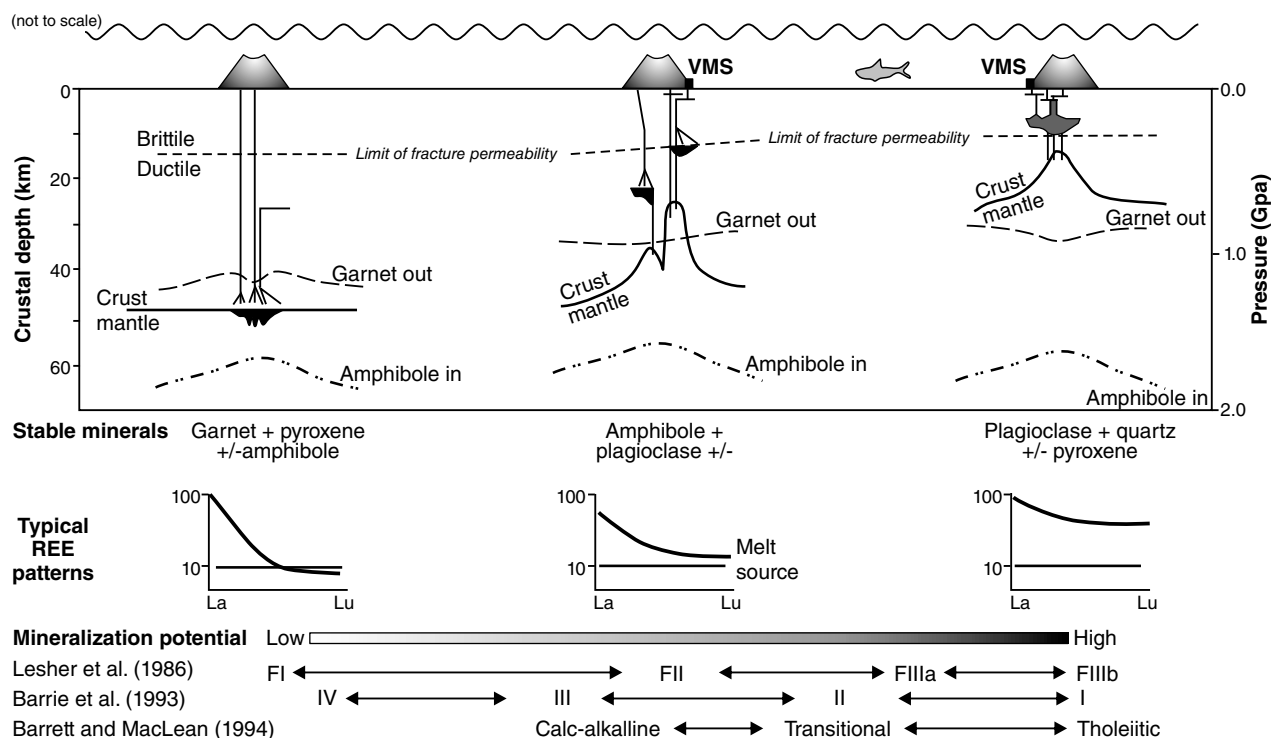


**Figure 40.** Conceptual petrogenetic model for the formation of FI-FII-FIII felsic volcanic rocks by partial melting at progressively shallower crustal depths in a rift environment. Combined high heat flow and an extensional-rift environment allow low pressure, higher-temperature crustal melting within the zone of brittle fracture permeability and promote convective seawater fluid flow. The complex arrangement of magma chambers depicted for FII felsic volcanic centres corresponds to the fact that FII felsic volcanic rocks forming below the maximum depth of convective fluid flow are barren, whereas those forming above this depth may be mineralized. From Hart et al. (2004).

Many VMS deposits show a shift of the AIOH absorption feature of the white micas to shorter (paragonitic) wavelengths towards sulfide mineralization, over a decametre scale (Herrmann et al., 2001; Jones et al., 2005; Hinchey, 2011; van Ruitenbeek et al., 2012), but this trend is not always evident and may even be reversed — for instance at the Hellyer VMS deposit in Tasmania (Yang et al., 2011). Similarly, the FeOH absorption feature for chlorite behaves inconsistently. Canadian Archean Noranda-type deposits typically have shorter wavelength FeOH features (Mg-rich chlorite) proximal to mineralization, whereas Mattabi-type deposits show longer wavelength FeOH features (Fe-rich chlorite) close to mineralization (Morton and Franklin, 1987). Care must be exercised if using shifts in wavelength of the AIOH or FeOH absorption features to vector to new VMS systems.

Rocks in drillcore from Golden Grove and Glenview display changes in both mineralogy and wavelengths of the AIOH and FeOH absorption features that could be attributed to the varying influence of hydrothermal fluids. At Golden Grove, the wavelength of the AIOH absorption feature in core from the non-mineralized CUDD001 hole, varies by 14 nm and generally correlates with changes in rock type (Fig. 23). Conversely, the 5–8 nm variation in wavelength of the AIOH absorption feature observed in core from all other studied holes from Golden Grove shows little change in response to rock composition (Figs 24–28), and is considered to represent the effect of increased hydrothermal alteration intensity, with less variation evident in domains that have undergone more intense alteration.

Drillcore from the non-mineralized RHDD034 hole also has white micas with shorter wavelengths for the AIOH absorption feature, suggesting significant hydrothermal alteration, although less intense than in the mineralized holes (Figs 26 and 31). The lack of VMS mineralization may possibly be due to absence of metals in the hydrothermal fluid. It should also be noted that the average wavelength of the AIOH absorption feature is slightly higher here than at the mineralized holes at Gossan Hill, indicating slightly less intense hydrothermal alteration (Fig. 31).

The white mica composition in mineralized holes at Gossan Hill gradually changes from muscovite to paragonite within 50–100 m of sulfide mineralization (Figs 24, 25, and 29), coinciding with a subsequent decrease in wavelength of the AIOH absorption feature (Fig. 30). This change is not evident in the non-mineralized CUDD001 hole, where muscovite is the dominant white mica mineral and shows no change in relation to the mineralized horizon (Figs 23 and 29).

The average wavelength of the white mica AIOH absorption feature is also shorter in VMS-mineralized holes SC107 and SC098D1 from Scuddles, than in the non-mineralized CUDD001 hole, suggesting that hydrothermal alteration at Scuddles is more intense. However, the decrease in the wavelength of the white mica AIOH feature at Scuddles is less than at Gossan Hill or in RHDD034. Possible explanations for the difference include: i) thermal overprinting of earlier alteration

effects during emplacement of abundant intrusions at Scuddles resulting in less distinctive patterns; or ii) originally less intense hydrothermal alteration by lower temperature fluids, as suggested by the lack of significant Cu-mineralization at Scuddles compared to Gossan Hill (Ashley et al., 1988; Gawlinski, 2004). The differences in alteration between the Scuddles and Gossan Hill deposits indicates that each deposit must be treated independently, and that comparisons of any two different deposits must be done with care.

At Glenview, the lack of variation in the AIOH absorption feature in the eastern drillholes suggests that hydrothermal alteration is the controlling factor on white mica composition in the east (Figs 36 and 37). In the west, the AIOH absorption feature varies significantly downhole, indicating that rock type is the controlling factor over white mica composition (Figs 34 and 35). Paragonite is the more prevalent white mica in the two eastern holes, and shows no discernible variation in abundance and only minimal shortening or lengthening of the AIOH wavelength (Figs 36 and 37). This uniformity suggests that hydrothermal alteration was more intense.

The average wavelength of the FeOH absorption feature for chlorite also shows broadly systematic variation with distance from sulfide mineralization. At Gossan Hill this feature shifts about 8 nm to longer wavelengths (more Fe-rich chlorite) when at the mineralized zone (Fig. 32). This shift is also evident in the non-mineralized RHDD034 hole (Fig. 32), suggesting that the chlorite FeOH absorption feature may be useful for identifying prospective units away from mineralization.

At Glenview, the chlorite FeOH absorption feature also shifts to longer wavelengths where sulfide stringer veins occur (Figs 34, 35, and 36), and in the two eastern holes, longer wavelength peaks tend to occur in volcanoclastic and volcanic breccia units, in places associated with chert horizons, which might therefore have potential to host massive sulfides.

TIR scanning can identify minerals and mineral groups that are currently undetectable using SWIR, such as feldspars and quartz; however, the accuracy of the results should be verified by petrological examination or XRD.

## Conclusions

The geological features of the Glenview prospect are very similar to those of the VMS-endowed Golden Grove region: i) both are dominated by felsic volcanic, volcanoclastic, and sedimentary successions deposited into a deep subaqueous environment (>500 m); ii) newly acquired crystallization ages of c. 2977 Ma for felsic rocks near Glenview are only slightly older than those of c. 2960 Ma for the entire dacitic succession at Golden Grove; iii) felsic volcanic geochemistry indicates eruption at both Golden Grove and Glenview in an active continental margin setting, a setting favourable for forming VMS deposits; iv) felsic volcanic rocks in both areas are also geochemically fertile for VMS mineralization; and v) both sequences have extensive hydrothermal sericite

and hydrothermal chlorite alteration. These similarities between Golden Grove and Glenview suggest that the latter region is prospective for significant VMS mineralization.

Changes in chlorite and white mica compositions provide measurable vectors towards sulfide mineralization at Golden Grove, and can be detected using mineral spectroscopy. White mica is progressively more Al rich (paragonitic) towards sulfide mineralization, and chlorite is more Fe rich immediately adjacent to sulfides. The intensity of hydrothermal alteration also increases towards sulfide mineralization, and is shown in spectral data by a decrease in variability of wavelength of the AIOH feature for white mica, and a shift to longer wavelengths for the FeOH feature for chlorite. A similar pattern is noted for white mica at Glenview, and suggests that the core of the mineralizing system here lies to the east of present exploration.

The confirmation that the volcano-sedimentary successions adjacent to the Glenview prospect are significantly older than the southern part indicates that the stratigraphy for this part of the Murchison Domain must be reassessed. This also has implications for previously proposed models for the tectonic and geodynamic setting in this region. Specifically, more geological mapping and geochronology are needed to further constrain the stratigraphy in the vicinity of the Weld Range; hence, providing a better understanding of the tectonostratigraphic evolution of the Murchison Domain. Particular attention should be paid to the pre-2900 Ma component and its significance for VMS mineralization.

## Acknowledgements

This report is derived from research undertaken as part of a Master of Economic Geology project completed through The University of Western Australia. I would like to thank the geological staff at MMG Limited, Golden Grove, and Hampton Hill Mining, Weld Range, for their knowledgeable assistance and donation of appropriate drillcore for this study, Wilson Forte (Hampton Hill Mining) for his field assistance and willingness to share knowledge on the Weld Range area, Scott Halley (Mineral Mapping) and Jon Huntington (CSIRO) for their assistance with analysing data using TSG, and Michael Verrall (CSIRO) for his assistance with operation of the SEM, Trevor Beardsmore and Tim Ivanic for their reviews and contributions to the text, Lena Hancock and Paul Duuring for their discussions on aspects of the project, Mark Barley for supervising my Master of Economic Geology project through The University of Western Australia, and Lee Hassan for supervising both the Master of Economic Geology project and this Report.

## References

- Allen, RL and Weihed, P 2002, Global comparisons of volcanic-associated massive sulphide districts: Geological Society, London, Special Publications, v. 204, no. 1, p. 13–36.
- Ashley, PM, Dudley, RJ, Lesh, RH, Marr, JM and Ryall, AW 1988, The Scuddles Cu–Zn prospect, an Archean volcanogenic massive sulfide deposit, Golden Grove District, Western Australia: *Economic Geology*, v. 83, no. 5, p. 918–951.
- Barley, ME 1992, A review of Archean volcanic-hosted massive sulfide and sulfate mineralization in Western Australia: *Economic Geology*, v. 87, no. 3, p. 855–872.
- Barley, ME, Kerrich, R, Reudavy, I and Xie, Q 2000, Late Archean Ti-rich, Al-depleted komatiites and komatiitic volcanoclastic rocks from the Murchison Terrane in Western Australia: *Australian Journal of Earth Sciences*, v. 47, no. 5, p. 873–883.
- Barrett, TJ and MacLean, WH 1999, Volcanic sequences, lithogeochemistry, and hydrothermal alteration in some bimodal volcanic-associated massive sulfide systems: *Reviews in Economic Geology*, v. 8, p. 101–131.
- Barrie, CT, Ludden, JN and Green, TH 1993, Geochemistry of volcanic rocks associated with Cu–Zn and Ni–Cu deposits in the Abitibi subprovince: *Economic Geology*, v. 88, no. 6, p. 1341–1358.
- Belford, SM 1996, Report on the Chemistry of VHMS Deposits with Particular Reference to the Mineralization, Alteration, and Potential of the Glenview Prospect Weld Range, WA: Hampton Hill Mining NL (unpublished), 15p.
- Belford, SM 2001, VMS deposits: nature, genesis and controls on formation and distribution of giant examples: University of Western Australia, Nedlands, Perth, Western Australia, Masters Thesis (unpublished), 76p.
- Binns, RA and Scott, SD 1993, Actively forming polymetallic sulfide deposits associated with felsic volcanic rocks in the eastern Manus back-arc basin, Papua New Guinea: *Economic Geology*, v. 88, no. 8, p. 2226–2236.
- Campbell, IH, Franklin, JM, Gorton, MP, Hart, TR and Scott, SD 1981, The role of subvolcanic sills in the generation of massive sulfide deposits: *Economic Geology*, v. 76, no. 8, p. 2248–2253.
- Campbell, IH, Coad, P, Franklin, JM, Gorton, MP, Scott, SD, Sowa, J and Thurston, PC 1982, Rare earth elements in volcanic rocks associated with Cu–Zn massive sulphide mineralization: a preliminary report: *Canadian Journal of Earth Sciences*, v. 19, no. 3, p. 619–623.
- Cas, RAF 1992, Submarine volcanism; eruption styles, products, and relevance to understanding the host-rock successions to volcanic-hosted massive sulfide deposits: *Economic Geology*, v. 87, no. 3, p. 511–541.
- Cas, RAF and Wright, JV 1987, Volcanic successions: modern and ancient: a geological approach to processes, products and successions: Allen & Unwin, London, UK, 529p.
- Cassidy, KF, Champion, DC, Krapez, B, Barley, ME, Brown, SJA, Blewett, RS, Groenewald, PB and Tyler, IM 2006, A revised geological framework for the Yilgarn Craton, Western Australia: Geological Survey of Western Australia, Record 2006/8, 8p.
- Cathles, LM 1983, An analysis of the hydrothermal system responsible for massive sulfide deposition in the Hokuroku Basin of Japan: *Economic Geology Monograph*, v. 5, p. 439–487.
- Clifford, BA 1992, Facies and palaeoenvironment analysis of the Archean volcanic-sedimentary succession hosting the Golden Grove Cu–Zn massive sulphide deposits, Western Australia: Monash University, PhD thesis (unpublished), 343p.
- Duuring, P and Hagemann, SG 2013, Genesis of superimposed hypogene and supergene Fe ore bodies in BIF at the Madoonga deposit, Yilgarn Craton, Western Australia: *Mineralium Deposita*, v. 48, no. 3, p. 371–395, doi:10.1007/s00126-012-0429-0.
- Fisher, RV and Schmincke, HU 1984, *Pyroclastic Rocks* (10th edition): Springer, Berlin, Germany, 472p.
- Franklin, JM, Lydon, JW and Sangster, DF 1981, Volcanic-associated massive sulfide deposits: *Economic Geology*, v. 75, p. 485–627.



- Galley, AG 1993, Characteristics of semi-conformable alteration zones associated with volcanogenic massive sulphide districts: *Journal of Geochemical Exploration*, v. 48, no. 2, p. 175–200.
- Galley, AG, Hannington, MD and Jonasson, IR 2007, Volcanogenic massive sulphide deposits, in *A synthesis of major deposit-types, district metallogeny, the evolution of geological provinces, and exploration methods* edited by WD Goodfellow: Geological Association of Canada, Mineral Deposits Division, Special Publication 5, p. 141–161.
- Gawliniski, S 2004, Recent exploration success at Golden Grove, Western Australia: Copper-zinc massive sulphide deposits in Western Australia. *CSIRO Explores*, v. 2, p. 33–37.
- Gole, MJ 1980, Mineralogy and petrology of very-low-metamorphic grade Archaean banded iron-formations, Weld Range, Western Australia: *American Mineralogist*, v. 65, p. 1–2.
- Gorton, MP and Schandl, ES 2000, From continents to island arcs: a geochemical index of tectonic setting for arc-related and within-plate felsic to intermediate volcanic rocks: *The Canadian Mineralogist*, v. 38, no. 5, p. 1065–1073.
- Hancock, EA and Huntington, JF 2010a, The GSWA HyLogger: rapid spectral analysis and its application in detecting mineralization, in *GSWA 2010 extended abstracts: promoting the prospectivity of Western Australia*: Geological Survey of Western Australia, Record 2010/2, p. 10–13.
- Hancock, EA and Huntington, JF 2010b, The GSWA NVCL HyLogger: rapid mineralogical analysis for characterizing mineral and petroleum core: Geological Survey of Western Australia, Record 2010/17, 21p.
- Hart, TR 1984, The geochemistry and petrogenesis of a metavolcanic and intrusive sequence in the Kamiskotia area, Timmins, Ontario: University of Toronto, Toronto, Canada, MSc thesis (unpublished), 179p.
- Hart, TR, Gibson, HL and Leshner, CM 2004, Trace element geochemistry and petrogenesis of felsic volcanic rocks associated with volcanogenic massive Cu–Zn–Pb sulfide deposits: *Economic Geology*, v. 99, no. 5, p. 1003–1013.
- Hawkesworth, CJ, Turner, SP, McDermott, F, Peate, DW and Van Calsteren, P 1997, U–Th isotopes in arc magmas: Implications for element transfer from the subducted crust: *Science*, v. 276, no. 5312, p. 551–555.
- Herrmann, W, Blake, M, Doyle, M, Huston, D, Kamprad, J, Merry, N and Pontual, S 2001, Short wavelength infrared (SWIR) spectral analysis of hydrothermal alteration zones associated with base metal sulfide deposits at Rosebery and Western Tharsis, Tasmania, and Highway-Reward, Queensland: *Economic Geology*, v. 96, no. 5, p. 939–955.
- Herzig, PM and Hannington, MD 1995, Polymetallic massive sulfides at the modern seafloor A review: *Ore Geology Reviews*, v. 10, no. 2, p. 95–115.
- Hinchey, JG 2011, Visible/infrared spectroscopy (VIRS) of volcanogenic massive sulphide hydrothermal alteration products, Tulks Volcanic Belt, central Newfoundland: An additional exploration technique?, in *Current Research: Newfoundland and Labrador* Department of Natural Resources, Geological Survey, Report 11-1, p. 97–108.
- Ishikawa, Y, Sawaguchi, T, Iwaya, S and Horiuchi, M 1976, Delineation of prospecting targets for Kuroko deposits based on modes of volcanism of underlying dacite and alteration haloes: *Mining Geology*, v. 26, p. 105–117.
- Ivanic, TJ 2009, Madoonga, WA Sheet 2444: Geological Survey of Western Australia, 1:100 000 Geological Series.
- Ivanic, TJ, Wingate, MTD, Kirkland, CL, Van Kranendonk, MJ and Wyche, S 2010, Age and significance of voluminous mafic–ultramafic magmatic events in the Murchison Domain, Yilgarn Craton: *Australian Journal of Earth Sciences*, v. 57, p. 597–614.
- Ivanic, TJ, Van Kranendonk, MJ, Kirkland, CL, Wyche, S, Wingate, MTD and Belousova, E 2012, Zircon Lu–Hf isotopes and granite geochemistry of the Murchison Domain of the Yilgarn Craton: evidence for reworking of Eoarchean crust during Meso–Neoproterozoic plume-driven magmatism: *Lithos*, v. 148, p. 112–127.
- John Martyn and Associates Pty Ltd 2000, Pre-petrology summary of progress in geological studies of the Ryansville project (unpublished), 33p.
- Jones, S, Herrmann, W and Gemmell, JB 2005, Short wavelength infrared spectral characteristics of the HW horizon: Implications for exploration in the Myra Falls volcanic-hosted massive sulfide camp, Vancouver Island, British Columbia, Canada: *Economic Geology*, v. 100, no. 2, p. 273–294.
- Kerr, A, Rafuse, H, Sparkes, G, Hinchey, J and Sandeman, H 2011, Visible/infrared spectroscopy (VIRS) as a research tool in economic geology: Background and pilot studies from Newfoundland and Labrador, in *Current Research: Newfoundland and Labrador* Department of Natural Resources, Geological Survey, Report 11-1, p. 145–166.
- Kerrich, R and Said, N 2011, Extreme positive Ce-anomalies in a 3.0 Ga submarine volcanic sequence, Murchison Province: Oxygenated marine bottom waters: *Chemical Geology*, v. 280, no. 1, p. 232–241.
- Large, RR 1992, Australian volcanic-hosted massive sulfide deposits: features, styles, and genetic models: *Economic Geology*, v. 87, no. 3, p. 471–510.
- Large, RR, Gemmell, JB, Paulick, H and Huston, DL 2001, The alteration box plot: A simple approach to understanding the relationship between alteration mineralogy and lithogeochemistry associated with volcanic-hosted massive sulfide deposits: *Economic Geology*, v. 96, no. 5, p. 957–971.
- Lentz, DR 1998, Petrogenetic evolution of felsic volcanic sequences associated with Phanerozoic volcanic-hosted massive sulphide systems: the role of extensional geodynamics: *Ore Geology Reviews*, v. 12, no. 5, p. 289–327.
- Leshner, CM, Goodwin, AM, Campbell, IH and Gorton, MP 1986, Trace-element geochemistry of ore-associated and barren, felsic metavolcanic rocks in the Superior Province, Canada: *Canadian Journal of Earth Sciences*, v. 23, no. 2, p. 222–237.
- Martin, NK, Kneewhaw, AD and Andrews, P 1997, Annual report for the period ending 28 February 1997 on E20/163, E20/168, E20/208, E20/220, E20/229-230, E20/258, E20/280, E20/284-288, E51/525, E51/527-528, M20-311, P20/1674-1681, P20/1686-1687, P51/2162; M.I.M. Exploration PTY. LTD.: Geological Survey of Western Australia, Statutory mineral exploration report, A51364 (Public).
- McCuaig, TC, Miller, JM and Beresford, S (compilers) 2010, Controls on giant mineral systems in the Yilgarn Craton — a field guide: Geological Survey of Western Australia, Record 2010/26, 164p.
- McDonough, WF and Sun, SS 1995, The composition of the Earth: *Chemical Geology*, v. 120, no. 3, p. 223–253.
- McPhie, J, Doyle, M and Allen, R 1993, Volcanic textures: a guide to the interpretation of textures in volcanic rocks: CODES, University of Tasmania, Hobart, Tasmania, 198p.
- Merry, N, Pontual, S and Gamson, P 1999, The Spectral Geologist v. 2.0 user manual: AusSpec International: Commonwealth Scientific and Industrial Research Organisation (CSIRO), Australia.
- MMG Limited 2012a, Scuddles and Gossan Hill Archaean VHMS deposits: p. 1–36 (unpublished).
- MMG Limited 2012b, Annual Report 2012, viewed 10 May 2013 <[http://www.mmg.com/en/Investors-and-Media/Reports-and-Presentations/~media/Files/Exchange%20Announcements/Investors%20and%20Media/News/2013/04/18/e\\_2013-04-19\\_2012%20Annual%20Report.aspx](http://www.mmg.com/en/Investors-and-Media/Reports-and-Presentations/~media/Files/Exchange%20Announcements/Investors%20and%20Media/News/2013/04/18/e_2013-04-19_2012%20Annual%20Report.aspx)>.

- Morris, PA 2007, Composition of the Bunbury Basalt (BB1) and Kerba Monzogranite (KG1) geochemical reference materials, and assessing the contamination effects of mill heads: Geological Survey of Western Australia, Record 2007/14, 22p.
- Morton, RL and Franklin, JM 1987, Two-fold classification of Archean volcanic-associated massive sulfide deposits: *Economic Geology*, v. 82, no. 4, p. 1057–1063.
- Mueller, WU, Stix, J, Corcoran, PL and Daigneault, R 2009, Subaqueous calderas in the Archean Abitibi greenstone belt: An overview and new ideas: *Ore Geology Reviews*, v. 35, no. 1, p. 4–46.
- Nakamura, N 1974, Determination of REE, Ba, Fe, Mg, Na and K in carbonaceous and ordinary chondrites: *Geochimica et Cosmochimica Acta*, v. 38, no. 5, p. 757–775.
- Nelson, DR 1995, 104963: biotite rhyolite, Penneshaw Formation; *Geochronology Record 21*: Geological Survey of Western Australia, 5p.
- Pearce, JA 1982, Trace element characteristics of lavas from destructive plate boundaries: *Orogenic andesites and related rocks*, p. 528–548.
- Pearce, JA 1996, A users guide to basalt discrimination diagrams: Trace element Geochemistry of volcanic rocks: applications for massive sulphide exploration. Geological Association of Canada, Short Course Notes, v. 12, p. 79–113.
- Pearce, JA 2008, Geochemical fingerprinting of oceanic basalts with applications to ophiolite classification and the search for Archean oceanic crust: *Lithos*, v. 100, no. 1, p. 14–48.
- Pidgeon, RT and Hallberg, JA 2000, Age relationships in supracrustal sequences of the northern part of the Murchison Terrane, Archaean Yilgarn Craton, Western Australia: a combined field and zircon U–Pb study: *Australian Journal of Earth Sciences*, v. 47, p. 153–165.
- Pontual, S 2008, GMEX spectral analysis guides for mineral exploration (3rd edition): AusSpec International, 10 vols.
- Schandl, ES and Gorton, MP 2002, Application of high field strength elements to discriminate tectonic settings in VMS environments: *Economic Geology*, v. 97, no. 3, p. 629–642.
- Sharpe, R 1999, The Archean Cu–Zn magnetite-rich Gossan Hill VHMS deposit, Western Australia: Evidence of a structurally-focused, exhalative and sub-seafloor replacement mineralising system: University of Tasmania, Hobart, Tasmania, PhD thesis (unpublished), 505p.
- Sharpe, R and Gemmell, JB 2001, Alteration characteristics of the Archean Golden Grove Formation at the Gossan Hill deposit, Western Australia: Induration as a focusing mechanism for mineralizing hydrothermal fluids: *Economic Geology*, v. 96, no. 5, p. 1239–1262.
- Sharpe, R and Gemmell, JB 2002, The Archean Cu–Zn magnetite-rich Gossan Hill volcanic-hosted massive sulfide deposit, Western Australia: genesis of a multistage hydrothermal system: *Economic Geology*, v. 97, no. 3, p. 517–539.
- Thurston, PC 1981, Economic evaluation of Archean felsic volcanic rocks, using REE geochemistry, in *Archean Geology edited by JE Glover and DI Groves*: Geological Society of Australia, Perth, Western Australia, Special Publication 7, p. 439–450.
- Thurston, PC and Fryer, BJ 1983, The geochemistry of repetitive cyclical volcanism from basalt through rhyolite in the Uchi-Confederation greenstone belt, Canada: *Contributions to Mineralogy and Petrology*, v. 83, no. 3–4, p. 204–226.
- Van Kranendonk, MJ 2008, New evidence on the evolution of the Cue-Meekatharra area of the Murchison Domain, Yilgarn Craton, in *Annual Review 2006–07*: Geological Survey of Western Australia, Perth, Western Australia, p. 32–42.
- Van Kranendonk, MJ and Ivanic, TJ 2009, A new lithostratigraphic scheme for the northeastern Murchison Domain, Yilgarn Craton, in *Annual Review 2007–08*: Geological Survey of Western Australia, Perth, Western Australia, p. 34–53.
- Van Kranendonk, MJ, Ivanic, TJ, Wyche, S, Wilde, SA and Zibra, I (compilers) 2010, A time transect through the Hadean to Neoproterozoic geology of the western Yilgarn Craton — a field guide: Geological Survey of Western Australia, Record 2010/19, 69p.
- Van Kranendonk, MJ, Ivanic, TJ, Wingate, MT, Kirkland, CL and Wyche, S 2012, Long-lived, autochthonous development of the Archean Murchison Domain, and implications for Yilgarn Craton tectonics: *Precambrian Research*, v. 229, p. 49–92.
- van Ruitenbeek, FJ, Cudahy, TJ, van der Meer, FD and Hale, M 2012, Characterization of the hydrothermal systems associated with Archean VMS-mineralization at Panorama, Western Australia, using hyperspectral, geochemical and geothermometric data: *Ore Geology Reviews*, v. 45, p. 33–46.
- Vearncombe, S 2010, Yilgarn volcanogenic massive sulphides, in *Abstracts edited by S Wyche*: Geological Survey of Western Australia; Fifth International Archean Symposium, Perth, Western Australia, 10 September 2010, p. 47–50.
- Wang, Q 1998, Geochronology of the granite–greenstone terranes in the Murchison and Southern Cross Provinces of the Yilgarn Craton, Western Australia: Australian National University, Canberra, PhD thesis (unpublished), 186p.
- Watkins, KP and Hickman, AH 1990, Geology of the Murchison Province granite–greenstone terrane, Western Australia, in *Third international Archean symposium, excursion guidebook edited by SE Ho, JE Grover, JS Myers, and JR Muhling*: University of Western Australia; p. 147–171.
- Winchester, JA and Floyd, PA 1977, Geochemical discrimination of different magma series and their differentiation products using immobile elements: *Chemical Geology*, v. 20, p. 325–343.
- Wingate, MTD, Bodorkos, S and Kirkland, CL 2008, 184112: metasandstone, Ram Well; *Geochronology Record 736*: Geological Survey of Western Australia, 6p.
- Wingate, MTD and Kirkland, CL 2013, Introduction to geochronology information released in 2013: Geological Survey of Western Australia, 5p.
- Wingate, MTD, Kirkland, CL, Ivanic, TJ, Wyche, S and Van Kranendonk, MJ 2013a, 155572: felsic volcanoclastic metasandstone, Weld Range; *Geochronology Record 1097*: Geological Survey of Western Australia, 5p.
- Wingate, MTD, Kirkland, CL, Van Kranendonk, MJ and Wyche, S 2013b, 155569: metarhyolite, Weld Range; *Geochronology Record 1096*: Geological Survey of Western Australia, 4p.
- Wingate, MTD, Kirkland, CL, Ivanic, TJ, Wyche, S and Van Kranendonk, MJ 2014, 155568: metasiltstone, Weld Range; *Geochronology Record 1171*: Geological Survey of Western Australia, 6p.
- Wood, DA, Joron, JL and Treuil, M 1979, A re-appraisal of the use of trace elements to classify and discriminate between magma series erupted in different tectonic settings: *Earth and Planetary Science Letters*, v. 45, no. 2, p. 326–336.
- Wyman, DA 1999, A 2.7 Ga depleted tholeiite suite: evidence of plume–arc interaction in the Abitibi greenstone belt, Canada: *Precambrian Research*, v. 97, no. 1, p. 27–42.
- Yang, K, Huntington, JF, Gemmel, JB and Scott, KM 2011, Variations in composition and abundance of white mica in the hydrothermal alteration system at Hellyer, Tasmania, as revealed by infrared reflectance spectroscopy: *Journal of Geochemical Exploration*, v. 108, no. 2, p. 143–156.
- Yeats, CJ, McNaughton, NJ and Groves, DI 1996, SHRIMP U–Pb geochronological constraints on Archean volcanic-hosted massive sulfide and lode gold mineralization at Mount Gibson, Yilgarn Craton, Western Australia: *Economic Geology*, v. 91, p. 1354–1371.

Appendix 1 – Geochemistry

Table 1.1. Major and trace-element geochemistry for Golden Grove and Weld Range samples

GSWA number	Deposit	Prospect	Drillhole	Easting (MGA)	Northing (MGA)	Depth (m)	Rock type	SiO <sub>2</sub>	TiO <sub>2</sub>	Al <sub>2</sub> O <sub>3</sub>	Fe <sub>2</sub> O <sub>3t</sub>	MnO	MgO	CaO	Na <sub>2</sub> O	K <sub>2</sub> O	P <sub>2</sub> O <sub>5</sub>	LOI	C	As	Ni	Co	Cr	V
								Detection 0.01	0.01	0.01	0.01	0.01	0.01	0.01	0.01	0.01	0.001	0.01	0.01	0.5	0.5	0.1	20	10
206501	Golden Grove	Gossan Hill	GG276D1	494330	6818575	973.1	Dacite	62.66	0.41	13.43	3.96	0.08	2.28	6.16	0.28	3.64	0.097	7.12	1.41	0.9	39.2	20.7	51	69
206502	Golden Grove	Gossan Hill	GG276D1	494330	6818575	1005.95	Dacite	63.22	0.43	14.04	3.32	0.1	2.03	5.58	2.66	2.46	0.107	5.63	1.16	0.5	22.4	19.9	57	69
206521	Golden Grove	Cullens	CUDD001	494489	6816796	1028.3	Dacite	54.99	0.9	12.89	12.72	0.08	11.51	0.48	0.03	0.02	0.213	6.07	0.11	1.2	8.1	34.3	<	168
206525	Golden Grove	Cullens	CUDD001	494489	6816796	936.25	Lava	73.99	0.41	10.99	4.67	0.03	3.17	0.42	0.08	2.62	0.11	2.96	0.14	0.9	<	18.5	<	<
206534	Golden Grove	Cullens	CUDD001	494489	6816796	565.75	Rhyodacite	73.06	0.43	13.2	1.97	0.03	0.74	1.14	3.04	2.84	0.096	2.64	0.45	0.6	2.8	19.5	<	32
206536	Golden Grove	Cullens	CUDD001	494489	6816796	504.95	Rhyodacite	69.93	0.41	12.72	4.85	0.06	1.8	1.53	3.51	1.75	0.09	2.8	0.39	1.5	6.4	22.3	23	27
206538	Golden Grove	Cullens	CUDD001	494489	6816796	582.15	Rhyodacite	70.15	0.4	12.54	3.43	0.06	1.14	3.13	1.4	3.09	0.09	4.49	0.8	1	2.9	15.1	<	26
206538*	Golden Grove	Cullens	CUDD001	494489	6816796	582.15	Rhyodacite	70.1	0.41	12.42	3.42	0.06	1.14	3.12	1.41	3.09	0.088	4.55	0.85	0.6	2.1	17.1	<	26
206542	Golden Grove	Cullens	CUDD001	494489	6816796	515.9	Rhyodacite	70.21	0.48	14.57	1.98	0.04	0.99	1.67	3.39	3.2	0.103	3.32	0.62	0.8	2.9	15.3	<	27
206543	Golden Grove	Cullens	CUDD001	494489	6816796	429.7	Dacite	66.46	0.46	15.73	2.07	0.05	1.27	2.67	3.96	2.84	0.118	4.46	0.93	1.7	10.5	14.6	75	69
206544	Golden Grove	Cullens	CUDD001	494489	6816796	415.95	Dacite	64.38	0.42	14.44	3.98	0.07	1.68	4.01	3.58	1.96	0.11	4.94	0.96	0.9	48.6	20	63	67
206545	Golden Grove	Cullens	CUDD001	494489	6816796	393	Sediments	72.18	0.29	11.34	6.3	0.08	2.62	1.1	0.1	2.24	0.058	3.52	0.29	1.8	1.1	9.3	<	<
206545*	Golden Grove	Cullens	CUDD001	494489	6816796	393	Sediments	71.9	0.28	11.35	6.29	0.08	2.61	1.1	0.09	2.24	0.055	3.56	0.29	0.5	<	9.8	<	<
206547	Golden Grove	Cullens	CUDD001	494489	6816796	318.7	Dacite	71.12	0.4	13.95	2.94	0.04	1.08	1.27	6.64	0.39	0.107	1.71	0.27	1.6	22.7	28.2	90	53
206548	Golden Grove	Cullens	CUDD001	494489	6816796	295.2	Dacite	69.82	0.47	13.7	3.79	0.05	1.81	1.63	4.29	1.31	0.094	2.73	0.36	2.5	6.7	19.6	33	42
206550	Golden Grove	Cullens	CUDD001	494489	6816796	276.3	Dacite	67.04	0.52	17.23	3.76	0.04	1.2	0.58	6.93	1.25	0.136	1.58	0.07	4.3	14.7	18.8	87	85
206555	Golden Grove	Cullens	CUDD001	494489	6816796	206.4	Rhyolite	68.58	0.49	16.47	2.12	0.02	0.74	1.15	8.56	0.23	0.118	1.4	0.22	1.4	4.8	25.4	89	43
206561	Golden Grove	Scuddles	RHDD034	496041	6821151	465.55	Dacite	62.78	0.46	15.56	4.59	0.06	1.98	3.35	4.4	1.63	0.122	4.41	0.75	1.3	43.5	21.6	75	70
206562	Golden Grove	Scuddles	RHDD034	496041	6821151	489.4	Dacite	66.04	0.46	15.06	3.93	0.06	1.48	3.24	1.61	3.11	0.126	4.75	0.75	1	31.9	13.6	71	71
206563	Golden Grove	Scuddles	RHDD034	496041	6821151	502.7	Rhyodacite	70.54	0.44	13.3	3.92	0.06	2.19	2.26	1.03	2.43	0.097	3.79	0.47	0.7	3.6	15.7	<	31
206565	Golden Grove	Scuddles	RHDD034	496041	6821151	543.7	Rhyodacite	72.97	0.41	12.41	3.16	0.03	1.19	2.25	0.21	3.38	0.093	3.79	0.54	1	3.1	17.3	<	23
206566	Golden Grove	Scuddles	RHDD034	496041	6821151	594.7	Rhyodacite	70.87	0.38	11.43	4.75	0.05	1.99	2.57	0.12	2.81	0.086	4.41	0.66	0.8	3.3	18	<	24
206574	Golden Grove	Scuddles	RHDD034	496041	6821151	715.15	Dacite	66.92	0.38	9.16	10.89	0.14	5.99	1.1	0.03	0.09	0.111	4.64	0.38	2.5	<	15.9	<	14
206570	Golden Grove	Scuddles	RHDD034	496041	6821151	642.3	Rhyodacite	73.29	0.24	9.53	5.86	0.12	3.82	1.76	0.08	1.3	0.033	4.03	0.37	<	3.8	15.6	20	<
206572	Golden Grove	Scuddles	RHDD034	496041	6821151	659.9	Rhyodacite	67.84	0.31	8.9	8.54	0.23	5.18	2.81	0.11	0.26	0.062	5.12	0.68	1.1	5	11.7	<	16
206575	Golden Grove	Scuddles	RHDD034	496041	6821151	732.6	Rhyodacite	63.11	0.46	10.74	14.53	0.17	4.85	0.19	0.06	0.47	0.132	4.48	0.01	8.9	6.3	33.2	<	18
206576	Golden Grove	Scuddles	RHDD034	496041	6821151	735.8	Andesite	38.3	0.58	6.79	8.11	0.23	11.6	15.74	0.06	0.02	0.473	15.01	3.1	34.7	617.8	58.2	959	106
206579	Golden Grove	Scuddles	SC107	493327	6820602	624	Rhyodacite	70.67	0.42	13	4.23	0.06	1.85	2.15	1.53	2.38	0.093	3.02	0.34	<	10.6	22.2	26	26
206579*	Golden Grove	Scuddles	SC107	493327	6820602	624	Rhyodacite	70.5	0.42	12.99	4.22	0.06	1.84	2.15	1.52	2.35	0.097	3.05	0.36	0.6	10.6	22.2	22	29
206584	Golden Grove	Scuddles	SC107	493327	6820602	779.2	Rhyodacite	71.73	0.42	12.99	4.13	0.06	2.3	2.56	1.3	2.46	0.096	1.57	0.12	1.9	6.7	27.7	35	22
209821	Golden Grove	Scuddles	SC098D1	496070	6822730	1499	Rhyodacite	74.46	0.39	12.08	3.98	0.05	2.2	1.19	1.05	2.88	0.088	1.38	<	<	4.5	27	20	20
209828	Golden Grove	Scuddles	SC098D1	496070	6822730	1325.5	Dacite	67.73	0.51	14.78	4.55	0.04	3.84	1.99	2.71	2.15	0.106	1.48	<	<	53.6	29.3	82	76
204833	Weld Range	Glenview	95WGD002	554853	7016607	202.9	Felsic hyaloclastite	62.72	0.62	16.53	5.14	0.1	3.02	0.13	0.08	5.03	0.092	6.25	1.1	62.2	20.1	48.4	44	66
204856	Weld Range	Glenview	95WGD004	555559	7016834	169.1	Rhyodacite	72.94	0.33	12.28	4.84	0.06	3.71	0.09	0.09	2.24	0.075	3.19	0.02	3.7	8.3	22.7	26	25
204857	Weld Range	Glenview	95WGD004	555559	7016834	182.8	Felsic hyaloclastite	77.22	0.3	11.17	3.6	0.04	1.83	0.08	0.12	2.55	0.071	2.44	0.02	29.9	15.3	70.2	29	25
204881	Weld Range	Glenview	95WGD004	555559	7016834	381.3	Felsic hyaloclastite	84.82	0.16	6.51	2.98	0.09	0.81	0.09	0.1	1.81	0.064	2.6	0.54	3.9	4.3	85.9	21	<
204882	Weld Range	Glenview	95WGD004	555559	7016834	392.2	Rhyodacite	74.29	0.44	10.79	6.26	0.05	2.6	0.18	0.1	1.96	0.132	2.44	0.11	1.5	18.2	21.1	37	53
204882*	Weld Range	Glenview	95WGD004	555559	7016834	392.2	Rhyodacite	74.16	0.44	10.89	6.29	0.06	2.61	0.17	0.11	1.97	0.135	2.85	0.11	1.9	18.2	14.1	40	58
204888	Weld Range	Glenview	95WGD004	555559	7016834	433.8	Rhyodacite	79.67	0.31	12.42	1.23	0.01	0.41	0.12	0.18	3.5	0.094	1.95	0.05	9.6	3.6	38.1	<	15
205611	Weld Range	Glenview	96GVDI001	556465	7017100	186.8	Felsic hyal.	75.38	0.21	11.6	5.32	0.23	1.41	0.06	0.17	2.72	0.048	3.28	0.44	3	3.3	29.2	<	<
205615	Weld Range	Glenview	96GVDI001	556465	7017100	206.25	Rhyodacite	80.55	0.15	8.64	1.37	0.08	0.81	1.81	0.2	2.37	0.031	3.91	0.81	1.3	5.9	61.2	37	<
205622	Weld Range	Glenview	96GVDI001	556465	7017100	239.3	Rhyodacite	62.79	0.34	14.59	10.04	0.15	4.59	0.12	0.14	2.19	0.093	4.52	0.26	2.8	8.3	36.5	21	24
205622*	Weld Range	Glenview	96GVDI001	556465	7017100	239.3	Rhyodacite	62.56	0.34	14.6	10.03	0.15	4.6	0.11	0.13	2.19	0.092	4.52	0.26	2.8	8.3	35.8	26	25
205634	Weld Range	Glenview	96GVDI001	556465	7017100	301.25	Felsic hyaloclastite	67.84	0.13	9.5	3.96	0.22	2.03	4.77	0.2	2.48	0.024	8.22	2	1.7	4.5	31.4	27	<
205635	Weld Range	Glenview	96GVDI001	556465	7017100	309.3	Rhyolite	82.1	0.16	7.77	3.86	0.22	0.63	0.08	0.12	2.05	0.057	2.88	0.62	1.2	6.7	42.5	23	15

NOTES: \* Indicates duplicates

Table 1.1. continued

<i>GSWA number</i>	<i>Cu (ppm)</i>	<i>Zn (ppm)</i>	<i>S (%)</i>	<i>Ga (ppm)</i>	<i>Pb (ppm)</i>	<i>Sr (ppm)</i>	<i>Rb (ppm)</i>	<i>Ba (ppm)</i>	<i>Zr (ppm)</i>	<i>Nb (ppm)</i>	<i>Ta (ppm)</i>	<i>Mo (ppm)</i>	<i>Th (ppm)</i>	<i>U (ppm)</i>	<i>Y (ppm)</i>	<i>W (ppm)</i>	<i>Cs (ppm)</i>	<i>La (ppm)</i>	<i>Ce (ppm)</i>	<i>Pr (ppm)</i>	<i>Nd (ppm)</i>	<i>Sm (ppm)</i>	<i>Eu (ppm)</i>	<i>Gd (ppm)</i>	<i>Tb (ppm)</i>	<i>Dy (ppm)</i>	<i>Ho (ppm)</i>
<i>Detection</i>	<i>0.5</i>	<i>1</i>	<i>0.01</i>	<i>0.1</i>	<i>0.5</i>	<i>0.2</i>	<i>0.1</i>	<i>0.5</i>	<i>1</i>	<i>0.1</i>	<i>0.1</i>	<i>0.1</i>	<i>0.5</i>	<i>0.5</i>	<i>0.5</i>	<i>1</i>	<i>0.05</i>	<i>0.2</i>	<i>0.5</i>	<i>0.05</i>	<i>0.1</i>	<i>0.05</i>	<i>0.05</i>	<i>0.05</i>	<i>0.02</i>	<i>0.05</i>	<i>0.02</i>
206501	14.9	48	0.01	14.6	7.7	63.6	78.3	450	136	4.8	0.4	1	4.83	1.3	9.3	63	1.22	15.1	27.2	2.93	10.9	1.92	0.56	1.84	0.25	1.57	0.33
206502	14.6	52	0.01	15.7	7.5	146.8	57.1	525.9	149	5.3	0.4	1	5.31	1.24	10.3	95	1.1	17.2	31.5	3.43	13	2.19	0.69	2.1	0.29	1.86	0.37
206521	<	63	<	14.6	2.5	9.1	0.8	5.5	157	5.4	0.3	0.4	3.12	0.76	30.4	24	0.33	14.8	30.7	3.7	16.3	3.02	1.06	3.55	0.6	4.38	1.12
206525	3	78	<	13.9	3.6	12.2	50.3	562.3	261	8.7	0.6	0.2	5.79	1.28	41.3	110	1	23.2	47.9	5.69	23.7	4.55	1.16	4.92	0.87	6.07	1.52
206534	73.9	33	0.02	14	5.7	40.9	69.9	551.5	297	12.3	0.8	0.9	8.76	1.84	42.9	134	1.42	28.3	56.9	6.5	27.1	5.33	0.83	5.37	0.9	6.56	1.55
206536	7.6	84	0.01	15.1	7.4	51.5	40	621	293	11.3	0.8	3.8	8.34	2.09	50.7	99	1.14	26	52.7	6.19	25.3	4.7	0.99	6.08	1.04	7.38	1.73
206538	22.3	72	0.02	14.5	6.7	38.9	74.2	460.3	278	11.5	0.8	0.3	8.08	1.89	49.1	79	1.5	30.5	60.6	7.03	28.2	5.57	1.05	6.25	1.08	7.27	1.64
206538*	22	69	0.02	13.9	9.8	39.8	74.8	477.3	286	11.4	0.8	0.3	8.13	1.9	49.4	79	1.5	29.9	59.4	6.88	28.4	5.29	0.99	6.12	1.05	7.45	1.7
206542	15.8	36	<	15.9	15.5	41.9	77	695.1	336	13.7	0.9	3.6	9.67	2.3	56	100	1.26	27.4	56.7	6.78	28.6	6	1.26	6.88	1.21	8.67	1.99
206543	4.6	55	<	18	8.4	75.8	80.4	597	183	6.5	0.5	0.2	6.83	1.5	11.1	65	1.41	22.7	41.9	4.44	16.5	2.74	0.74	2.55	0.34	2.17	0.45
206544	12.6	91	0.02	15.7	6.4	120.8	59.6	441.2	171	5.9	0.4	0.1	6.09	1.47	11.8	49	1.04	20	36.5	3.79	14.3	2.26	0.75	2.27	0.32	1.98	0.47
206545	39.6	149	0.02	15.2	7.4	66.7	70.4	327.4	335	12.1	0.8	0.5	7.35	1.73	74.7	54	1.31	28.8	61.2	7.33	31.4	6.55	1.51	8.11	1.46	11	2.64
206545*	42	161	<	15.2	6.8	65.2	69.6	327	342	12.3	0.7	0.5	7.13	1.77	74.8	55	1.25	28.7	59.6	7.32	31.5	6.44	1.46	7.84	1.44	10.53	2.66
206547	23.6	75	0.11	13.1	9.1	165.7	11.3	157.5	165	5.9	0.4	0.5	5.81	1.4	11	129	0.37	19	33.8	3.54	13.8	2.24	0.67	2.13	0.32	1.98	0.42
206548	55.6	100	0.04	14.9	13.4	171	44.5	810.3	276	11	0.7	1.6	8.07	1.95	42.6	94	0.91	27.3	52.7	5.97	24.7	4.73	0.9	5.27	0.88	6.25	1.44
206550	9.4	83	0.23	20.9	8.8	125.6	40.7	754.3	203	7.7	0.5	1.9	7.44	1.71	14.9	86	0.83	21.9	40.9	4.38	16.4	2.85	0.83	2.83	0.36	2.29	0.49
206555	<	56	<	13.4	4.7	135.8	9	52	203	6.9	0.5	0.1	6.81	1.28	15.7	158	0.29	21.4	38.7	4.04	15.4	2.64	0.85	2.56	0.4	2.6	0.55
206561	24	59	0.02	16.4	5.9	117.2	48	263.9	179	7	0.5	0.4	7.07	1.72	13.3	60	0.79	22.9	41.9	4.43	16.8	2.99	0.93	2.66	0.41	2.3	0.48
206562	5.8	60	<	16.3	8.7	49.7	81.9	479.7	178	6.7	0.5	0.3	6.81	1.63	12.4	43	1.38	19.9	36.7	3.85	14.8	2.75	0.77	2.32	0.32	2.12	0.4
206563	21.2	71	0.01	14.6	10	59.5	77.4	348.9	282	11.8	0.7	1.2	8.32	2.05	44.7	65	1.25	28.9	57.4	6.86	27.4	5.42	1.01	5.95	0.98	6.6	1.63
206565	35	99	<	14.2	7.1	32.5	75.6	260.3	287	11.8	0.8	0.5	8.19	1.85	38.3	91	1.68	27	55	6.42	26.6	5.1	0.98	5.26	0.9	6.27	1.39
206566	15	85	<	12.5	6.3	30.3	59.1	231.2	257	10.3	0.7	1.3	7.67	1.82	42.2	85	1.48	26	51.9	5.96	24.7	4.84	0.93	5.16	0.94	6.34	1.49
206574	183.9	331	0.03	15.1	3.8	6.3	2.2	55.9	194	7.2	0.4	0.6	4.79	1.27	40.9	59	0.3	18.7	38.9	4.59	19.5	3.74	1.22	4.4	0.81	5.69	1.42
206570	43.3	202	0.01	12.1	7.6	16.9	37.7	244.7	229	9	0.6	0.7	5.46	1.46	46.9	94	0.56	26.7	55.8	6.51	26.1	5.47	1.24	5.92	1.06	7.63	1.74
206572	119.6	373	0.04	11.1	11.9	14.4	6.8	87.1	168	6.8	0.5	0.2	4.04	1.11	39.8	52	0.28	20.5	44.1	5.11	20.4	4.43	1.08	5.55	1.01	6.43	1.64
206575	20.1	493	1.63	12.2	13.6	6	9.9	108.1	181	6.9	0.4	2.7	4.51	1.18	41.6	94	0.33	14.2	29.9	3.66	14.2	3.57	1.03	4.6	0.98	6.67	1.63
206576	268.3	1831	1.47	7.5	<	73.4	1.3	7.4	99	38.2	1.2	0.2	13.02	1.55	17.7	25	0.64	89.2	189.3	22.24	79.4	10.82	1.43	6.54	0.72	3.7	0.69
206579	40.2	82	0.01	13.1	35.8	38.9	66.5	471.2	233	10.5	0.8	1.3	7.49	1.78	44	83	1.21	29.5	58.7	6.68	25.9	5.31	1.01	6.06	1.06	6.79	1.64
206579*	41	71	0.02	13.9	17.6	40.9	69.3	467.6	251	10.8	0.8	1.4	8.09	1.96	46.3	86	1.02	30.5	60.9	7.08	27.5	5.49	0.9	5.88	1.09	6.92	1.78
206584	29.3	62	0.01	13.4	10.2	28.3	75.2	302.1	229	9.9	0.7	0.7	7.07	1.84	40.4	128	1.53	27.6	56.5	6.39	24	5.35	0.96	5.4	0.99	6.25	1.52
209821	10.8	66	0.01	12.7	9.2	26	64.7	303.1	215	9.5	0.7	0.6	7.02	1.52	39.3	147	3.18	24.1	48.1	5.57	20.8	4.36	0.82	5.17	0.91	6.17	1.53
209828	<	57	0.01	16	8.3	81.1	46.7	425.3	164	6.1	0.5	<	5.94	1.46	13.8	95	2.2	21.6	40.9	4.47	16.7	3.47	0.81	2.92	0.48	2.57	0.57
204833	520.1	207	0.54	18.8	64.5	3.4	104.5	478.1	215	10.1	0.9	2.4	11.25	2.89	29.7	196	1.58	28.6	55.3	6.15	22.9	4.94	0.81	5.18	0.84	5.02	1.09
204856	1.4	212	0.03	13.8	6.1	6.5	54.7	269.4	191	8.1	0.8	1.8	13.68	3.43	28.9	97	2.12	28.8	57.4	6.28	22.3	4.84	0.64	4.65	0.81	4.96	0.98
204857	3.9	118	0.5	12.5	16.2	6.3	61.6	324.8	183	8.3	0.8	1.9	13.39	3.52	35.5	387	1.52	29.8	59.5	6.43	23.3	4.59	0.81	5.33	0.96	5.45	1.24
204881	635.9	25	0.16	6.4	7.3	5.6	46.9	344.6	88	3.3	0.3	0.2	2.96	0.72	12.5	522	0.94	8.2	17.2	2	7.7	1.81	0.42	2.17	0.39	2.14	0.46
204882	320.7	148	0.04	12.4	5.7	5.2	49	469.1	106	4.6	0.3	0.9	2.79	0.83	12.1	69	1.05	8.3	18.7	2.24	9.1	2.18	0.45	2.39	0.43	2.27	0.44
204882*	355.5	151	0.04	12.5	8.1	5.3	49.8	474.6	106	4.7	0.4	0.9	2.93	0.85	13.3	45	1.15	7.7	16.6	2	8.5	1.89	0.43	2.36	0.42	2.22	0.51
204888	8.6	17	0.19	14.2	7	9	81.8	723.2	174	9.2	0.8	1.9	11.87	2.56	30.8	203	2.33	29.6	60.5	7.03	25	5.6	1.08	5.79	0.96	5.45	1.16
205611	1.3	54	0.03	13.2	3	8.3	64.8	360.6	210	7.8	0.6	1.5	7.25	1.86	24.1	187	1.39	21.5	43.4	4.94	18.1	3.37	1.02	3.97	0.69	4.03	0.9
205615	2	21	<	6.7	10.3	10.6	53.4	347.9	137	6.1	0.6	<	9.53	2.49	28.7	373	1.57	22.9	44.3	4.74	17.3	3.47	0.69	4.43	0.83	5.03	1.03
205622	1.5	301	0.02	16.7	7.9	5.1	55.2	421.4	234	10.3	0.9	0.6	13.03	3.15	39.8	177	0.88	32	63.8	7.2	26.2	5.69	0.92	6.05	1.09	6.58	1.46
205622*	1.2	308	0.02	15.9	6.9	5.2	55.2	421.3	238	10.2	0.8	0.6	13.47	3.31	39.9	179	0.78	31.2	62.2	6.79	26.4	5.76	0.91	5.74	1.13	6.42	1.33
205634	14.8	34	0.07	8.9	6.7	16.9	56.4	406.9	132	6.5	0.6	0.4	10.39	2.45	26.1	183	1.27	28.3	53.6	5.85	20.2	4.34	0.82	4.17	0.79	4.47	0.98
205635	1.1	25	0.01	7.2	3	5.7	49.7	303.4	94	4.4	0.5	0.2	8.44	2.04	14.9	263	0.88	15.9	31.3	3.5	12.4	2.46	0.54	2.11	0.43	2.48	0.54

NOTE: \* Indicates duplicates

Table 1.1. continued

GSWA number	Er (ppm)	Tm (ppm)	Yb (ppm)	Lu (ppm)	Re (ppm)	SO <sub>3</sub> (%)	Ge (ppm)	Hf (ppm)	Ti (ppm)	Sb (ppm)	Se (ppm)	Sn (ppm)	BaO (%)	Be (ppm)	Bi (ppm)	Cd (ppm)	In (ppm)	Li (ppm)	Te (ppm)	Ag (ppm)
Detection	0.05	0.05	0.05	0.2	0.002	0.002	0.05	0.1	0.02	0.05	0.5	1	0.005	0.05	0.01	0.02	0.005	0.1	0.05	0.01
206501	0.96	0.19	0.91	0.15	0.006	0.014	0.69	3.3	0.44	0.42	<	2	0.047	0.87	0.03	0.11	0.023	16.3	0.07	0.07
206502	0.98	0.23	0.91	0.18	0.005	0.006	0.69	3.7	0.2	1.05	0.7	2	0.057	1.08	0.04	0.14	0.024	13.5	0.09	0.1
206521	3.36	0.61	3.79	0.7	0.008	<	0.81	3.9	<	0.25	0.7	2	<	0.73	0.02	0.07	0.064	34	0.06	0.02
206525	4.74	0.75	5.27	89	0.005	0.01	0.77	6.5	0.15	0.19	0.8	2	0.065	1.34	0.05	0.09	0.075	14.6	0.06	0.05
206534	4.66	0.74	5.1	0.91	0.008	0.031	0.93	7.5	0.16	0.24	0.8	4	0.055	1.53	0.04	0.13	0.056	3.6	0.06	0.26
206536	5.46	0.88	6.04	0.97	0.008	0.023	0.98	7.6	0.11	0.22	0.8	3	0.065	1.11	0.04	0.1	0.041	11.8	0.05	0.19
206538	5.2	0.9	5.38	0.94	0.007	0.036	1.06	7.1	0.17	0.3	0.7	3	0.049	1.45	0.05	0.1	0.054	9.5	0.09	0.18
206538*	5.06	0.83	5.4	0.94	0.007	0.034	0.95	7.4	0.18	0.31	1	3	0.051	1.35	0.06	0.1	0.057	9.5	0.07	0.05
206542	5.88	0.97	6.3	1.09	0.005	0.01	0.87	8.3	0.18	0.21	0.5	4	0.072	1.63	0.15	0.14	0.064	5.6	0.06	0.31
206543	1.15	0.21	0.89	0.17	0.007	0.019	0.75	4.5	0.21	0.31	<	2	0.067	0.99	0.03	0.13	0.026	4.5	<	0.11
206544	1.22	0.2	1.03	0.19	0.005	0.034	0.75	4.1	0.15	0.31	0.7	2	0.046	1.02	0.02	0.1	0.024	14.7	<	0.03
206545	8.17	1.35	9.13	1.52	0.007	0.025	1.02	8.3	0.21	0.34	0.8	3	0.039	1.47	0.09	0.08	0.118	23.8	0.09	0.09
206545*	8.28	1.34	9.03	1.49	0.005	0.025	1.14	8.4	0.22	0.36	0.5	3	0.036	1.29	0.08	0.1	0.117	25.1	0.09	0.11
206547	1.13	0.18	0.95	0.19	0.006	0.268	0.74	4	0.08	0.64	0.9	2	0.016	0.72	0.16	0.13	0.023	9.6	0.08	0.09
206548	4.56	0.74	4.74	0.78	0.005	0.091	1.07	6.9	0.41	1.01	0.7	4	0.09	1.49	0.14	0.12	0.058	14.4	0.08	0.09
206550	1.48	0.23	1.38	0.25	0.007	0.524	1.31	4.7	0.56	1.73	0.8	3	0.08	1.51	0.17	0.14	0.05	9.3	0.06	0.18
206555	1.43	0.24	1.25	0.2	0.008	0.002	0.81	5	0.14	3.31	1	2	<	0.81	0.02	0.07	0.022	8.8	0.08	0.03
206561	1.29	0.25	1.28	0.23	0.005	0.03	0.72	4.3	0.18	0.61	0.9	2	0.026	1.18	0.02	0.08	0.027	17.5	0.07	0.04
206562	1.2	0.21	1.13	0.21	0.005	0.003	0.81	4.2	0.32	0.47	0.6	2	0.052	1.28	0.03	0.09	0.028	14.6	0.07	0.03
206563	4.91	0.83	5.39	0.88	0.006	0.02	1	7.2	0.3	0.52	<	3	0.039	1.44	0.05	0.13	0.061	23.1	0.07	0.03
206565	4.28	0.69	4.69	0.81	0.007	0.012	0.9	7.2	0.25	0.62	0.9	3	0.03	1.45	0.03	0.11	0.048	10.3	0.06	0.1
206566	4.49	0.77	5.01	0.85	0.006	0.006	1.01	6.6	0.27	0.71	<	3	0.031	1.09	0.04	0.11	0.05	14.2	0.07	0.07
206574	4.46	0.75	5.06	0.87	0.005	0.081	0.9	4.8	0.07	0.98	0.8	4	<	0.67	1.32	0.41	0.187	16	1.55	1.34
206570	5.81	0.94	6.71	1.2	<	0.029	0.98	6.3	0.35	0.78	<	2	0.029	1.19	0.02	0.05	0.089	27.6	<	0.87
206572	4.94	0.8	5.23	0.88	<	0.102	0.83	4.8	0.11	2.41	<	1	0.011	0.62	0.08	0.16	0.12	50.1	<	1.87
206575	5.04	0.84	5.47	0.98	<	4.702	1.25	4.9	0.65	2.72	<	2	0.01	1.19	0.05	0.09	0.044	33.1	0.05	0.53
206576	1.88	0.29	1.57	0.27	<	4.029	0.73	2.8	0.13	61.12	<	1	<	0.85	0.1	2.81	0.015	8.9	<	13.14
206579	5.37	0.78	5.72	0.92	<	0.021	0.91	6.5	0.23	0.64	<	3	0.051	1.52	0.09	0.14	0.061	13.8	<	0.28
206579*	5.5	0.85	5.92	0.98	<	0.019	0.91	6.6	0.23	0.47	<	3	0.049	1.44	0.09	0.1	0.057	14.1	<	0.54
206584	5.01	0.8	5.5	0.91	<	0.014	1.02	6.7	0.28	0.59	<	2	0.032	1.42	0.03	0.04	0.058	19.4	<	0.03
209821	5.09	0.82	5.63	0.92	<	0.024	0.86	6.3	0.22	0.22	<	3	0.034	1.15	0.02	0.03	0.047	18.1	<	0.79
209828	1.56	0.27	1.49	0.28	<	0.004	0.87	4.5	0.13	0.47	<	2	0.05	1.16	0.02	<	0.031	36.4	<	0.11
204833	3.39	0.53	3.25	0.44	<	1.351	0.82	6.4	1.43	6.66	<	7	0.053	1.52	3.04	0.57	0.052	7	<	1.54
204856	3.18	0.53	2.98	0.5	<	0.076	0.84	5.5	0.5	2.55	<	10	0.027	0.96	0.08	-0.02	0.043	23.4	<	0.18
204857	3.8	0.59	3.58	0.57	0.003	1.248	0.86	5.2	0.7	5.82	<	12	0.032	1.18	0.41	0.08	0.046	12.5	<	0.35
204881	1.31	0.2	1.14	0.18	0.003	0.383	1.16	2.3	0.2	4.9	0.8	17	0.043	0.57	0.89	0.64	0.113	1.7	0.08	0.97
204882	1.37	0.25	1.25	0.26	<	0.107	1.16	3.1	0.23	3.81	<	4	0.053	0.7	0.65	0.34	0.118	25.9	<	0.64
204882*	1.42	0.23	1.34	0.24	<	0.115	1.05	3	0.23	3.32	0.5	4	0.055	0.8	0.64	0.21	0.12	26.8	<	0.65
204888	3.53	0.53	3.28	0.51	<	0.493	1.07	4.9	0.35	3.64	<	2	0.077	1.3	0.5	<	0.047	2.2	<	0.18
205611	2.61	0.45	2.93	0.42	<	0.063	0.92	5.9	0.35	1.39	<	3	0.039	1.23	0.07	<	0.052	9.8	<	0.02
205615	3.1	0.46	2.81	0.44	0.003	0.005	0.6	4.2	0.27	1.19	<	4	0.036	0.7	0.07	0.04	0.038	0.9	<	0.27
205622	4.62	0.64	4.21	0.68	<	0.037	1.17	6.9	0.25	1.79	<	7	0.042	0.95	0.05	0.05	0.037	35.2	<	0.08
205622*	4.31	0.66	4.09	0.68	<	0.036	1.16	6.8	0.24	1.85	<	7	0.04	1.3	0.04	<	0.039	37	<	0.07
205634	2.94	0.46	2.87	0.52	<	0.169	0.56	4.2	0.28	1.48	<	4	0.047	0.7	0.23	0.16	0.045	3.2	<	0.28
205635	1.63	0.29	1.6	0.28	<	0.013	0.89	2.9	0.21	0.89	<	2	0.026	0.64	0.02	<	0.02	2.6	<	0.07

NOTE: \* Indicates duplicates



Table 1.2. Major and trace-element geochemistry for recorded and measured standards

Sample	Al <sub>2</sub> O <sub>3</sub> (%)	CaO (%)	Fe <sub>2</sub> O <sub>3</sub> (%)	K <sub>2</sub> O (%)	MgO (%)	MnO (%)	Na <sub>2</sub> O (%)	P <sub>2</sub> O <sub>5</sub> (%)	SiO <sub>2</sub> (%)	SO <sub>3</sub> (%)	TiO <sub>2</sub> (%)	Ba (ppm)	Ce (ppm)	Cr (ppm)	Cs (ppm)	Dy (ppm)	Er (ppm)	Eu (ppm)	Ga (ppm)	Gd (ppm)	Hf (ppm)	Ho (ppm)	La (ppm)	Lu (ppm)	Nb (ppm)	Nd (ppm)	Pr (ppm)
BB1 standard	15.33	8.71	12.22	0.46	4.72	0.16	3.03	0.25	51.82	0.16	2.02	152	26.8	150	0.2	7.27	3.95	2.01	23	7.26	4	1.46	10.95	0.49	7.6	18.75	3.63
BB1 measured	15.55	8.75	12.3	0.45	4.69	0.16	3.13	0.246	52.39	0.15	2.08	158.2	28.8	153	0.4	7.01	3.69	2.02	22.3	7.53	4.1	1.49	11.8	0.54	7.3	18.3	3.92
BB1 measured	15.54	8.76	12.32	0.45	4.68	0.16	3.12	0.244	52.41	0.15	2.07	156.5	27.4	156	0.41	6.84	3.67	2	21.4	7.06	4.2	1.47	11.4	0.46	6.9	19.4	3.96
BB1 measured	15.53	8.77	12.35	0.46	4.67	0.16	3.09	0.242	52.52	0.15	2.08	158.9	27.6	252	0.35	7.66	3.99	2.14	23.7	7.93	4.4	1.57	11.2	0.5	8	20.1	3.96
BB1 measured	15.59	8.73	12.28	0.45	4.68	0.16	3.1	0.244	52.44	0.14	2.07	157.6	27.7	245	0.36	7.76	4.08	2.13	23.5	8.16	4.6	1.61	11.2	0.51	7.9	20.5	3.97
KG1 standard	14.95	2.16	2.08	3.47	0.48	0.04	4.07	0.08	71.37	0.03	0.24	1373	71.3	170	2.2	0.8	0.4	0.8	20	1.5	5	0.1	43.8	0.1	9.5	22.4	6.6
KG1 measured	15.07	2.15	2.07	3.47	0.48	0.04	4.22	0.069	71.66	0.01	0.23	1448	72	227	2.12	0.91	0.49	0.7	21	1.58	5.5	0.2	43.6	0.09	10.5	23.9	6.97
KG1 measured	15.04	2.13	2.07	3.47	0.46	0.04	4.22	0.067	71.32	0.01	0.24	1430.6	72.4	214	2.17	0.93	0.49	0.69	20	1.55	5.2	0.18	43.3	0.09	10.6	23.6	7.07
KG1 measured	15.15	2.14	2.06	3.48	0.47	0.04	4.22	0.067	71.54	0.01	0.24	1407.6	75.3	182	2.11	0.82	0.49	0.79	19.6	1.48	5.8	0.16	45.7	0.09	9.3	22.7	7.33
MW1 standard	4.39	3.68	9.7	0.04	31.24	0.15	0.04	0.02	40.52	0.07	0.22	24.1	2.3	2128	0.9	0.85	0.54	0.19	4.9	0.76	0.37	0.19	0.96	0.08	0.49	1.55	0.31
MW1 measured	4.39	3.68	10.09	0.04	31.26	0.15	0.11	0.019	40.72	0.08	0.22	27.5	2.7	2188	0.93	0.96	0.56	0.18	4.6	0.78	0.4	0.23	1	0.1	0.4	1.9	0.36

NOTES: BB = Bunbury Basalt KG1 = Kerba Monzogranite MW1 = Murphy Well Komatiite

Table 1.2. continued

Sample	Rb (ppm)	Sm (ppm)	Sn (ppm)	Sr (ppm)	Ta (ppm)	Tb (ppm)	Th (ppm)	Tl (ppm)	Tm (ppm)	U (ppm)	V (ppm)	W (ppm)	Y (ppm)	Yb (ppm)	Zr (ppm)	Ag (ppm)	As (ppm)	Cd (ppm)	Co (ppm)	Cu (ppm)	Mo (ppm)	Ni (ppm)	Pb (ppm)	Sc (ppm)	Zn (ppm)
BB1 standard	12.4	5.69	1.8	245	0.5	1.22	1.8	-0.1	0.53	0.3	245	-0.3	39.8	3.32	153	0.1	5.2	-	37	82	1.8	41	4.4	27.7	116
BB1 measured	11.4	5.87	2	240	0.5	1.21	1.78	0.09	0.51	0.34	246	<	35.2	3.27	141	0.06	4.5	0.13	37.8	74.3	2.2	40	4	26	113
BB1 measured	10.7	5.61	2	232.5	0.4	1.2	1.7	0.09	0.5	0.32	247	1	34.1	3.07	136	0.05	4.9	0.16	37.5	74.4	2.3	41	4.3	26	114
BB1 measured	12	5.55	3	264.1	0.5	1.26	1.94	0.1	0.59	0.37	260	<	41.7	3.16	172	0.11	4.5	0.19	35.4	72.1	2	39.9	4.5	18	114
BB1 measured	11.9	5.67	3	264.7	0.5	1.31	1.91	0.1	0.58	0.38	257	<	41.5	3.35	173	0.15	4.2	0.16	37	71.4	2.1	36.9	4.1	18	113
KG1 standard	96	2.8	1.8	515	1	0.2	17.4	-	-	4.2	14.6	-	4.5	0.5	190	0.01	1	-	-	6.2	1.7	8	40	2.4	41
KG1 measured	101.3	2.98	3	592.4	1	0.18	17.97	0.47	0.09	4.47	17	<	5.1	0.48	221	0.1	0.9	0.09	3.4	3.9	1.9	2.5	48.7	<	48
KG1 measured	100.1	2.78	3	576.4	1	0.18	18.26	0.49	0.11	4.3	17	<	5	0.4	216	0.05	0.8	0.08	3.4	3.9	2.2	3	38.9	<	52
KG1 measured	94.5	2.9	2	532.1	1	0.18	16.77	0.52	0.13	4.01	16	<	4.6	0.5	203	0.09	0.8	0.03	4.5	6.6	2.6	7	<	<	51
MW1 standard	1.8	0.5	0.2	13.6	-0.08	0.14	0.12	-0.5	0.09	0.04	85	0.18	5.2	0.54	13	0.4	1	0.13	104	122	0.5	1779	3.9	18	82
MW1 measured	2	0.71	<	13.8	<	0.15	0.17	0.02	0.06	0.1	92	<	4.5	0.5	15	0.11	<	0.16	109.1	146.3	0.7	1779.3	4	18	82

NOTES: BB = Bunbury Basalt KG1 = Kerba Monzogranite MW1 = Murphy Well Komatiite

## Appendix 2 – SEM

Results of SEM analysis on white mica and chlorite samples from Golden Grove and Glenview. The results were compared with white mica and chlorite species depicted by HyLogger analysis.

Table 2.1. SEM data for white mica from Golden Grove

GSWA number	SWIR mineral	Drillhole	Depth (m)	SiO <sub>2</sub>	Al <sub>2</sub> O <sub>3</sub>	K <sub>2</sub> O	Na <sub>2</sub> O	FeO	MgO	TiO <sub>2</sub>	SO <sub>2</sub>	ZnO	CaO
206540	Muscovite	CUDD001	564.6	48.47	30.57	7.89	-	8.44	3.8	0.82	-	-	-
				46.87	29.68	6.11	-	11.16	6.18	-	-	-	-
				51.89	32.73	10.44	-	3.99	-	0.95	-	-	-
				53.77	32.35	10.55	-	3.32	-	-	-	-	-
				50.85	29.34	10.28	-	7.53	-	1.99	-	-	-
	Averages			50.37	30.93	9.05	-	6.89	2.0	0.75	-	-	-
209847	Paragonite	GG274	1018.8	47.78	36.85	7.72	3.02	1.8	-	-	2.83	-	-
				48.42	37.48	8.05	2.25	1.67	-	-	2.13	-	-
				47.79	38.11	7.75	2.58	1.53	-	-	2.23	-	-
				48.44	37.58	7.99	-	2.56	-	-	3.42	-	-
				48.95	36.95	6.88	2.8	1.85	-	-	2.58	-	-
	Averages			48.28	37.39	7.68	2.13	1.88	-	-	2.64	-	-
209855	Paragonite	GG274	952.5	52.68	36.34	10.07	-	0.9	-	-	-	-	-
				49.19	36.43	9.86	-	1.26	-	-	1.07	2.19	-
				51.04	37.26	10.52	-	1.18	-	-	-	-	-
				51.74	36.91	10.14	-	1.21	-	-	-	-	-
				52.59	36.07	9.92	-	1.42	-	-	-	-	-
	Averages			50.23	34.96	9.8	5.75	-	-	-	-	-	8.42
				34.95	8.62	1.02	1.06	1.47	-	-	-	-	-
			52.38					-	-	0.15	0.31	1.20	-
209858	Paragonite	GG274	945.9	50.56	38.23	10.07	-	1.14	-	-	-	-	-
				52.37	38.43	9.2	-	-	-	-	-	-	-
				48.83	37.99	9.49	-	1.11	-	-	-	2.59	-
				51.17	38.81	10.03	-	-	-	-	-	-	-
				51.65	38.21	10.13	-	-	-	-	-	-	-
	Averages		50.92	38.33	9.78	-	0.45	-	-	-	0.518	-	-

**Table 2.2. SEM data for chlorite from Golden Grove**

<i>GSWA number</i>	<i>SWIR mineral</i>	<i>Drillhole</i>	<i>Depth (m)</i>	<i>SiO<sub>2</sub></i>	<i>Al<sub>2</sub>O<sub>3</sub></i>	<i>FeO</i>	<i>MgO</i>	<i>TiO<sub>2</sub></i>	<i>SO<sub>2</sub></i>	<i>ZnO</i>
209846	Fe-chlorite	GG274	1022.8	29.01	27.31	28.28	7.46	-	4	-
				29.17	27.79	29.67	8.25	-	2.95	2.16
				27.76	26.26	37.74	6.58	-	-	1.67
				28.63	27.99	33.93	6.79	-	-	2.66
				27.98	26.92	35.27	7.05	-	-	2.78
				27.43	26.28	37.35	6.27	1.31	-	1.36
				Averages	28.33	27.09	33.71	7.07	0.22	1.16
	209842	FeMg-chlorite	GG274	1049.2	32.61	25.76	25.05	15.97	-	-
31.1					25.24	24.73	15.37	-	-	-
32.67					25.31	25.09	16.4	-	-	-
32.36					25.74	26.67	14.72	-	-	-
32.59					24.34	25.92	15.51	-	-	-
32.44					24.7	28.13	13.96	-	-	-
Averages					32.3	25.18	25.93	15.32	-	-

**Table 2.3. SEM data for white mica from Glenview**

<i>GSWA number</i>	<i>SWIR mineral</i>	<i>Drillhole</i>	<i>Depth (m)</i>	<i>SiO<sub>2</sub></i>	<i>Al<sub>2</sub>O<sub>3</sub></i>	<i>K<sub>2</sub>O</i>	<i>Na<sub>2</sub>O</i>	<i>FeO</i>	<i>MgO</i>	<i>SO<sub>2</sub></i>
204831	Muscovite	95WGD002	210.2	53.76	35.86	10.38	-	-	-	-
				52.8	35.15	12.04	-	-	-	-
				53.5	35.34	11.16	-	-	-	-
				53.18	35.28	11.54	-	-	-	-
				54.24	34.08	10.62	-	1.06	-	-
				51.32	35.43	10.64	-	-	2.61	-
				53.34	34.99	11.47	-	-	-	-
				51.07	34.7	10.7	-	1.22	2.31	-
				52.91	34.33	10.29	-	-	2.46	-
	Averages									
			52.9	35.0	11.0	-	0.25	0.82	-	
204842	Musc/phengite	95WGD002	163.2	51.48	28.8	9.05	-	2.88	4.62	3.17
				54.22	27.51	8.24	-	2.68	3.88	3.2
				53.01	27.86	7.94	1.35	2.59	4.38	2.87
				49.44	30.02	9.05	-	2.89	3.31	4.65
				48.96	31.14	9.6	-	3.01	3.92	3.36
				Averages						
			51.422	29.066	8.776	0.27	2.81	4.022	3.45	
205614	Paragonite	96GVDI001	203.8	50.46	30.76	10.37	2.2	1.8	-	4.41
				53.35	34.88	9.12	1.37	1.28	-	-
				58.22	30.97	8.84	-	1.96	-	-
				51.95	34.25	10	-	3.8	-	-
				64.27	28.2	7.53	-	-	-	-
				74.82	20.26	4.92	-	-	-	-
				52.18	35.57	10.56	-	1.68	-	-
				60.19	29.74	8.52	-	1.55	-	-
				53.49	35.58	9.3	-	1.63	-	-

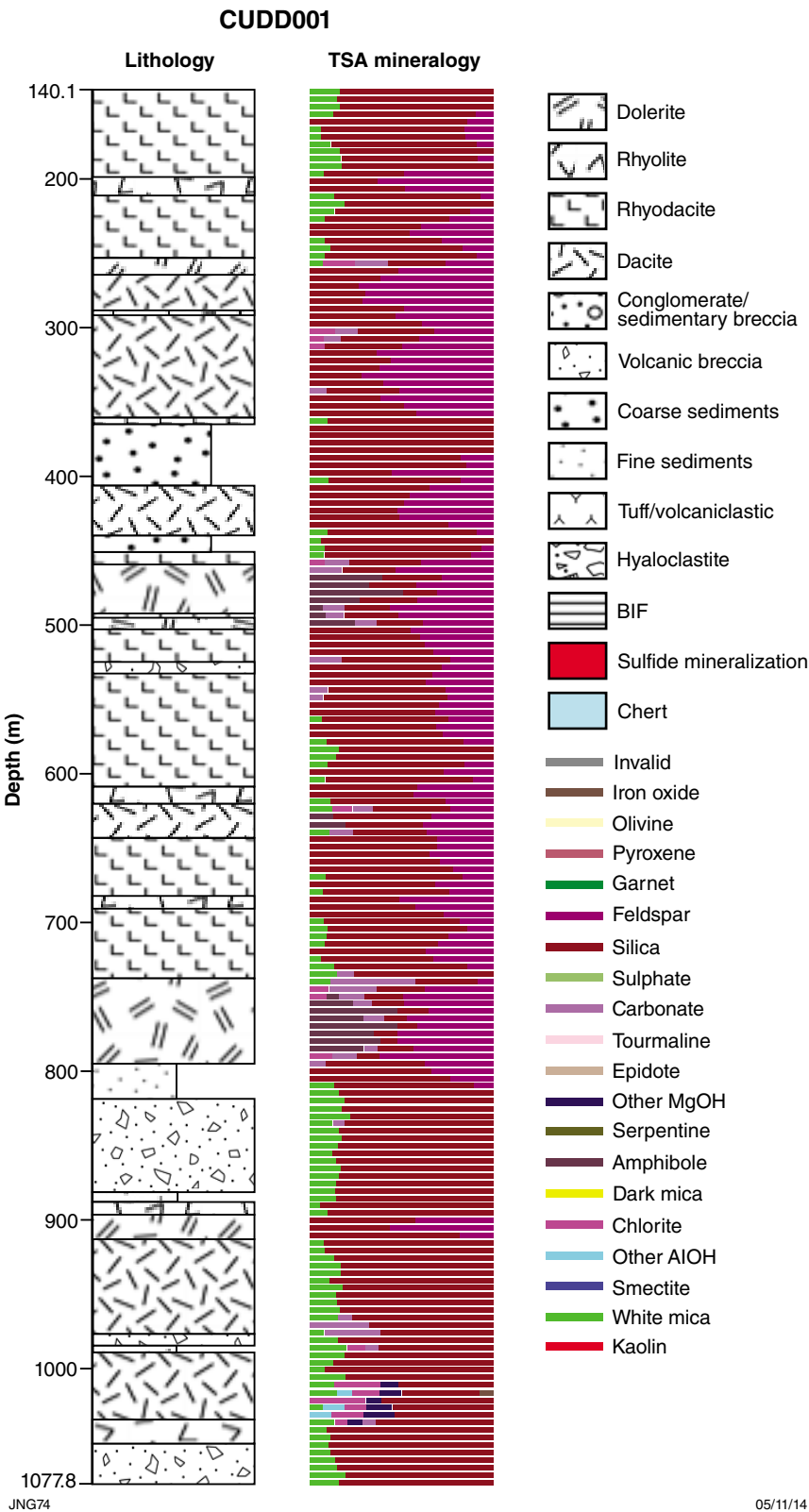
Table 2.3. continued

GSWA number	SWIR mineral	Drillhole	Depth (m)	SiO <sub>2</sub>	Al <sub>2</sub> O <sub>3</sub>	K <sub>2</sub> O	Na <sub>2</sub> O	FeO	MgO	SO <sub>2</sub>
				56.31	33.14	8.4	-	2.15	-	-
				54.54	34.21	9.57	-	1.68	-	-
				53.25	35.21	9.66	-	1.88	-	-
	Averages			56.92	31.9	8.9	0.3	1.62	-	0.37
205618	Paragonite	96GVDI001	221.5	50.68	37.98	9.8	-	1.54	-	-
				49.14	38.73	9.63	-	1.29	-	1.21
				48.88	36.96	9.21	-	2.22	-	2.74
				49.71	38.54	9.7	-	2.06	-	-
	Averages			49.6	38.05	9.59	-	1.78	-	0.99

Table 2.4. SEM data for chlorite from Glenview

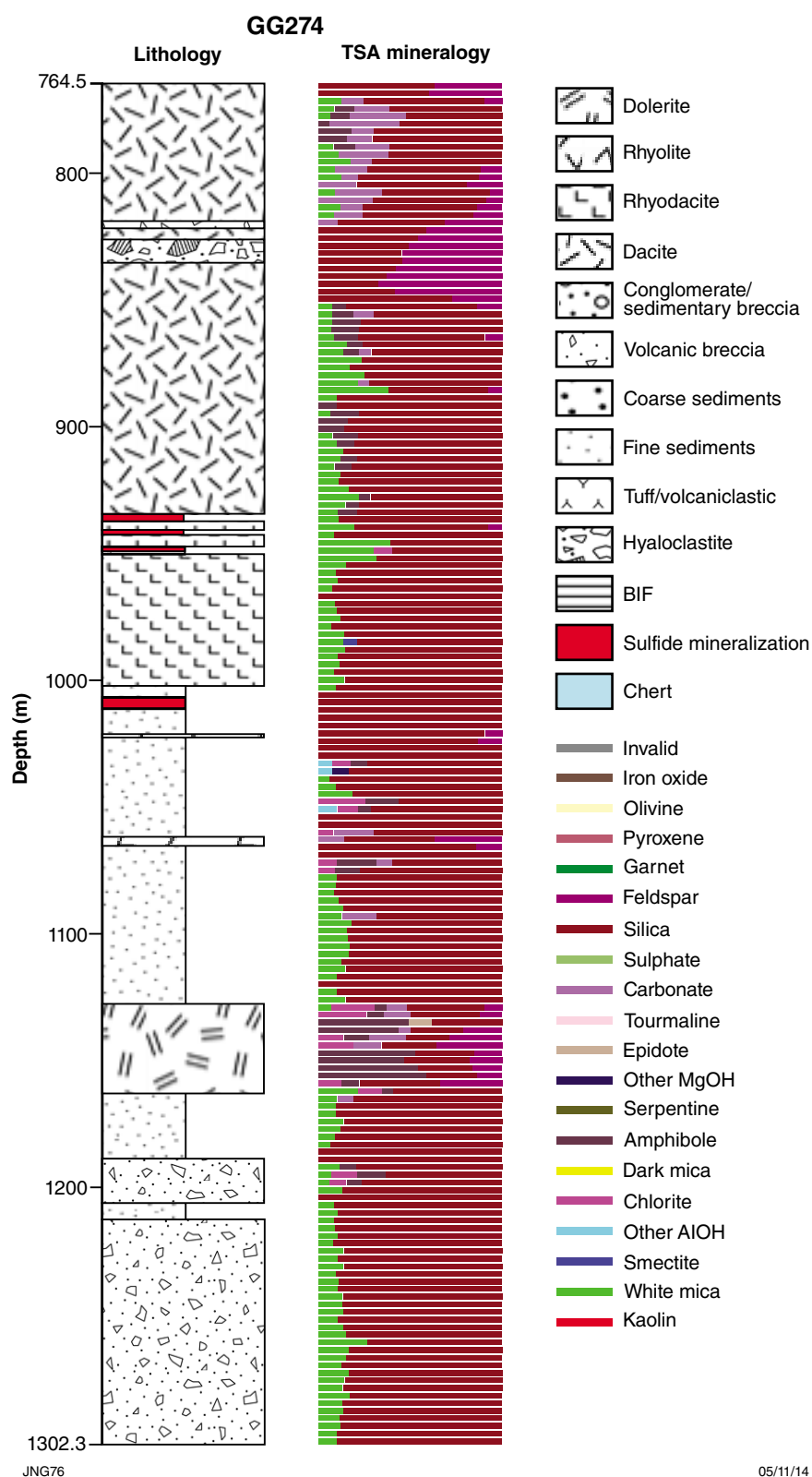
GSWA number	SWIR mineral	Drillhole	Depth (m)	SiO <sub>2</sub>	Al <sub>2</sub> O <sub>3</sub>	K <sub>2</sub> O	FeO	MgO	SO <sub>2</sub>
205618	FeMg-chlorite	96GVDI001	221.5	31.88	28.72	-	24.19	11.53	2.88
				30.24	25.05	0.41	30.17	10.21	3.93
				33.19	28.76	-	23.32	11.35	3.38
				33.49	27.93	-	23.4	11.44	3.73
				30.29	28.21	-	27.19	11.21	3.1
				30.54	28.9	-	25.66	11.94	2.96
				30.9	27.64	-	26.07	12.46	2.94
				34.42	29.26	-	25.29	9.81	1.22
				40.37	32.34	-	19.03	7.13	1.13
				31.6	28.46	-	25.48	12	1.62
				33.15	27.36	-	25.17	11.49	-
				30.29	28.21	-	27.19	11.21	3.1
				30.54	28.9	-	25.66	11.94	2.96
				30.9	27.64	-	26.07	12.46	2.94
				34.42	29.26	-	25.29	9.81	1.22
				40.37	32.34	-	19.03	7.13	1.13
				31.6	28.46	-	25.48	12	1.62
				33.15	27.36	-	25.17	11.49	-
	Averages			32.85	28.6	0.02	24.94	10.92	2.21

# Appendix 3 – TIR results

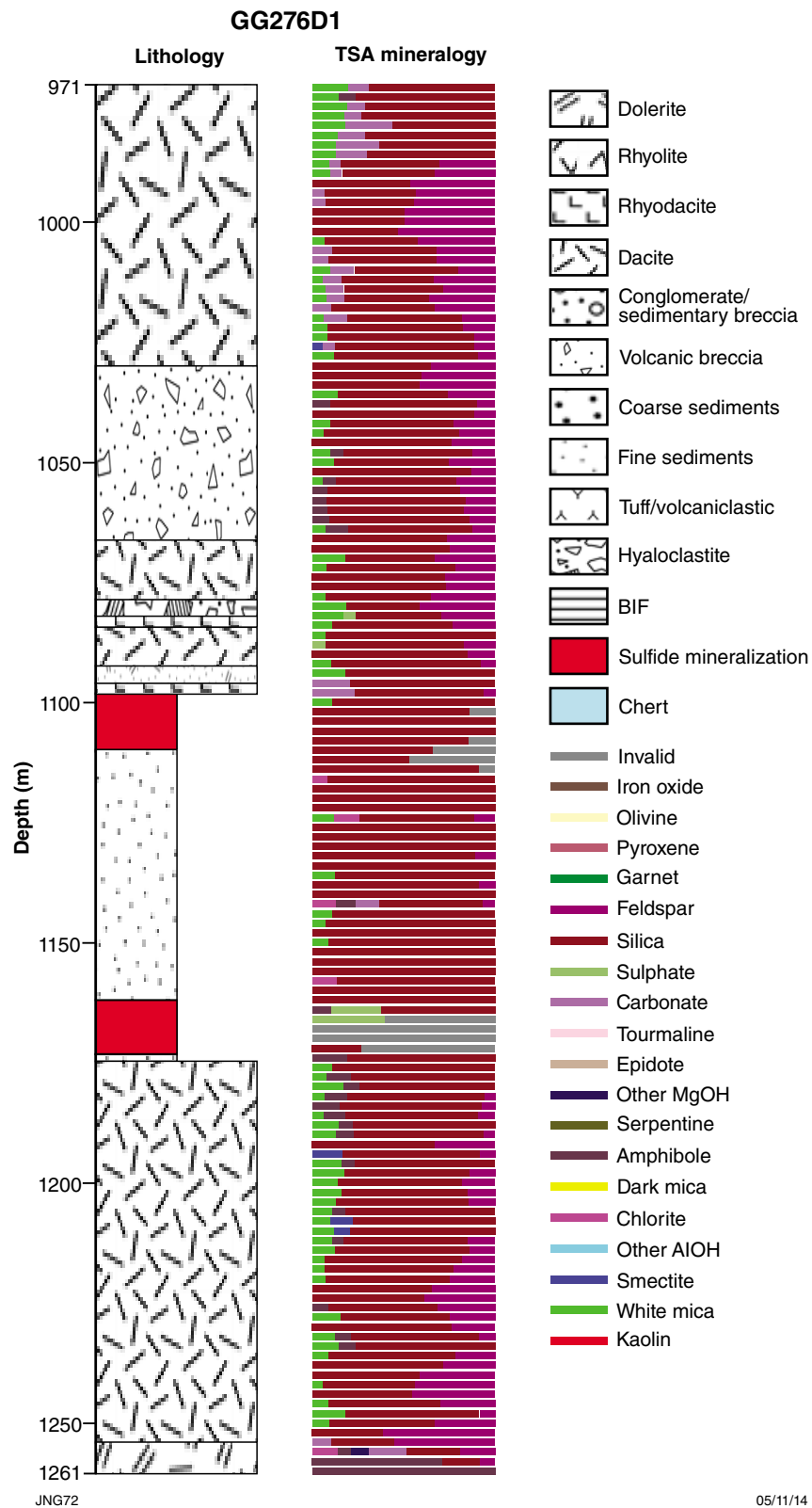


Appendix 3a. Graphic log of Golden Grove drillhole CUDD001 showing lithology and TSG TIR predicted mineral species.

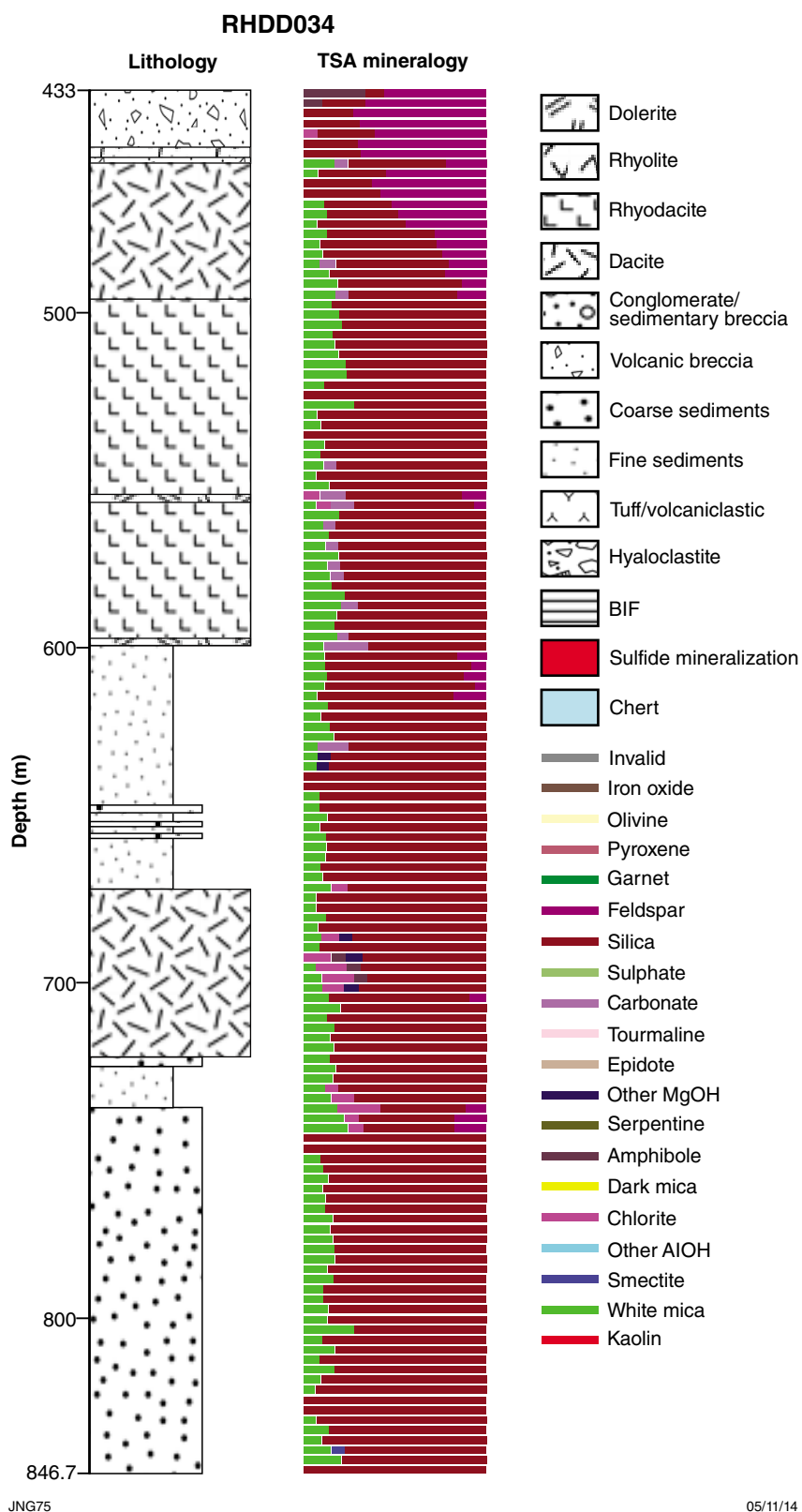




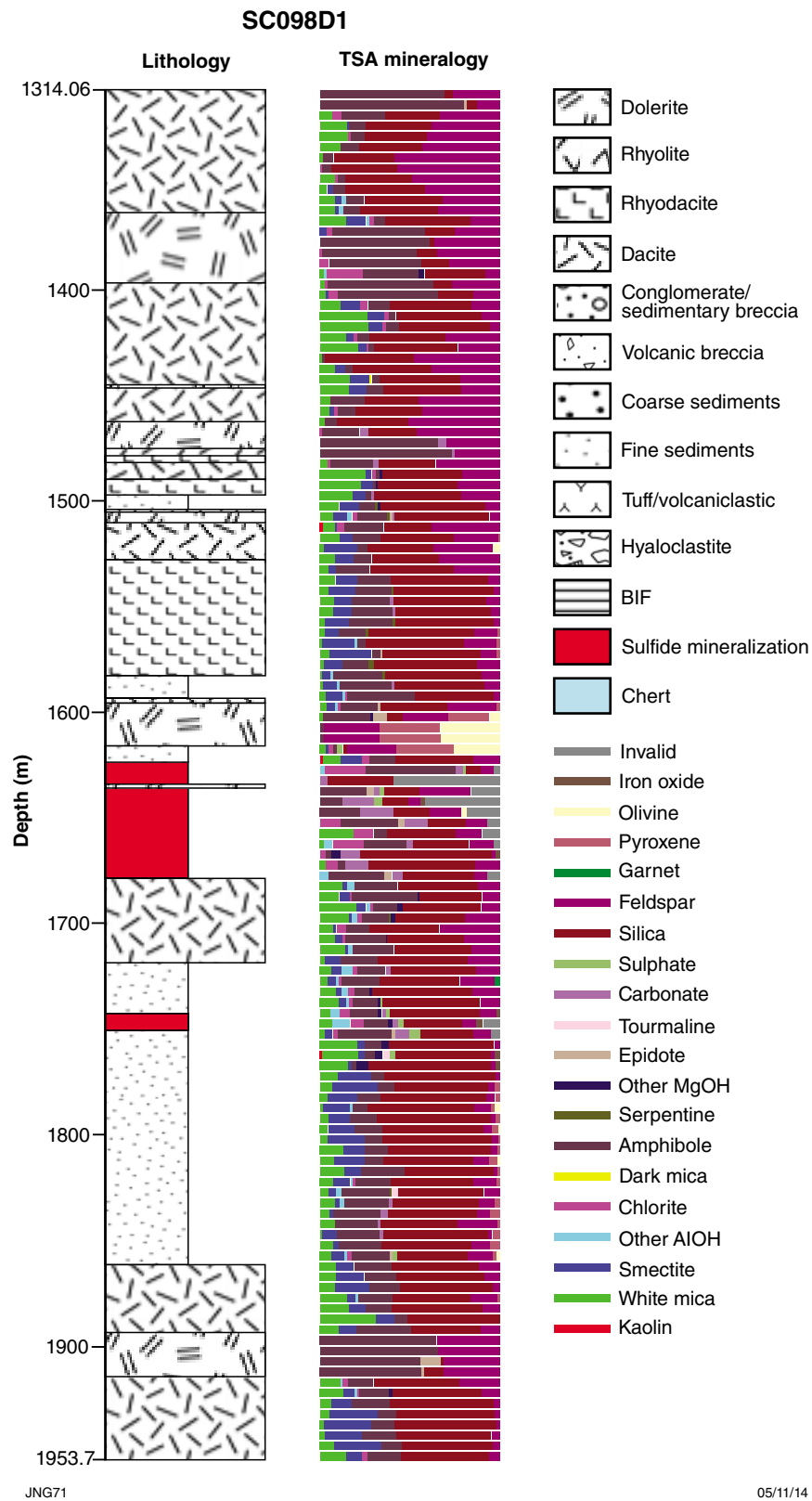
**Appendix 3b. Graphic log of Golden Grove drillhole GG274 showing lithology and TSG TIR predicted mineral species.**



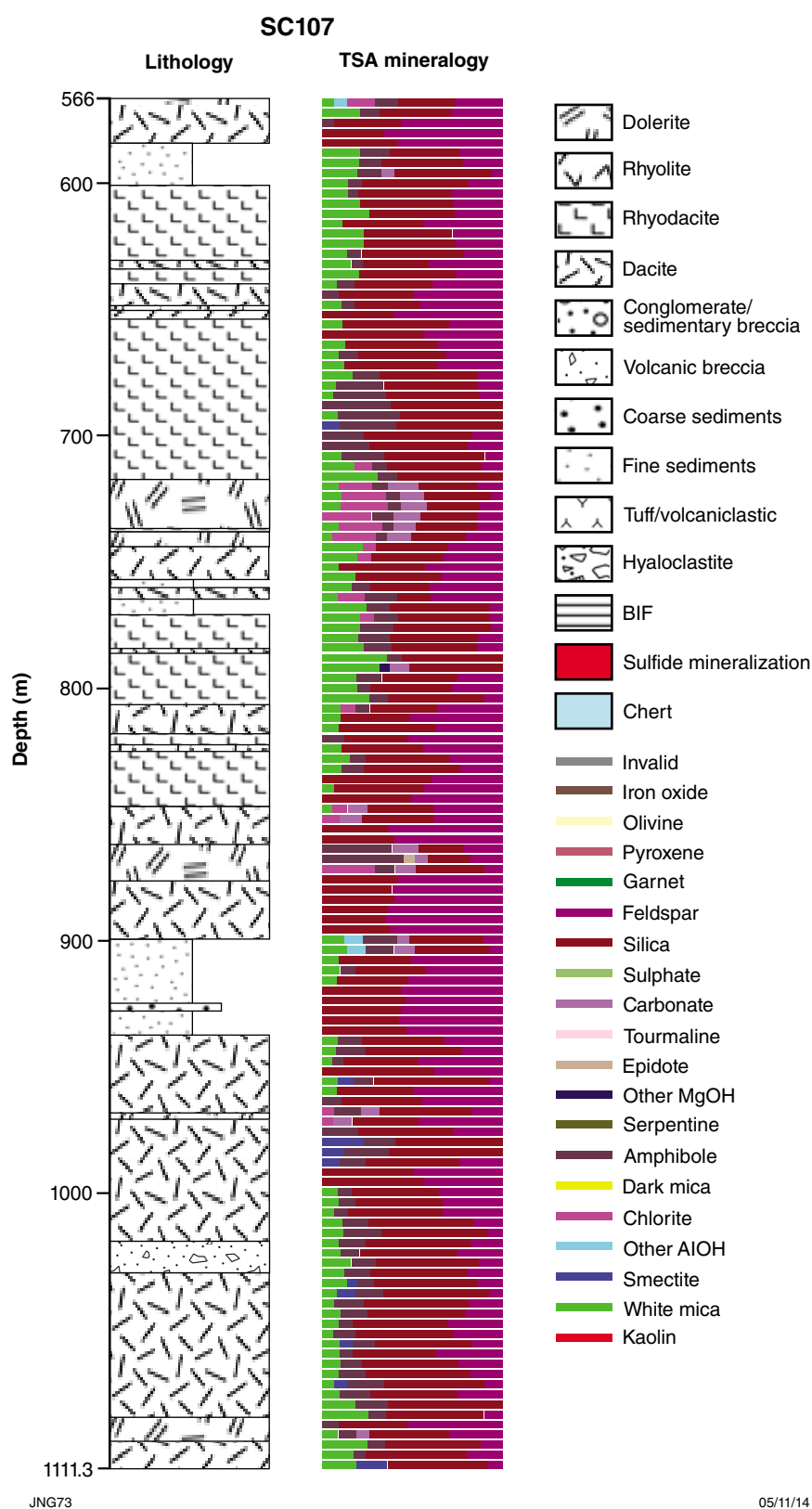
**Appendix 3c. Graphic log of Golden Grove drillhole GG276D1 showing lithology and TSG TIR predicted mineral species.**



**Appendix 3d. Graphic log of Golden Grove drillhole RHDD34 showing lithology and TSG TIR predicted mineral species.**

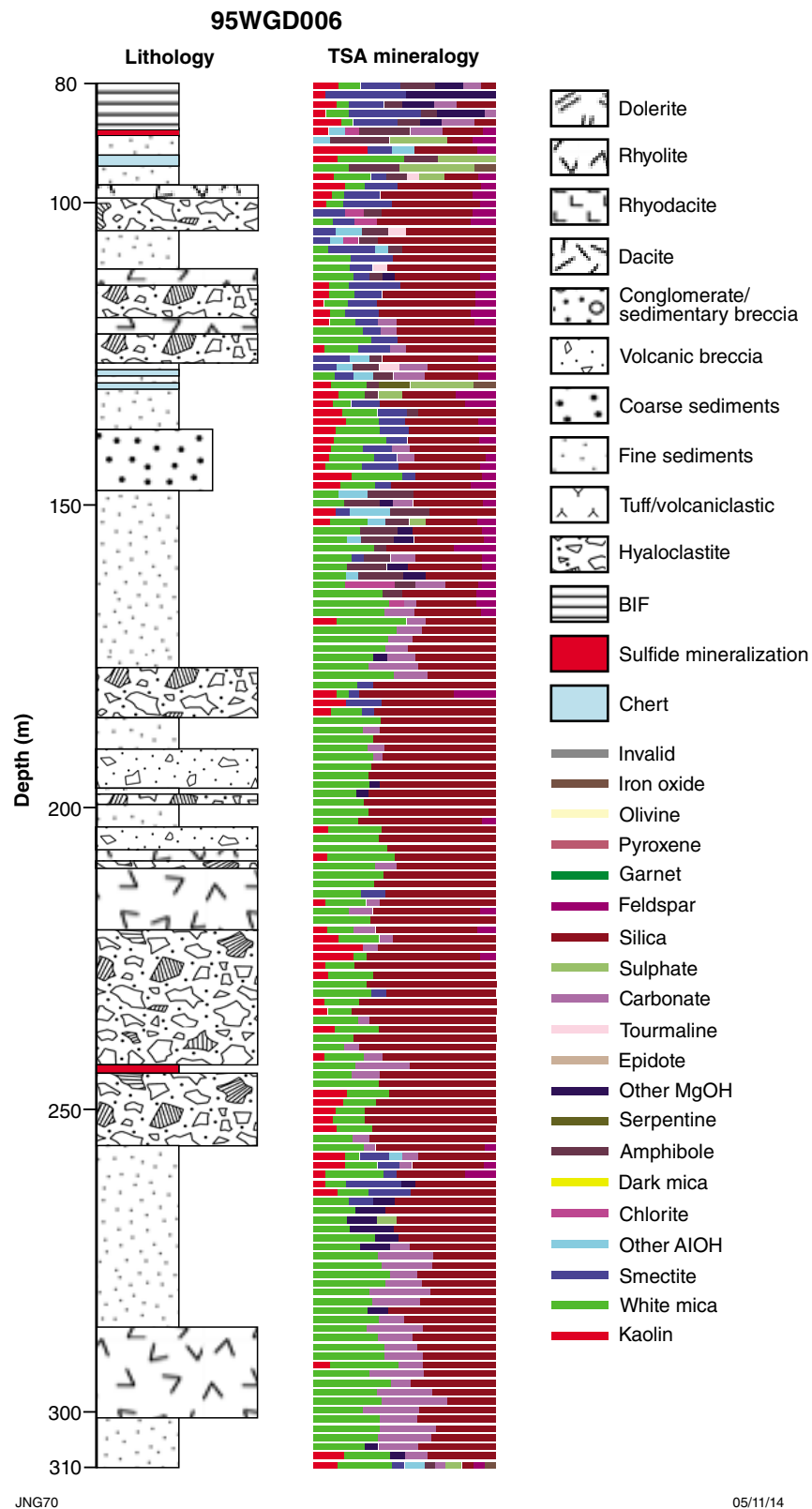


**Appendix 3e. Graphic log of Golden Grove drillhole SC098D1 showing lithology and TSG TIR predicted mineral species.**

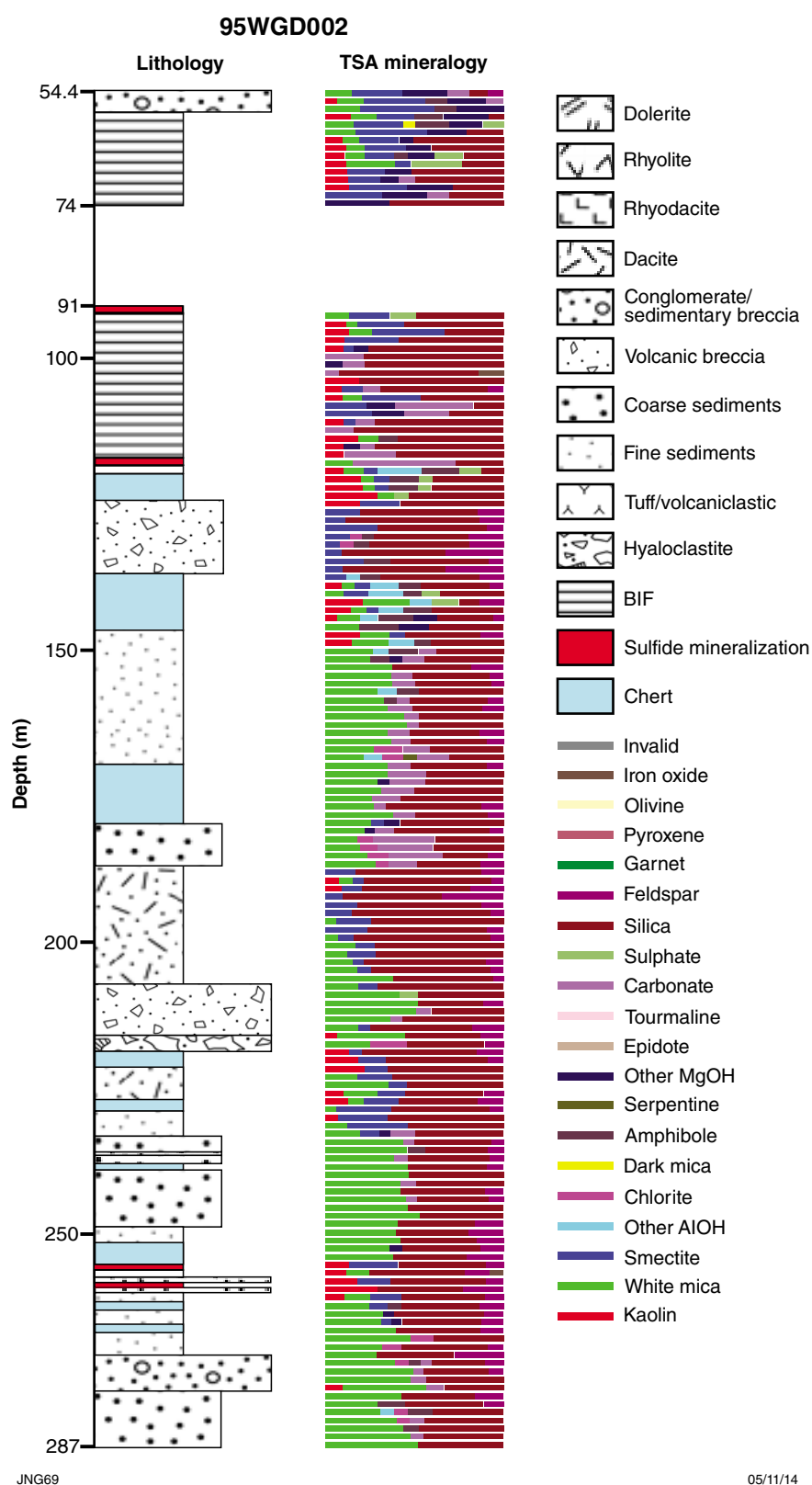


**Appendix 3f. Graphic log of Golden Grove drillhole SC107 showing lithology and TSG TIR predicted mineral species.**

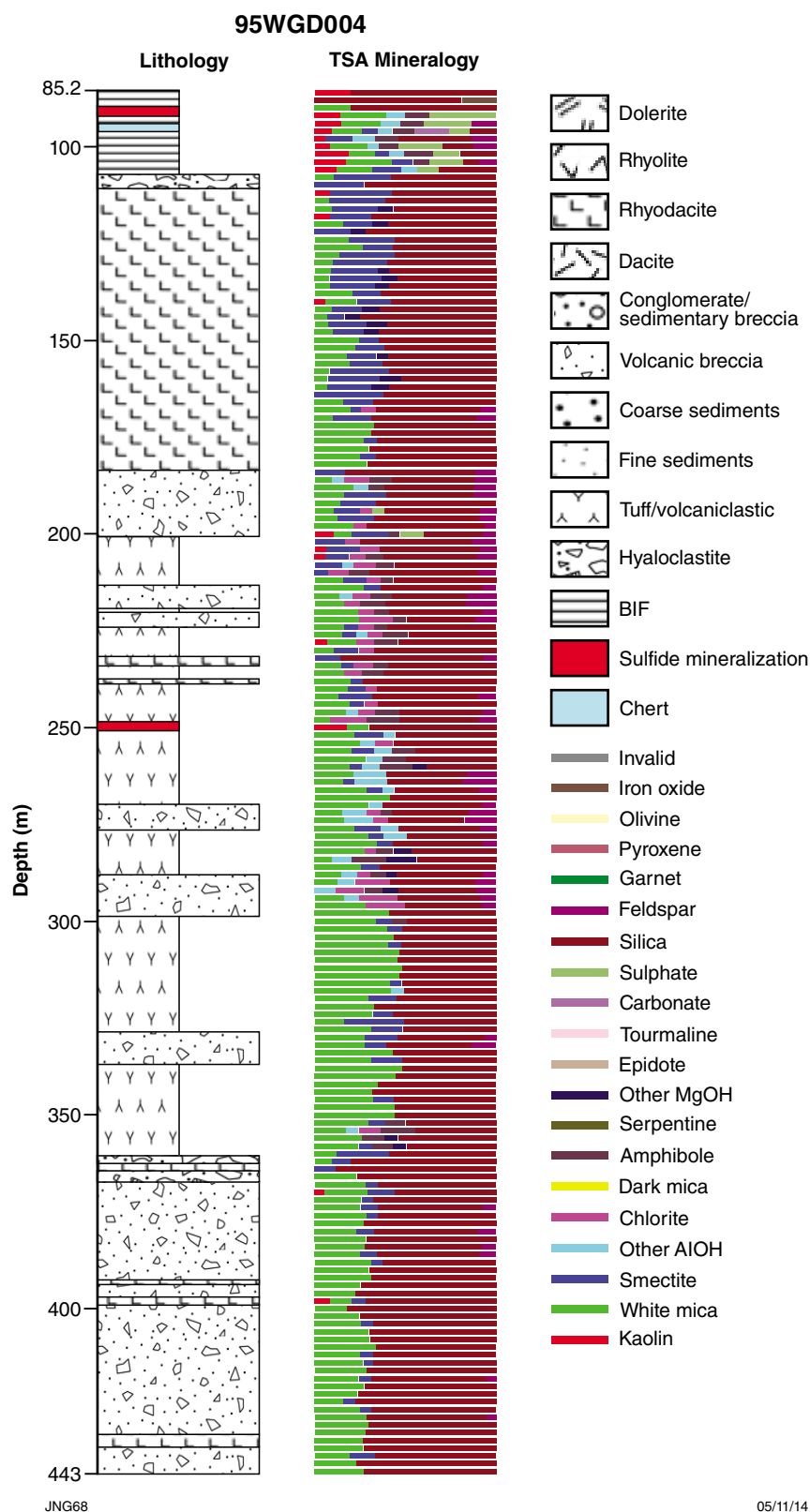




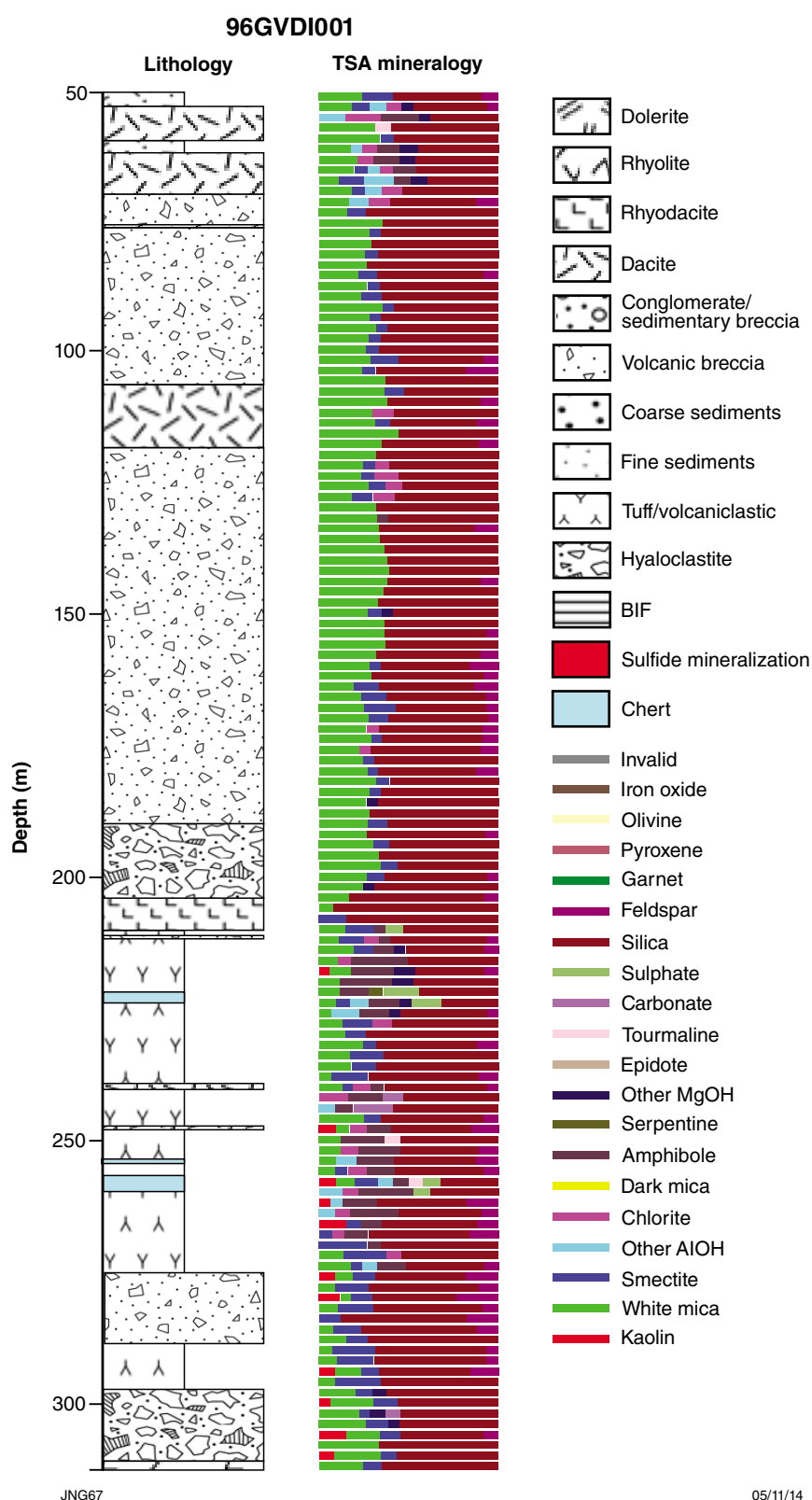
**Appendix 3g. Graphic log of Glenview drillhole 95WGD006 showing lithology and TSG TIR predicted mineral species.**



**Appendix 3h. Graphic log of Glenview drillhole 95WGD002 showing lithology and TSG TIR predicted mineral species.**



**Appendix 3i. Graphic log of Glenview drillhole 95WGD004 showing lithology and TSG TIR predicted mineral species.**

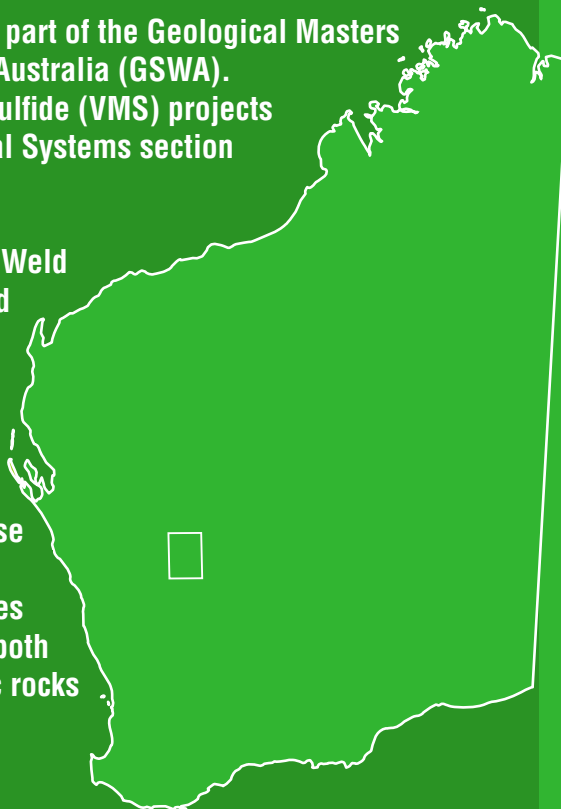


**Appendix 3j. Graphic log of Glenview drillhole 96GVDI001 showing lithology and TSG TIR predicted mineral species.**

This Report is the culmination of work conducted as part of the Geological Masters Program through the Geological Survey of Western Australia (GSWA). It is one of several Archean volcanogenic massive sulfide (VMS) projects in the Murchison region being studied by the Mineral Systems section of GSWA.

The geological features of the Glenview prospect at Weld Range are very similar to those of the VMS-endowed Golden Grove region. Both sequences comprise felsic volcanic, volcanoclastic, and sedimentary rocks that were deposited into a deep subaqueous environment, likely more than 500 m below sea level. Crystallization ages of c. 2977 Ma for felsic rocks near Glenview are only slightly older than those of c. 2960 Ma for the entire dacitic succession at Golden Grove. Felsic volcanic geochemistry indicates eruption in an active continental margin setting for both Golden Grove and Glenview, and that felsic volcanic rocks from both areas are geochemically fertile for VMS mineralization.

Both Golden Grove and Glenview have extensive hydrothermal white mica and chlorite alteration. Mineral spectroscopy of drillcore from Golden Grove showed that white mica and chlorite alteration changed systematically in chemistry and intensity with respect to sulfide mineralization, and provide a vector towards VMS mineralization. When applied to Glenview, such changes in white mica and chlorite alteration suggest the core of the system lies east of the present focus of exploration.



Further details of geological products and maps produced by the Geological Survey of Western Australia are available from:

Information Centre  
Department of Mines and Petroleum  
100 Plain Street  
EAST PERTH WA 6004  
Phone: (08) 9222 3459 Fax: (08) 9222 3444  
[www.dmp.wa.gov.au/GSWApublications](http://www.dmp.wa.gov.au/GSWApublications)